Development of Kinetics and Mathematical Models for High Pressure Gasification of Lignite-Switchgrass Blends

Final Report

Reporting Period: October 1, 2010 – September 30, 2015

Principal Investigator
Pradeep K. Agrawal

Submitted: December 20, 2016

Georgia Tech Research Corporation
Georgia Institute of Technology
311 Ferst Drive NW
Atlanta, Georgia 30332-0100

DOE Award Number: DE-FE0005339

ABSTRACT

The overall objective of the current project was to investigate the high pressure gasification characteristics of a feed containing both coal and biomass. The two feed types differ in their ash contents and ash composition, particularly the alkali content. Gasification of a combined feed of coal and biomass has the potential for considerable synergies that might lead to a dramatic improvement in process economics and flexibility. The proposed study aimed to develop a detailed understanding of the chemistry, kinetics, and transport effects during high pressure gasification of coal-biomass blend feed. Specifically, we studied to develop: (a) an understanding of the catalytic effect of alkali and other inorganic species present in the biomass and coal, (b) an understanding of processing conditions under which synergistic effects of the blending of coal and biomass might be observed. This included the role of particle size, residence time, and proximity of the two feed types, (c) kinetics of high pressure gasification of individual feeds as well as the blends, and (d) development of mathematical models that incorporate kinetics and transport models to enable prediction of gasification rate at a given set of operating conditions, and (e) protocols to extend the results to other feed resources. The goal was to provide a fundamental understanding of the gasification process and guide in optimizing the configurations and design of the next generation of gasifiers.

The approach undertaken was centered on two basic premises: (1) the gasification for small particles without internal mass transfer limitations can be treated as the sum of two processes in series (pyrolysis and char gasification) , and (2) the reactivity of the char generated during pyrolysis not only depends on the pressure and temperature but is also affected by the heating rates. Thus low heating rates (10-50 ^{o}C/min) typical of PTGA fail to produce char that would typically be formed at high heating rates (~10^4 ^{o}C/sec), encountered in entrained flow gasifiers. The char morphology, also a function of the heating rate, would influence the transport rates during the char gasification phase. Thus, heating rate plays a critical role through which both, pyrolysis and char gasification, are interconnected. We utilized two complementary gasification experiments: PEFR (pressurized entrained flow gasifier) and PTGA (pressurized thermo-gravimetric analyzer). The PEFR allowed us to study gasification at pressures, temperatures, and heating rates relevant for coal-biomass gasifiers. The PTGA work was useful in understanding the basic chemistry of the evolution of various gaseous species during pyrolysis. These results helped improved our understanding of the chemistry and chemical changes during pyrolysis. The role alkali metals and other inorganics in char gasification using steam and/or CO_2 was investigated. Finally, the mathematical models for char gasification without the transport effects were developed at commercial operating conditions.

TABLE OF CONTENTS

Background

Coal gasification is a relatively well-developed technology which can be used to produce syngas (CO + H_2) for liquid fuels (F-T synthesis) or hydrogen (via water-gas shift reaction). Because of greenhouse gas (GHG) emissions, there is renewed interest in an integrated gasification combined cycle (IGCC) which is not only more energy efficient, but it also facilitates CO_2 capture from the more concentrated streams. The gasifier comprises the central component of the IGCC technology. The advantage of gasification approach is that a variety of feeds (other than coal) can be utilized. There are two primary reasons for interest in biomass as a source of energy, chemicals, and/or fuels. Firstly, utilization of biomass involves using a domestic and renewable feedstock. Secondly, biomass is CO_2–neutral. The biomass gasification technologies are currently under development, but because of the heterogeneity of the biomass sources (e.g., wood, agricultural waste, forest residue, pulp & paper industry waste) there can be significant variations in the composition and quality of the syngas produced. Therefore, there is increased interest in the use of coal and biomass as potential feedstocks for the production of syngas that can be used to generate electricity (IGCC), hydrogen, chemicals, and liquid fuels. It is envisaged that the existing coal gasifiers can be fed with a blend of coal and biomass, provided a detailed understanding of the chemistry, kinetics, and transport effects is well developed. Biomass has a lower sulfur content and higher volatile content, as compared to coal. Thus, a feedstock blend of low quality coal with biomass waste is attractive for economic as well as environmental considerations. Recently, several groups[1-3] have reported results from co-gasification of coal and biomass. However, owing to the wide variations in the composition of the biomass and incomplete characterization, the results do not lend themselves to generalization. In the absence of fundamental understanding of the role of various species (including ash), it is not possible to extend the results from one study to next. Larson and co-workers[4] have reported economic performance of a gasification study using Illinois coal and biomass to produce electricity and fuels along with CO_2 capture and storage. With strong carbon mitigation policy, they find the economic aspects for such a process attractive. Also, while some groups report synergies during co-feed gasification, others claim to observe no such effect. Undoubtedly, the proximity between the two feeds, particle size, and residence time all are expected to play a role in the potential synergies of using co-feeds. A lack of adequate attention to these variables has rendered many studies to an optimization exercise for a specific set of coal and biomass feed.

According to the billion ton report,[5] America's forests can provide 368 million tons of biomass as unmerchantable wood, forest residuals, and waste from industrial conversion of wood on a sustainable basis. The heating value of this biomass ranges between 16-20 MJ/Kg. None or very little of the unmerchantable timber and harvesting residues is presently utilized. The annual liquid fuel production

from these residues could exceed 15 billion gal/year as gasoline equivalent. Both the scale and the economy of using biomass provide a strong impetus for using it as co-feed in the gasification.

It is helpful to briefly consider the chemical and structural differences between coal and biomass. Coal is highly heterogeneous in nature, and several analytical techniques are needed for its characterization so as to predict its behavior in gasification[6]. Coal consists primarily of polycyclic aromatic hydrocarbons (PAH). Conventional analyses such as proximate analysis, ash content and composition, ash fusion temperature assume coal to be a homogeneous material. Several advanced bulk analytical techniques, such as FTIR and ^{13}C NMR, provide information on the organic structure of coal. Lignite coal may have up to 12% ash, which is primarily composed of SiO_2, Al_2O_3, Fe_2O_3, CaO, and MgO; only small amounts (less than 1 wt%) of alkali (Na_2O & K_2O) are present in the lignite ash. In contrast, biomass consists of cellulose, hemicellulose, and lignin. Cellulose and hemicellulose are polymers of various sugars, whereas lignin can be considered to be a polymer made of phenyl propane monomer units connected through ether linkages. Almost 40-45% of the biomass is oxygen. Thus when biomass is exposed to heat, almost 70-80% of the biomass undergoes devolatilization at temperatures between 300-600 ^oC. The gaseous products evolved during this stage consist of CO, CO_2, H_2, CH_4, C_2-C_4 hydrocarbons, tars etc. The residue char consists primarily of carbon, small amounts of hydrogen and oxygen, and ash. Biomass ash is relatively rich in alkali metals and may have up to 7-8 wt% alkali present as Na_2O and K_2O. When one speaks of biomass gasification, it really involves two processes that occur in series- pyrolysis or devolatilization, to be followed by gasification.

Project Objectives

The overall objective of this project is to investigate the high pressure gasification characteristics of a feed containing both coal and biomass. The study aims to define the impact of biomass addition on coal reactivity. Specifically, we seek to develop: (a) an understanding of the catalytic effect of alkali and other inorganic species present in the biomass and coal, (b) an understanding of processing conditions under which synergistic effects of the blending of coal and biomass are observed. This will include the role of particle size, residence time, and proximity of the two feed types, (c) kinetics of high pressure gasification of individual feeds as well as the blends, (d) development of mathematical models that incorporate kinetics and transport models to enable prediction of gasification rate at a given set of operating conditions, and (e) protocols to extend the results to other feed resources. The results will help provide a fundamental understanding of the gasification process and guide in optimizing the configurations and design of the next generation of gasifiers.

There are several technology gaps: (1) larger particles/briquettes/pellets made from blending coal and biomass would likely have intraparticle heat and mass transfer limitations which can lead to incomplete gasification of carbon, (2) biomass gasification is well known to produce tars which not only contribute to an efficiency loss, but also create problems for IGCC power generation, and (3) potential synergies between coal and biomass require a detailed understanding of the chemistry and kinetics of the gasification process and the catalytic role played by the presence of ash and other inorganic species present in the feeds. The pellets and briquettes are made to overcome the feeding complications, without an understanding or consideration of the potential synergies which will be impacted by the proximity of the two feed types as well as the particle

size of individual feed. The chemical structure and chemical composition of coal and biomass differ significantly. Without a detailed understanding of the chemistry and catalytic role played by inorganic matter, it is not possible to develop a quantitative model for predicting either the gasification rates or the carbon in the ash.

Technical Approach/Rationale

The approach to be undertaken is centered on two basic premises: (1) the gasification for small particles without internal mass transfer limitations can be treated as the sum of two processes in series (pyrolysis and char gasification) , and (2) the reactivity of the char generated during pyrolysis not only depends on the pressure and temperature but is also affected by the heating rates. Thus low heating rates (10-50 ^{o}C/min) typical of PTGA fail to produce char that would typically be formed at high heating rates (~10^4 ^{o}C/sec), encountered in entrained flow gasifiers. The char morphology, also a function of the heating rate, would influence the transport rates during the char gasification phase. Thus, heating rate plays a critical role through which both, pyrolysis and char gasification, are interconnected.

We utilized two complementary gasification experiments: PEFR (pressurized entrained flow gasifier) and PTGA (pressurized thermo-gravimetric analyzer). The PEFR allowed us to study gasification at pressures, temperatures, and heating rates relevant for coal-biomass gasifiers. The PTGA was useful in understanding the basic chemistry of the evolution of various gaseous species during pyrolysis. In addition, solid residues generated at various stages of pyrolysis can be removed and analyzed using solid state NMR and FT-IR for functional groups in the solid residue. These results will help build an improved understanding of the chemistry and chemical changes during pyrolysis. Char gasification using steam and/or CO_2 is known to be catalyzed by alkali metals present in the biomass and coal. This study will generate intrinsic kinetic rate data (free of any transport limitations) for char gasification. The catalytic role of various inorganic matters (including alkali) will be examined. Finally, the proposed study aims to build mathematical models that incorporate the intrinsic kinetics of pyrolysis and char gasification with the transport effects.

In order to achieve the project objectives, the overall project was divided into 14 tasks, some of which are closely intertwined. However, these are expressed as separate tasks due to the nature of the equipment/tool used or the sequence in which these tasks were performed.

Task 1.0 – Project Management and Planning

The project has been divided into 14 separate tasks, each identified according to the work element or the end result. In preparing the Project Timetable, the time and effort to be devoted to each task were estimated. Certain tasks must be completed before undertaking the next task either due to the outcome of a previous task providing critical components needed or due to the fact that a given piece of equipment can be used for only one task at a given time. These factors were used in preparing the Project Timetable but there would be deviations from the original plans, since not all hurdles have been anticipated in preparing the Project Timetable. Adequate personnel resources and attention were devoted to ensure that milestones are not missed because progress in one area kept the next task from being pursued. Quarterly progress reports and financial reports were submitted peridiocally. These reports also addressed any deviations from and revisions to the original plans.

The entire project has been divided into two Phases: Phase 1 is to be completed at the end of first year which is the GO/No GO decision point. A total of five tasks have been identified for the Phase 1. We expect to have completed more than 50% of the work associated with the pyrolysis experiments (in both PEFR and PTGA). Looking at the Timetable, the following milestones can be identified:

Mathematical Models of pyrolysis for Blends	(end of Year 2)
Role of pyrolysis Conditions on Char Morphology	(end of Year 2)
Identification of Synergies for the Blends	(about 1.5 years)
Char Gasification Kinetic Models	(near the end of Year 3)
Mathematical Models for kinetics and transport	(near the end of Year 3)
Validation of Mathematical Models in PEFR	(end of Year 3)
Catalytic effect of alkali, metals etc	(end of Year 3)

Task 2.0 Collection and Preparation of Coal/Biomass Blend Samples

North Dakota or Texas lignite coals were chosen as the coal feed. The biomass candidate chosen for this study was switchgrass because of its high alkali content. A second biomass species (cornstover) was tested to a more limited extent as part of the fuel blends. The switchgrass was chosen because of its ready availability and abundance in different parts of the U.S., whereas cornstover is a suitable candidate for agriculture or biomass residue. Both the biomass and the coal samples were milled and sieved in order to prepare a good representative sample for each experiment. All studies were carried out using a feed of 180-250 μm. This size was small enough to create entrained flow in the PEFR pyrolysis runs, but also large enough to make sure that the feed powder did not form clumps which would have stopped the flow altogether. Due to the higher particle density of coal particles, it was necessary to use smaller particle size (90-106 μm) to enable entrained flow operation. The samples prepared were stored in a large refrigerator to minimize changes. In the last phase of the project, work was done using Illinois # 6 bituminous coal.

Task 3.0 Proximate and Elemental Analyses of Coal and Biomass Feed

The samples (ground and sieved) of coal and biomass were sent for proximate analysis, C-H-O-N-S analysis, and ICP elemental analysis of inorganic content. At least two samples of each (different sizes) were analyzed to quantify sample-to-sample variation and minimize any variations in inorganic content due to particle size. It is important to define the elemental composition in terms of the C, H, O, N, S, Cl, K or Na, Fe etc. This kind of information is critical to understanding the similarities and differences between gasification behaviors with different biomass.

Feed	C	H	N	O	S	Total %
Texas	56.44	4.29	1.21	22.8	0.76	85.5

Lignite	56.31	4.33	1.19	22.94	0.80	85.57
N. Dakota Lignite	60.33 60.21	3.94 4.02	1.15 1.01	24.36 24.24	1.2 1.05	90.98 90.53
Switchgrass	47.04	6.19	0.44	44.1	0.04	97.81

It is noteworthy that duplicate samples yielded similar results. More importantly, there was no significant difference in the elemental composition of the two lignites. The sulfur content is closer to 1%, in contrast with 3-5% sulfur in bituminous coals. Another noteworthy item, though expected, was that the sulfur content of switchgrass is significantly lower than that for the lignite samples. We had hoped to distinguish between the two lignites in their ash content and composition. This would likely affect the gasification and pyrolysis rates where the presence of inorganics might play a catalytic role. ICP analysis of these two lignite coals suggested that not to be the case, and all out studies were carried out using Texas lignite coal.

The below table provides proximate analyses of the feed materials:

	Volatiles	**Fixed Carbon**	**Ash**
Switchgrass	79.20%	17.70%	3.10%
Texas Lignite	32.00%	56.40%	11.50%
North Dakota Lignite	25.70%	62.00%	12.30%
Illinois # 6 Bituminous	36.8%	48.5%	9.38%

ICP data for Cornstover

			AVERAGE
	Corn Stover	**Corn Stover**	**Corn Stover**
	Oven Dried	**Oven Dried**	**Oven Dried**
	Biomass basis	**Biomass basis**	**Biomass basis**
element	**(mg/kg)**	**(mg/kg)**	**(mg/kg)**
Ash (%)			11.69%
Major Species			

Al	1134	1075	1105
Ca	3378	3320	3349
Fe	166	1613	890
K	5950	5833	5892
Mg	1344	1309	1327
Mn	63.5	62.5	63.0
Na	155	145	150
P	1485	1461	1473
S	489	470	479
Si	75.9	55.7	65.8
Si (Caustic Fusion)	32090	29120	30605

ICP data for Switchgrass

			AVERAGE
	Switch Grass	**Switch Grass**	**Switch Grass**
Matrix:	**Oven Dried**	**Oven Dried**	**Oven Dried**
	Biomass basis	**Biomass basis**	**Biomass basis**
element	**(mg/kg)**	**(mg/kg)**	**(mg/kg)**
Ash (%)			**6.65%**
Major Species			
Al	156	162	159
Ca	2879	2820	2850
Fe	177	190	183
K	10175	10175	10175
Mg	1636	1676	1656
Mn	100	100	100
Na	110	152	131
P	1124	1144	1134
S	751	778	765
Si	142	136	139
Si (Caustic Fusion)	11408	11245	11326

ICP data for North Dakota Lignite

			AVERAGE
	ND Lignite	**ND Lignite**	**ND Lignite**

	Oven Dried	Oven Dried	Oven Dried
	Basis	Basis	Basis
element	(mg/kg)	(mg/kg)	(mg/kg)
Ash (%)			11.70%
Major Species			
Al	4996	5066	5031
B	108	107	108
Ba	709	702	706
Ca	13689	13923	13806
Fe	4563	4411	4487
K	456	435	446
Mg	4083	4294	4189
Na	3077	3124	3101
S	10577	10869	10723
Si	426	424	425
Si (Caustic Fusion)	10153	10358	10255
Sr	493	504	498
Ti	158	157	157

ICP data for Texas Lignite

			AVERAGE
	TX Lignite	TX Lignite	TX Lignite
	Oven Dried	Oven Dried	Oven Dried
	Basis	Basis	Basis
element	(mg/kg)	(mg/kg)	(mg/kg)
Ash (%)			13.33%
Major Species			
Al	5505	5425	5465
B	220	220	220
Ba	315	308	311
Ca	14263	14396	14330
Fe	2373	2399	2386
K	227	216	221
Mg	2986	3013	2999
Na	245	240	243

S	5319	5639	5479
Si	296	376	336
Si (Caustic Fusion)	25212	25676	25444
Sr	293	303	298
Ti	513	519	516

Task 4.0 Pressurized Entrained Flow Reactor (PEFR) Pyrolysis Studies

The pressurized entrained flow reactor (PEFR) is schematically illustrated in Figure 1. Fine particles of biomass and nitrogen as carrier gas (so called primary gas) enter the reactor via a liquid cooled injector, shown in green in the upper section of the reactor assembly. Secondary gases, consisting of N_2 with different mixtures of oxidizing gases (H_2O and CO_2) and product gases (H_2 and CO) enter the reactor at the top of the preheat section, shown in orange in the below figure. As the secondary gases flow down the preheat section, they are heated to the reaction temperature by electric heaters. At the end of the preheat section, the hot secondary gas flows through a flow straightener that imparts a flat vertical velocity profile to the gas as it enters the reactor section. The outer wall of the reactor section is maintained at the desired reactor temperature by electric heaters. Biomass particles and the primary gas are heated rapidly by radiation from the reactor walls and convectively by the hot secondary gas.

The particles flow along the vertical center line of the reactor as they pass through it. The residual mass in the particles is collected by a liquid-cooled collector. The position of the moveable collector within the reactor is the primary method by which particle residence time is varied. Cool nitrogen is injected radially in the top of the collector to rapidly quench the gas-particle mixture. Char residues are separated by a cyclone with a nominal 50% cut size of 3 μm, located at the exit of the water-cooled collector. The gas exiting the cyclone is filtered by a heated glass fiber fume filter with a nominal cut size of 0.01 μm. The offgas is analyzed with a combination of Fourier-Transform Infra-Red analyzer and gas chromatograph. The organic carbon content in the char residue is measured and the extent of carbon conversion calculated.

Three different feeds (two lignite coals and switchgrass) were studied in the pressurized entrained flow reactor (PEFR) at three different pressures: 5, 10, and 15 bars and three different temperatures: 600 ^oC, 800 ^oC, and 1000 ^oC. Due to extensive heat losses, it was difficult to maintain the 1000 ^oC temperature at 20 bars. A few runs were carried out at 20 bars, but at lower temperatures only. The pyrolysis runs were conducted in flowing N_2 with a residence time of ~ 30 seconds. A few runs were also conducted at shorter residence times. The goal of shorter duration runs was to identify, if any, primary pyrolysis products. This is particularly true of the gaseous products and tars formed.

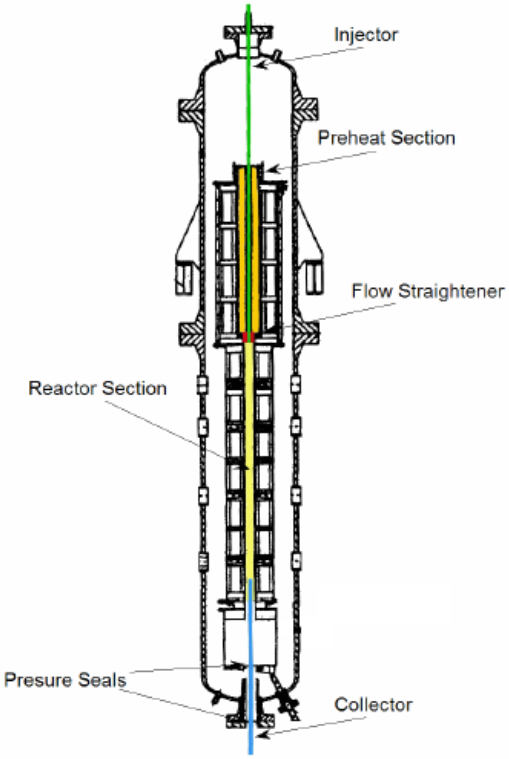

Figure 1. The Pressurized Entrained Flow Reactor at Georgia Institute of Technology. Diagram of the pressurized entrained-flow reactor (PEFR). The height of the reactor section is 2 m whereas the height of the whole equipment including the biomass feed system and the collector and gas sampling assembly (not shown in the schematic drawing) is 12 m.

The condensed residues were tested for (i) tars, (ii) C,H,O, and N, and (iii) inorganics using ICP (for carbon balance). Large char amounts were generated for PTGA study (Tasks 8 and 9) and characterization (Task 6). For each feed type, there were at least 9 runs (three temperatures and three pressures). Several runs were also made in atmospheric pressure laminar entrained flow reactor (LEFR) at 600, 800, and 1000 C respectively. Chars were characterized using SEM, surface area (N_2 and CO_2), C, H, N, O analysis, ICP for inorganic elements. Gases evolved during the pyrolysis were analyzed using a GC for CO, CO_2, CH_4, H_2, and C_2-C_4 hydrocarbons. It was not feasible to analyze the gaseous products for H_2O. Typically gas samples were collected during the pyrolysis runs in Tedlar bags and were analyzed using the GC within the next 10-15 hrs. Thus the moisture cannot be determined with accuracy due to condensation. Attempts were made to do a mass balance on carbon and H. The characterization results for chars generated from this study are provided under Task 6.0. In this sub-section, we present the results on tars collected and gas compositions obtained in PEFR pyrolysis runs.

	600 ^{o}C	800 ^{o}C	1000 ^{o}C
1 bar	x	x	x
5 bars	x	x	x
10 bars	x	x	x
15 bars	x	x	x

The gas composition at different pyrolysis pressures is presented in the below tables. Several observations can be made from the pyrolysis gas compositions reported here:

(i) Major products include CO, CH_4, H_2, and CO_2. The main minor product is ethylene, but a distant fifth species.

(ii) The four major gas species vary greatly depending on the pyrolysis pressure and temperature: (a) at lower temperatures (600 ^{o}C), CH_4 and CO are the major products, but at higher temperature (1000 ^{o}C), CH_4 is greatly reduced and CO amount is increased. Apparently, both steam reforming of methane and water gas shift (WGS) reactions play a role in the gaseous compositions. (b) the minor gaseous species (C_2-C_4) are reduced at higher pressures.

Species	Gas Composition (mole%) at **5 bars**		
	600 ^{o}C	**800 ^{o}C**	**1000 ^{o}C**
CO	45.2	41.2	61.0

CO_2	16.7	16.9	12.1
H_2	8.9	24.5	21.9
CH_4	21.1	16.6	4.75
C_2H_6	1.42		
C_2H_4	5.70	0.52	0.10
C_2H_2	0.09	0.22	0.15
C_3H_8	0.03		
C_3H_6	0.66		
C_4H_{10}			
C_4H_8			
C_4H_6	0.14		

Species	Gas Composition (mole%) at **10 bars**		
	600 ^oC	**800 ^oC**	**1000 ^oC**
CO	45.2	41.2	61.0
CO_2	16.7	16.9	12.1
H_2	8.9	24.5	21.9
CH_4	21.1	16.6	4.75
C_2H_6	1.42		
C_2H_4	5.70	0.52	0.10
C_2H_2	0.09	0.22	0.15
C_3H_8	0.03		
C_3H_6	0.66		
C_4H_{10}			

C_4H_8			
C_4H_6	0.14		

Species	Gas Composition (mole%) at **10 bars**		
	600 ^oC	**800 ^oC**	**1000 ^oC**
CO	45.2	41.2	61.0
CO_2	16.7	16.9	12.1
H_2	8.9	24.5	21.9
CH_4	21.1	16.6	4.75
C_2H_6	1.42		
C_2H_4	5.70	0.52	0.10
C_2H_2	0.09	0.22	0.15
C_3H_8	0.03		
C_3H_6	0.66		
C_4H_{10}			
C_4H_8			
C_4H_6	0.14		

This table shows the effect of residence time on the evolution of smaller olefins.

Temperature (°C)	800	1000	600				800				1000			
RT (s)	4s		28 s				28 s				28 s			
Pressure (bar)	5	5	5	10	15	20	5	10	15	20	5.0	10	15	
Carbon Monoxide	54.8	55.4	58.1	55.1	52.5	54.5	52.9	47.4	51.1	49.1	52.1	65.2	61.6	
Carbon Dioxide	12.3	7.3	6.9	8.7	9.9	10.7	9.6	13.1	15.9	18.9	10.6	6.8	5.9	
Hydrogen	11.3	16.7	9.5	10.8	14.2	9.5	20.5	27.9	19.7	14.6	30.9	26.0	30.0	
Methane	15.8	15.7	18.8	21.5	21.9	23.3	16.2	11.2	13.1	17.3	6.0	1.9	2.5	
Ethane	1.3	0.6	0.7	0.5	0.04	0.1								
Ethylene	3.6	3.5	5.6	3.3	1.5	1.9	0.5	0.3	0.1	0.1	0.2	0.1	0.01	
Acetylene	0.1	0.4	0.2	0.1	0.02		0.3				0.2			
Propane	0.1	0.01												
Propylene	0.7	0.3	0.3	0.04										
Butane														
1-Butene	0.02													
1,3-Butadiene	0.1	0.1												

The gas composition during lignite pyrolysis was monitored using the micro-GC. Below table shows the results obtained at 5 bars and three different temperatures. Overall, the only gaseous species observed are CO, CO_2, H_2, and CH_4 (moisture content could not be reliably measured). The amount of gases evolved are much lower than those observed during the switchgrass pyrolysis. This observation is not entirely surprising since lignite has very small amounts of H and O elements (which are present in abundance in a biomass like switchgarss). Secondly, the pyrolysis of switchgrass showed the formation of C_2-C_4 hydrocarbons. With lignite, only

methane is observed, presumably as a decomposition of functional group (methyl or methoxy) attached to lignite components.

PEFR Texas Lignite Pyrolysis at 5 bars (Exit Gas Composition)

Species	Gas Composition (mole fractions) at **5 bars**		
	600 °C	**800 °C**	**1000 °C**
CO	0.030	0.022	0.070
CO_2	0.035	0.032	0.026
H_2	0.019	0.035	0.131
CH_4	0.019	0.008	0.012

Switchgrass Tar Characterization

The tars evolved during switchgrass pyrolysis were collected on a filter at the exit of the reactor. Tars species were extracted using DCM (dichloromethane) and analyzed using GC-MS. The below table shows the results obtained at 600 °C and 800 °C (5 bars).

Compound name	Structure	600 _5 bar	800_5bar
Phenol, 2-methoxy	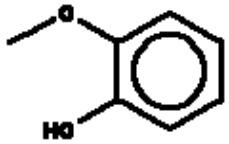	73.13	
Phenol, 4-ethyl		55.81	39.16
Phenol,3-ethyl	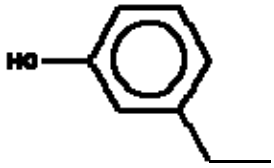		38.61

1,2-Benzenediol	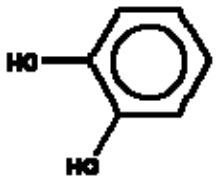	**91.04**	**77.85**
1,2-Benzenediol,3-methyl	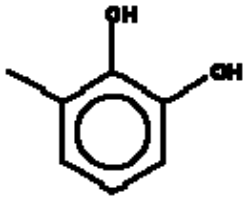	**95.24**	**61.83**
Hydroquinone		58.84	36.04
1,2,3-Propanetriol,diacetate	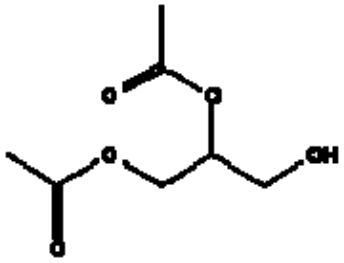	**79.24**	**67.04**
Phenol,2-metyhyl-6(2-propenyl)			
Biphenyl	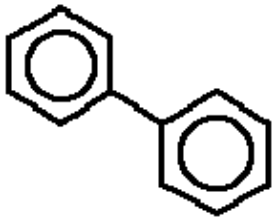	**77.92**	**64.38**
Biphenylene	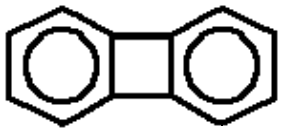	64.31	68.34

Dibenzofuran	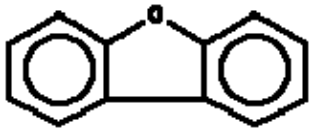	**90.95**	**97.49**
O-hydroxybiphenyl	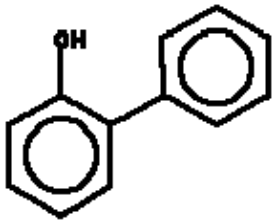	**76.84**	**77.95**
Napthalene,1-isocyano	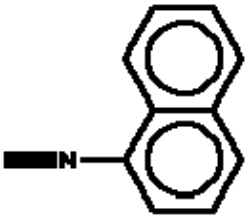	**63.70**	**85.85**
Fluorene	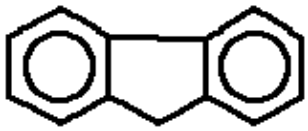	**94.47**	**94.72**
2-Napthalenol	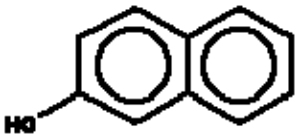	70.88	
2-fluoreneamine	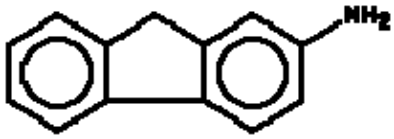	66.17	67.37
Napthalene,1-(1-methylethyl)-	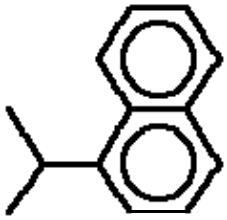	61.42	76.18

Phenanthrene	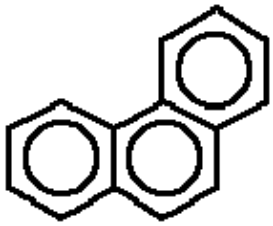	**82.89**	**85**
2-Tridecanone	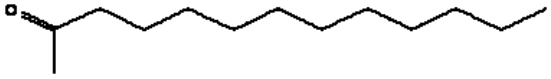	68.43	38.94
p-hydroxybiphenyl	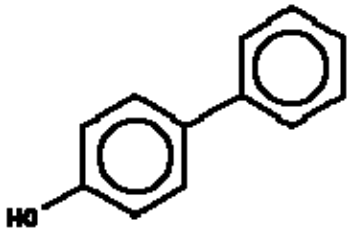	**76.19**	**77**
2-fluorenecarboxaldehyde	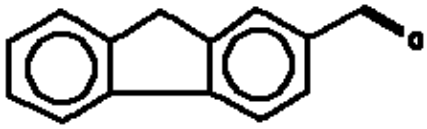	**93**	**93**
9-(chloromethyl)anthracene	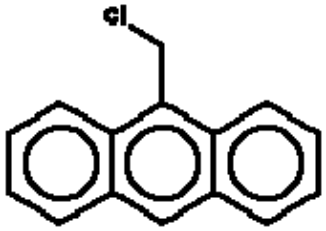	**82.73**	**87.61**
Azulene	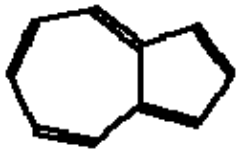		48.65
Resourcinol	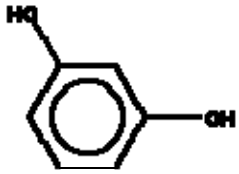		40.55

Napthalene,1-methyl	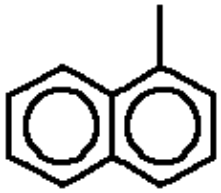		52.14
Napthalene,2-methyl	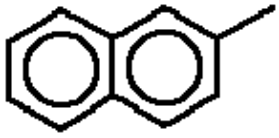		48.55
Benzenemethanol,.alpha.-ethyl-	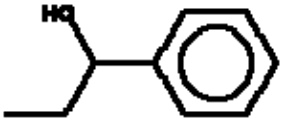		63.82
1,2-benzenedicarboxaldehyde	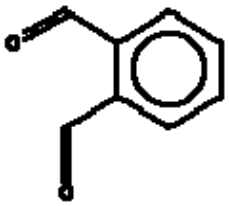		54.88
1,1'-Biphenyl,2-methyl	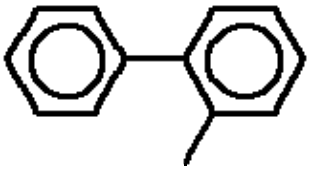		47.82

The last two columns in the above table show the probability of species identification. Where large numbers are indicated, the degree of confidence is high and those results are marked in bold. Mostly these tar species are aromatic in nature, with significant fraction being phenolic species. It is important to minimize the formation of tars as not only do they represent a loss of carbon efficiency, but these also impose heavy burden on downstream processing. It is important to note that not all tars are collected and identified as will be discussed under Task 6.0. It was not possible to quantify the total tars formed. One can only guess based on carbon balance as to the fraction left unidentified. Based on the results obatiend from short residence time studies and PTGA, the following appears to be a reasonable representation of primary, secondary, and tertiary tar formation.

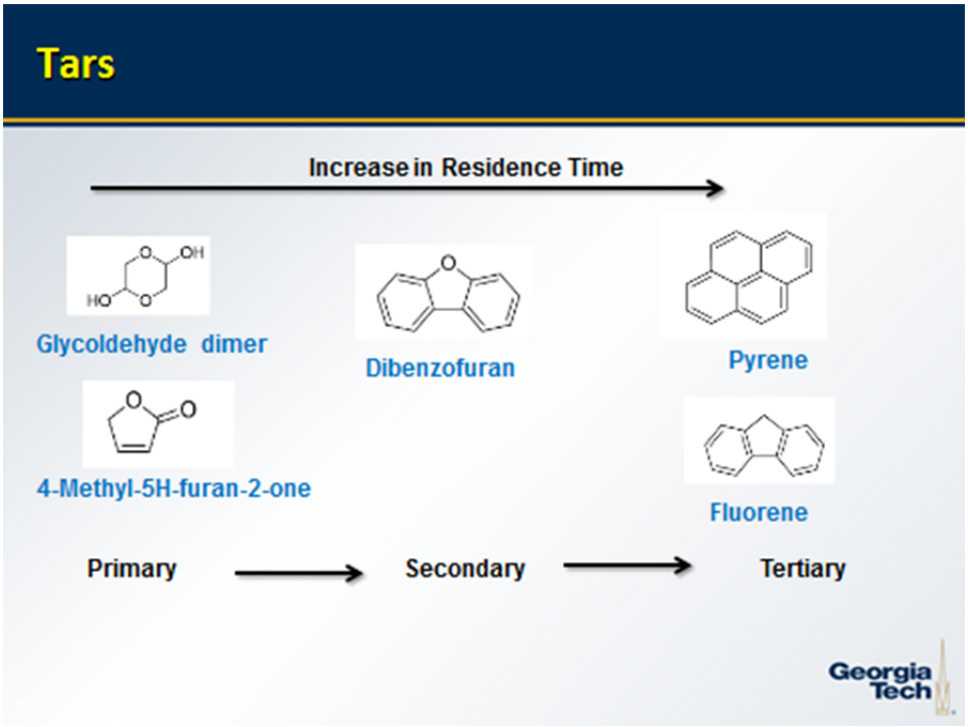

Tars have been classified as:- 1. *Primary*: characterized by cellulose-derived products such as levoglucosan, hydroxyacetaldehyde, and furfurals; analogous hemicellulose-derived products; and lignin-derived methoxyphenols; 2. *Secondary*: characterized by phenolics and olefins; 3. *Alkyl tertiary tars*: methyl derivatives of aromatics, such as methyl acenaphthylene, toluene, and indene; 4. *Condensed tertiary tars*: Poly-Aromatic Hydrocarbon (PAH) series: naphthalene, acenaphthylene, anthracene/phenanthrene

Tar evolution

Short residence time (4 s) → Long residence time (28 s)

Primary

Formula	Probable Compound	Derived from
$C_4H_8O_4$	Glycolaldehyde dimer	Cellulose
$C_3H_6O_3$	2-Propanone, 1-hydroxy-	Cellulose
$C_4H_6O_2$	Butanedial	Cellulose
$C_4H_6O_2$	2(5H)-Furanone	Cellulose
$C_5H_6O_2$	4-Methyl-5H-furan-2-one	Cellulose
$C_5H_6O_3$	2-Furancarboxaldehyde, 5-[hydroxymethyl]-	Cellulose
$C_3H_8O_2$	R-(-)-1,2-propanediol	
C_6H_6O	Phenol	Lignin
$C_5H_8O_4$	5-Oxotetrahydrofuran-2-carboxylic acid	

Secondary

Formula	Probable Compound
$C_{12}H_{10}$	Biphenyl
$C_{12}H_8O$	Dibenzofuran
$C_{20}H_{12}O$	Benzo[b]naphtho[2,3-d]furan
$C_{13}H_{10}O_2$	[Benzenediol?]

Tertiary

Formula	Probable Compound	Formula	Probable Compound
$C_{15}H_{10}$	Phenanthrene	$C_{16}H_{12}$	Phenanthrene, 3-methyl-
$C_{16}H_{10}$	Fluoranthene	$C_{13}H_{10}$	[Benzo[7]indene?]
$C_{14}H_{10}$	Anthracene	$C_{15}H_{12}$	Anthracene, 1-methyl-
$C_{16}H_{10}$	Pyrene	$C_{16}H_{12}$	Naphthalene, 2-phenyl-
$C_{16}H_{10}$	Fluorene	$C_{15}H_{12}$	Anthracene, 9-ethenyl-
$C_{17}H_{10}$	4H-Cyclopenta[def]phenanthrene	$C_{12}H_8$	Acenaphthene
$C_{15}H_8$	[acephenanthrylene?]		
$C_{12}H_8$	Acenaphthylene		

- PAH formation confirms that free radical molecular weight growth reactions occur at long residence times. [1]

Georgia Tech

[1]Jarvis et.al. Energy & Fuels 2010, 25, (1), 324-338

Pyrolysis Tars

Low temperatures and residence times		High temperatures and long residence times	
Cellulose/Hemicellulose Derived		**Polynuclear Aromatic Hydrocarbons (PAHs)**	
Acetic Acid[1]	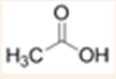	Phenanthrene	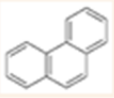
Protein Derived[1,2]		Fluorenthene	
Indole		Anthracene	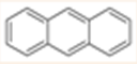
Carbazole	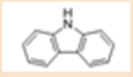	Acenapthylene	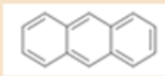
1-Napthalenecarbonitrile	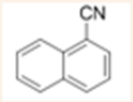		

- PAHs are products of tertiary pyrolysis reactions.

Georgia Tech

[1]Mullen et al, Energy & Fuels 2008, 22, 2104-2109
[2]Sharma et al, ACS Fuel Chem. Div. Pre. 2002, 47(1), 399

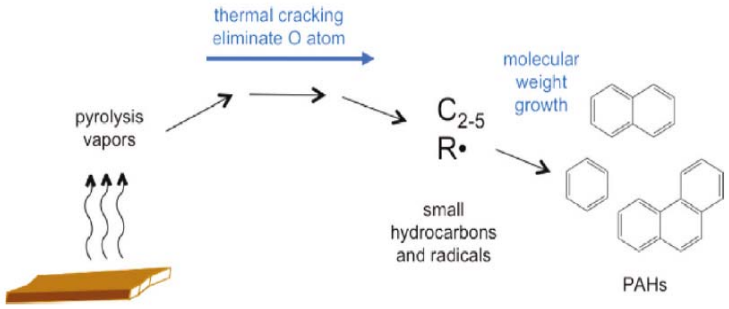

Model for PAH formation during pyrolysis

Total oxygen content of tar decreases with increasing temperature, favoring formation of CO, CO_2, oxygen-free aromatics and PAHs. The average molecular weight of pyrolysis tars from white-oak particles in an entrained flow reactor decreased due to cracking of tars until 750 °C; after which molecular weight growth was observed at temperatures higher than 900 °C due to formation of PAH. The proportion of 3-4 ring aromatic PAH increased above 800 ^{o}C.

A PAH formation mechanism has been hypothesized based on these observations. Pyrolysis vapors are formed from the decomposition of bio-polymers. Degradation of hemicellulose and lignin is observed at lower temperatures, while cellulose degrades at slightly higher temperatures. Pyrolysis vapors thus formed, crack into smaller molecular fragments (furans, aldehyde, ketones), releasing H_2, CO, CO_2. Eventually these fragments crack into smaller hydrocarbons.

As this size reduction occurs, O in these molecules is liberated as CO or CO_2. Likewise, lignin products form smaller molecular species and radicals. These radicals and small molecules combine to produce aromatic compounds by molecular weight growth by free-radical reactions. Tertiary tars grow in molecular weight with reaction severity and do not crack at high temperatures. The decision to run a gasifier at higher severity should be thus balanced by the consideration of the remaining tar composition which could be "refractory tars.

Task 5.0 Pyrolysis in Pressurized Thermal Gravimetric Analyzer (PTGA) Studies

One GT researcher worked under the direct supervision of the NREL co-PI. Five different feeds (as outlined in Task 4.0) were investigated at two different heating rates (10 ^{o}C/min and 30 ^{o}C/min). In summary, this part was used for developing an improved understanding of pyrolysis chemistry and the evolution of various gaseous species.

Figure 2. ThermMax500 pressurized thermogravimetric analyzer.

The experimental work at NREL to study the reactivity of biomass-coal mixtures was done using a Thermo Scientific TherMax500 pressurized thermogravimetric analyzer equipped with a Nicolet FTIR analyzer and an ONYX mass spectrometer.

The Thermo Scientific TherMax500 is capable of operating at pressures up to 100 bar and temperatures of up to 1100°C. The sensitivity of the balance is 100 micrograms, and the capacity up to 100 grams. However, at high pressures, the noise-to-signal ratio increases and the effective sensitivity increases.

The flows of the gases are regulated by mass flow controllers. For evolved gas analysis, the PTGA is equipped with a Thermo Onix ProLab mass spectrometer and a Nicolet Fourier-transform infra-red analyzer. The lines between the thermobalance and the analyzers are heated to 250°C.

The Thermo Onix ProLab mass spectrometer is a triple filter quadrupole mass analyzer capable of analyzing through mass number 300. The mass spectrometer has a dual (Faraday/channeltron multiplier) detector assembly. The minimum detectable concentrations are <10 ppm for the Faraday detector and <50 ppb for the Channeltron with UHP inlet for non-overlapping peaks. GasWorks software is utilized for the analysis of the results.

The FTIR analyzer is a Nicolet iS10 FT-IR spectrometer paired with the Nicolet iZ10 module. Omnic software is used for the analysis. An example spectrum for biomass pyrolysis is shown

below. Coal and switchgrass char devolatilization and gasification experiments were conducted in a Thermax 500 pressurized thermogravimetric analyzer (PTGA). The PTGA can operate up to temperatures of 1100°C and pressures of 100 bar. For evolved gas analysis, the PTGA is equipped with a Thermo Onix ProLab mass spectrometer (MS) and a Nicolet iS10 Fourier-transform infra-red analyzer (FTIR) paired with a Nicolet iZ10 module. The lines between the thermobalance and the analyzers are heated to 250°C.

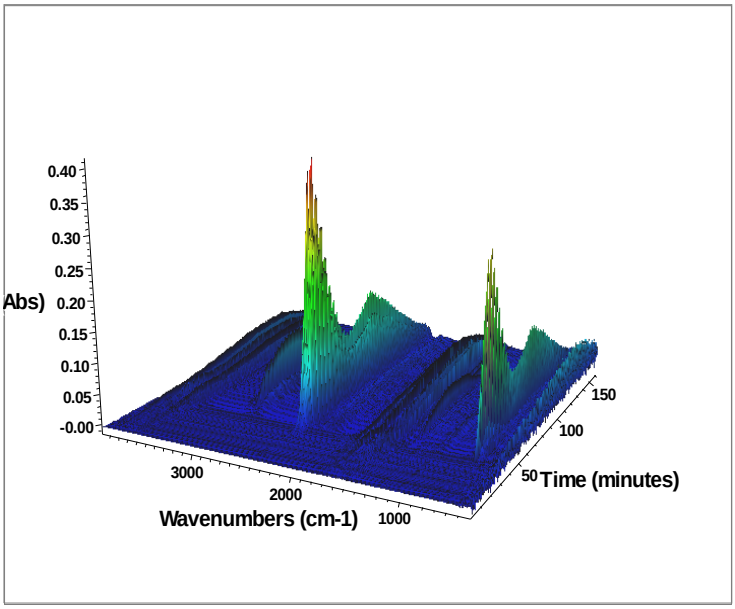

Figure 3. An example FTIR spectrum for biomass pyrolysis.

The devolatilization experiments were performed by heating the feeds at a constant heating rate to 1000°C in inert gas atmospheres. The evolved gases were measured by the MS and FTIR. The gasification reactions were performed isothermally. A weighed amount of char was placed in the sample holder and the reactor was closed and pressurized to the reaction pressure. The reactor was heated at a rate of 20°C/min under inert gas (He or N_2) to the reaction temperature and held at that temperature for a minimum of 5 minutes, after which the gas concentrations were switched to the predetermined values. When the gases included CO or H_2, the reactor was pressurized three times to a minimum of 10 bar prior to the experiment with an inert gas to remove any traces of oxygen from the system. Water was introduced via an HLPC pump and vaporized prior to introduction into the reactor and water vapor was condensed after the reactor in a chilled condensation loop.

Switchgrass and lignite and their blends were pyrolyzed in the PTGA at pressures of 5-20 bar and heating rates of 5-20°C/min. Example results for the two chars are shown in the below Figure. For switchgrass, a typical mass loss curve for biomass was obtained. The large mass loss

peak around 300-400°C is largely due to cellulose decomposition; hemicellulose volatilizes at slightly lower temperatures and contributed to the widening of the peak at lower temperatures. Lignin devolatilizes at a wider temperature range and is responsible for the peak at 450-700°C. The final mass loss at 800-900°C is associated with char carbonization reactions.

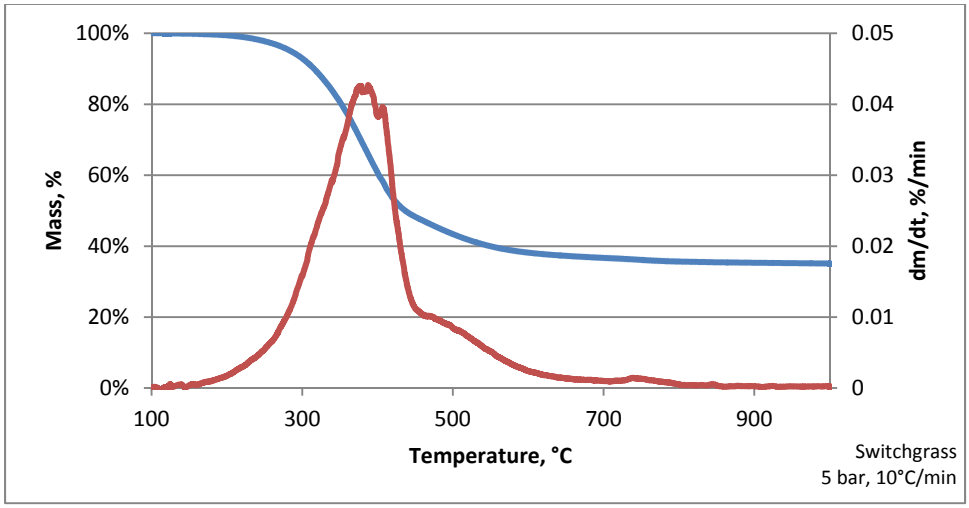

Water vapor (H_2O, m/z 18), carbon dioxide (CO_2, m/z 44), and carbon monoxide (CO, m/z 28) were the major gas components formed during cellulose decomposition whereas lignin decomposition was associated with the release of carbon monoxide and methane (CH_4, m/z 16). Char graphitization leads to the formation of hydrogen (H_2, m/z 2) and additional CO. Both CO and ethene (C_2H_4) have molar masses of 28.

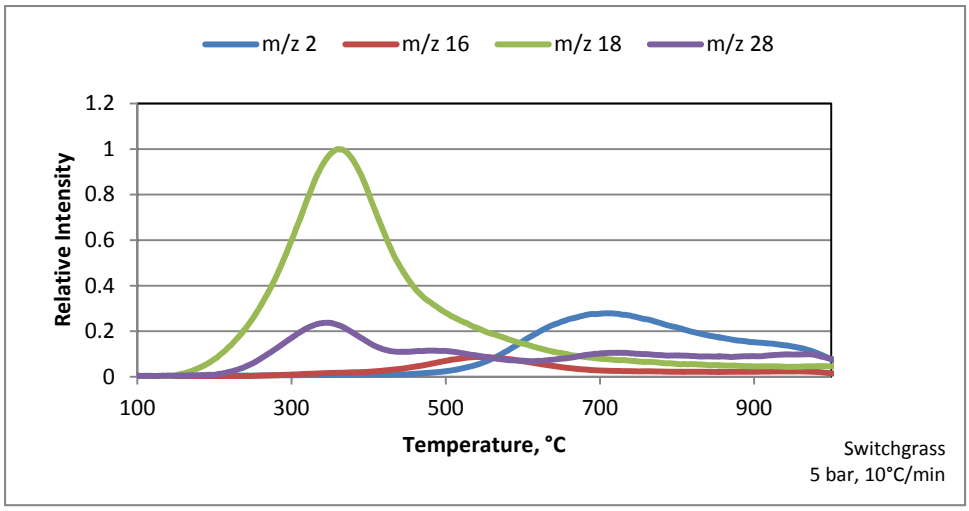

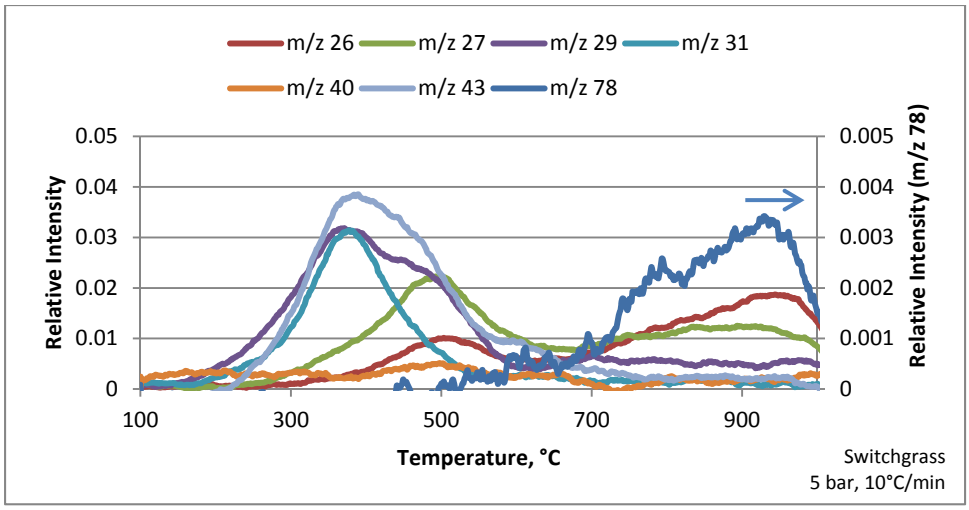

Figure 4. Devolatilization of switchgrass. Pressure 5 bar, heating rate 10°C/min, particle size 106-180 µm. Top: mass loss and derivative mass loss; middle: normalized MS intensities of major gas species; bottom: normalized MS intensities of minor gas species.

A comparison to the intensity of m/z 27 (-C_2H_3 fragment) suggested that during cellulose decomposition, the m/z at 28 peak was due almost exclusively to CO whereas during lignin decomposition and char carbonization, CO and C_2H_4 were both evolved. Several minor gas components were identified as well. Cellulose decomposition gave peaks for components with m/z 43, 29, 31, and 32, which likely correspond to the acetyl group (-CH_2CHO), ethyl group, (–C_2H_5), methoxy group (-CH_3O), and methanol (CH_3OH). The decomposition of lignin leads to m/z 27 and 29, likely -C_2H_3 and –C_2H_5. The final char graphitization showed m/z 26 and 27 (likely $C_2H_2$and –C_2H_3). A small amount of benzene (m/z 78) was detected during char carbonization.

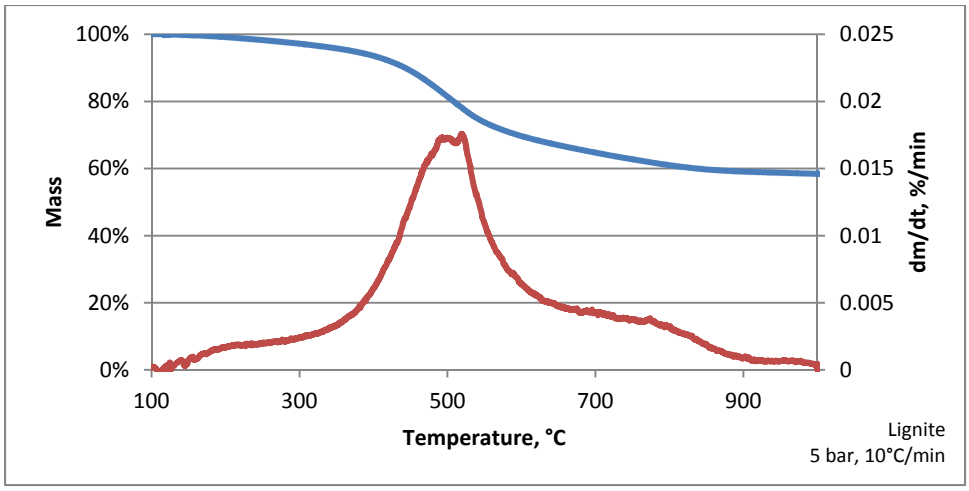
100%
80%
60%
40%
20%
0%
Mass
0.025
0.02
0.015
0.01
0.005
0
dm/dt, %/min
100
300
500
700
900
Temperature, °C
Lignite
5 bar, 10°C/min

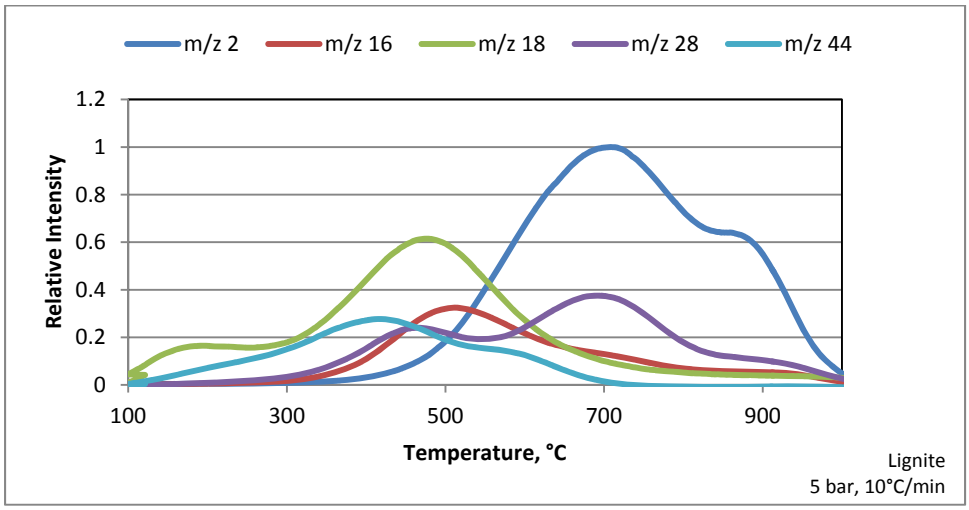
m/z 2
m/z 16
m/z 18
m/z 28
m/z 44
1.2
1
0.8
0.6
0.4
0.2
0
Relative Intensity
100
300
500
700
900
Temperature, °C
Lignite
5 bar, 10°C/min

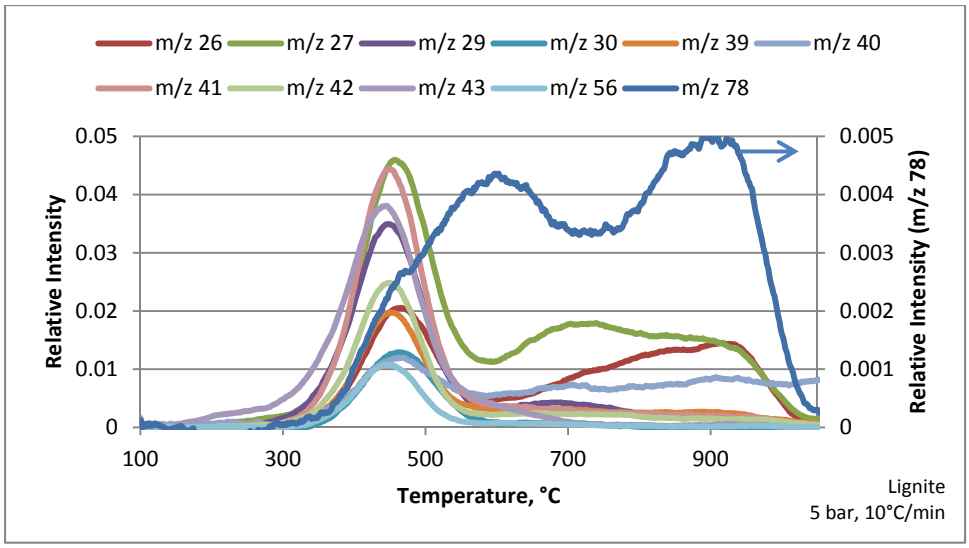

Figure 5. Devolatilization of lignite. Pressure 5 bar, heating rate 10°C/min, particle size 106-180 µm. Top graph: mass and derivative of mass; middle graph: normalized MS intensities of major gas species, and bottom: normalized MS intensities for minor gas species.

Lignite gave a higher char yield (58% vs. 35%) than switchgrass did, consistent with the higher volatile content of biomasses than coals. The peak devolatilization rate occurred at a higher temperature than for switchgrass and the peak was wider. Consequently, the peak devolatilization rate was lower than for switchgrass. A minor second peak, also attributed to char carbonization, occurred around 800°C. The highest MS signal intensity was for H_2 during char carbonization. The oxygen content of lignite is much lower than that of switchgrass, and consequently the intensities of oxygenated compounds are lower than for switchgrass. H_2O, CO_2, and CO/C_2H_2 were released during the main devolatilization peak and CO during char carbonization. Several minor peaks were detected during devolatilization (m/z 26, 27, 29, 30, 39, 40, 41, 42, 43, and 50, likely hydrocarbons and their fragments), and m/z 26 and 27 (likely C_2H_2, $-C_2H_3$) during char carbonization. The compounds detected during char carbonization were similar to those during switchgrass char carbonization, suggesting similar reactions during this stage for the two materials. During the main devolatilization phase, however, there were differences (e.g. peaks at different temperatures corresponding to the decomposition of different biopolymers for switchgrass but not for lignite, and no methanol during lignite decomposition). The evolution of benzene was different: one peak for switchgrass corresponding to char carbonization but evolution during a wider temperature range with two peaks for lignite.

Mixtures of lignite and switchgrass in mass ratios of 90:10, 70:30, and 50:50 were pyrolyzed at 5 bar and 30 bar. The mass losses for the mixtures were identical to the linear combinations of the pure materials as shown in below figure. Thus the materials pyrolyzed independently of each

other as would also be expected. The mass losses were not either affected by the pyrolysis pressure.

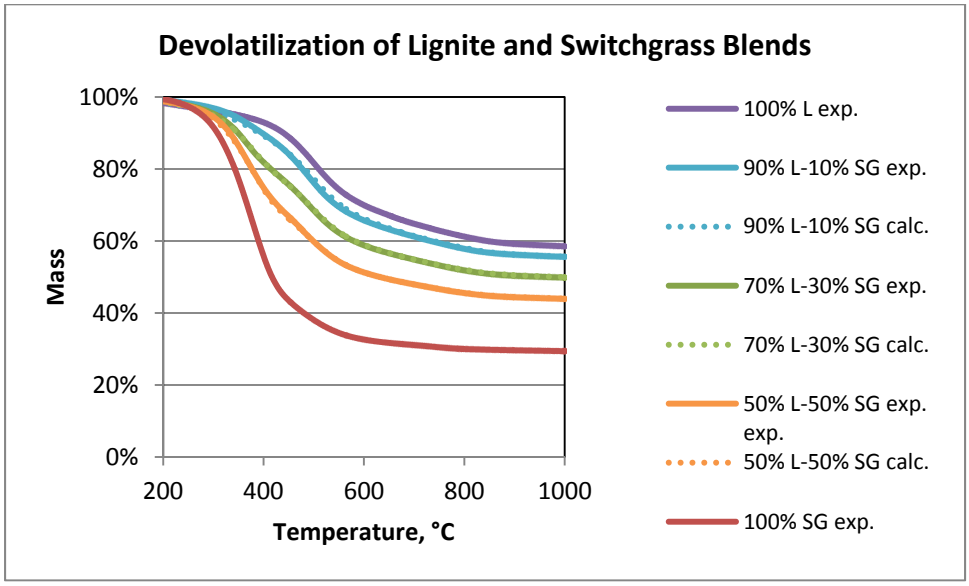

Figure 6. Mass loss during devolatilization of mixtures of lignite (L) and switchgrass (SG); exp. = experimental values, calc. = calculated linear combinations of the starting materials. Pressure 5 bar, heating rate 10°C/min.

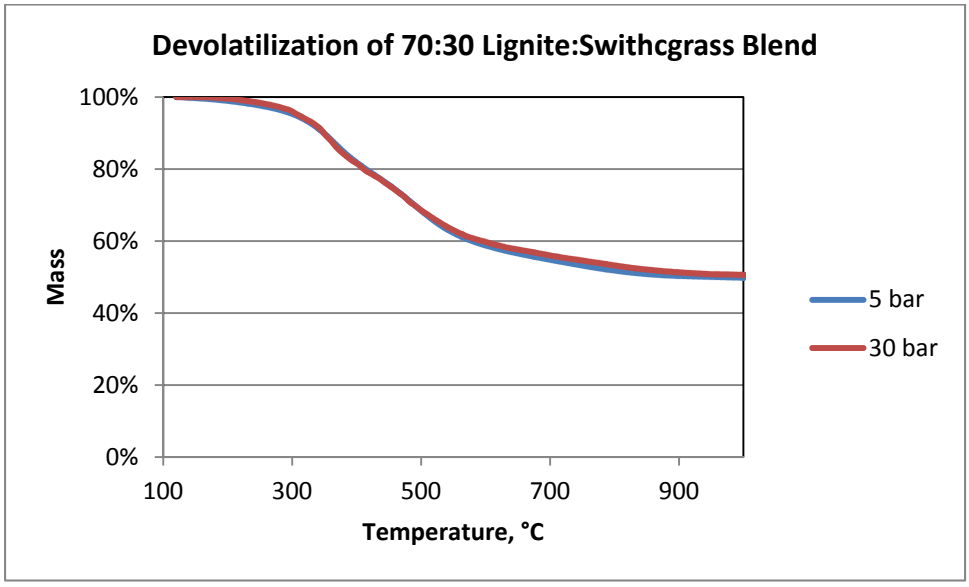

Figure 7. Mass loss during devolatilization of 70% lignite and 30% switchgrass at 5 bar and 30 bar. Heating rate 10°C/min.

Task 6.0 Characterization of Chars Generated from PEFR

The chars were characterized using a number of techniques: (i) morphology using SEM images, (ii) crystallinity using XRD, (iii) surface areas as measured using N_2 physisoprtion (BET) at 77 K and CO_2 physisorption at 273 K, (iv) H/C and O/C ratios from C,H,N,O analysis, and (v) ICP analyses for inorganics present in the char. The first four of these characterizations will be discussed below and how these are affected by the pyrolysis variables: pressure, temperature, and residence time. The ICP results (inorganics analyses) would be relevant to char gasification reactivity, to be discussed in a later section.

Effect on Char Morphology: Char morphology is affected by all three variables- pressure, temperature, and residence time. SEM results show that the char obtained from pyrolysis at the 600_5_4s possesses morphological features similar to untreated biomass. The char at 15 s appears to be slightly molten, with a hint of swelling. The shape of char is transformed significantly at a residence time of 28 s: the char has a highly swollen oblong shape with a nearly complete molten surface.

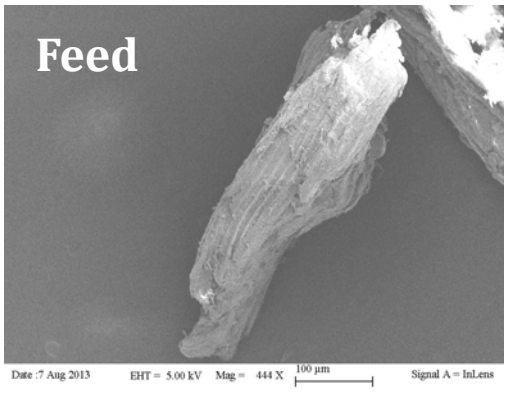

(A)

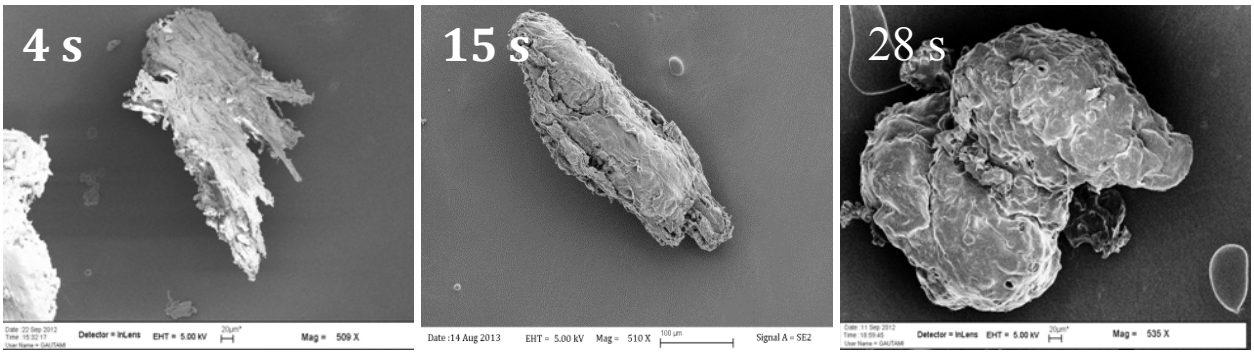

(B)

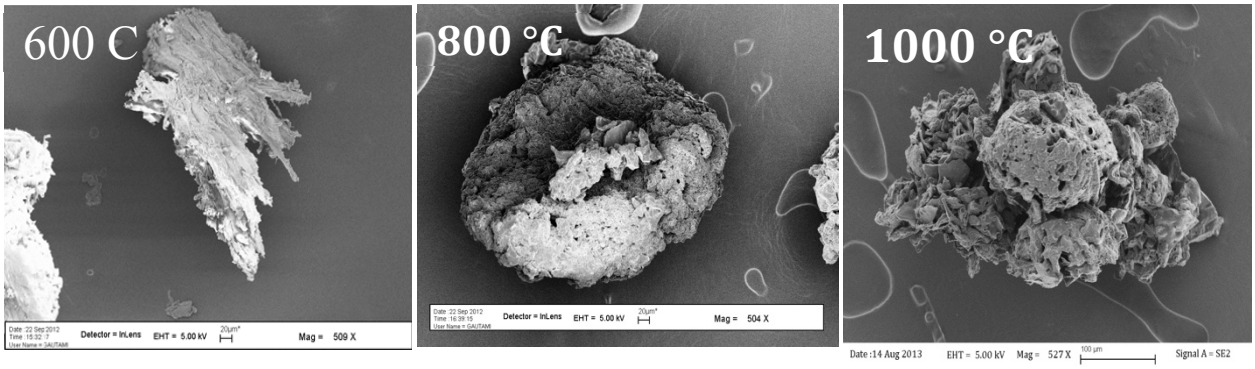

(C)

(D)

Figure 8. SEM Images of A. Untreated biomass (180-250 µm); B. Effect of Residence Time at 600 °C, 5 bar; C. Effect of Temperature at 5 bar RT= 4 s; D. Effect of Pressure at 600 °C

Above figures 8C show the effect of temperature at short residence time (4 s) and pyrolysis pressure of 5 bar. As temperature is increased beyond 600 ^{o}C, the biomass particle is seen becoming more molten and has a higher degree of swelling. At 1000 °C the molten particles tend to agglomerate and stick together. This effect also extends to longer residence times, where the char at 1000 °C appears to be a fusion of two char particles. Figure 8D above shows char morphology obtained at 600 ^{o}C, larger residence time (28 s), with varying pyrolysis pressure. As pyrolysis pressure is increased from 5 bar to 15 bar, the char particles become more rounded, sphere-like and have distinct bubbles on the surface.

These morphological changes can be best explained if we consider two events taking place simultaneously: (i) the biomass particles approach their surroundings temperature at a very high heating rate (~ 10^3 ^{o}C/s) in an entrained flow reactor and assume liquid-like properties, and

(ii) cellulose, hemicellulose, and lignin decompose releasing gases (e.g., CO, CO_2, H_2O, CH_4, and H_2). Some gases might be secondary decomposition products from the primary tars or other volatiles. These gases are trapped inside the molten biomass particle and try to escape even as more gases are formed from the decomposition reactions. Increase in reactor temperature increases the amount of gases released. This creates a balloon-like effect and results in the particles becoming swollen. If gases are allowed to be trapped for sufficient duration which could be both due to residence time or reactor pressure, the swollen particle is likely to assume a spherical morphology. Pyrolysis pressure directly impacts on the char morphology, since pressure differential (between inside and outside the particle) acts as a driving force for the trapped gases to escape. At low external pressure, the volatiles released attempt to escape through the char particle surface expanding it in the process. The extent of swelling decreases as the external pressure increases. Increase in external pressure makes it difficult for the volatiles to escape from the char surface causing a build-up of overpressure inside the particle. The surface of the char stretches like an elastic film (partially visible on the 15 bar char) when gas is trapped inside the char. Inside this elastic film are gas-filled pockets as shown in the below figure 9.

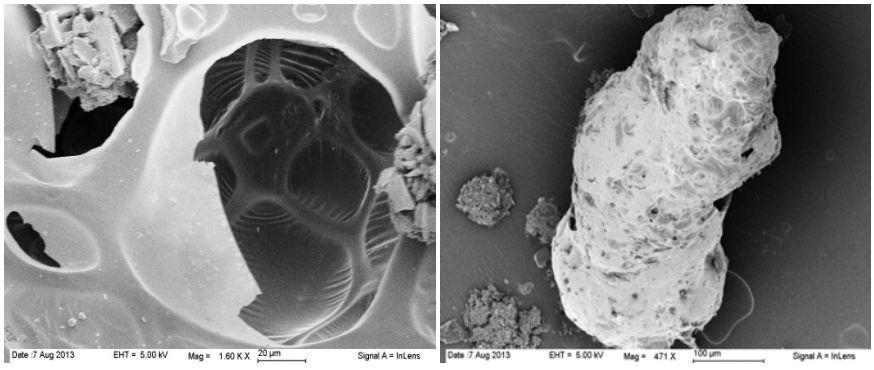

Figure 9. Inside the gas filled pockets of 600_20; B. The elongated, smooth texture of 1000_10 char

The effect of pressure on swelling is not as dramatic in chars at 800 °C and 1000 °C. The swelling increases from 5 to 10 bar, and negligible differences in morphology are observed at higher pressures. Furthermore, higher pyrolysis pressure leads to lower driving force and gases are trapped for longer time within the particle, leading to increased secondary pyrolysis reactions and an increasingly altered gas composition and tar species.

Evolution of morphology in set-ups like TGA/PTGA, where the particle heating rate ranges at ~ 1 ^{o}C/s is very different from high heating rate set-ups like the entrained flow reactor(or drop tube furnaces). As the biomass particles are heated at slow heating rates, decomposition of hemicelluloses and cellulose begins (~ 250-300 ^{o}C) well before the biomass components reach a

softening temperature (~ 600 ^{o}C). By the time particle reaches 600 ^{o}C, the particle has lost ~ 70% of its starting mass. It no longer is a biomass containing hemicelluloses and cellulose. Therefore, even as biomass is losing upto 80% of its starting mass, the final char product is a skeleton of its starting material, with little or no change in morphology. On the other hand, in an entrained flow reactor, decomposition of cellulose and hemicellulose occurs at the same time as the char starts melting. Hence the volatile release leads to the development of highly spherical chars, different in appearance from the starting biomass.

Texas lignite particles (90-106 µm) were pyrolyzed at 800 ^{o}C and 1000 ^{o}C at 5 bar. The below SEM images show the morphology of the starting material and a few pyrolyzed samples. There is no evidence of particle swelling or becoming spherical as has been observed with switchgrass feed. This is not surprising because unlike biomass, lignite and other coals have low volatiles content. In addition, it is the cellulosic and hemi-cellulosic content of the biomass that becomes fluid-like at elevated temperatures resulting in the formation of nearly spherical particles. On the other hand, coal particles do not become fluid-like.

Texas Lignite (feed material)

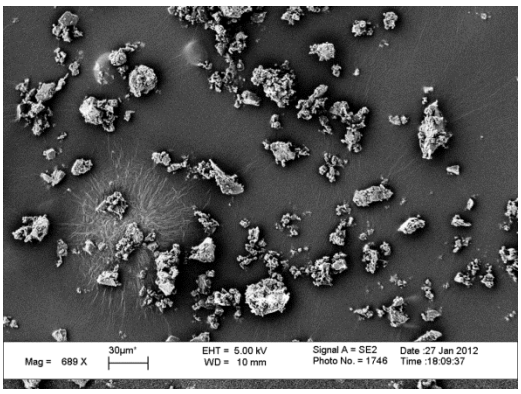

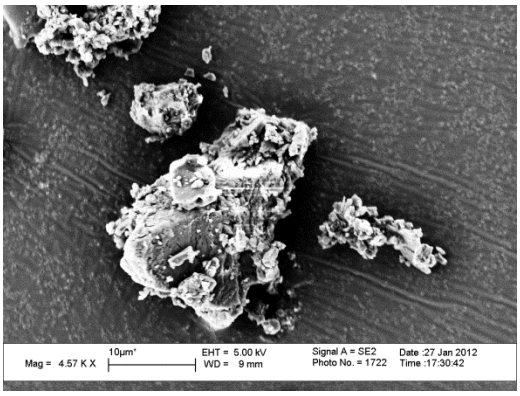

Texas Lignite (Pyrolysis Conditions: 5 bar, 800 ^{o}C)

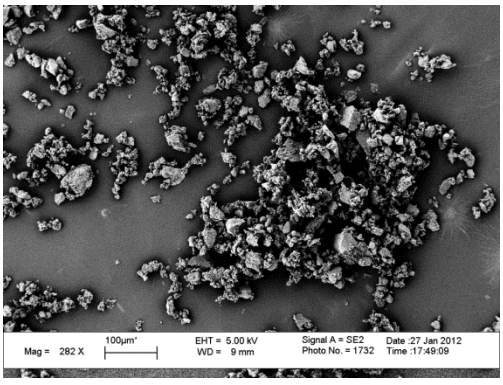

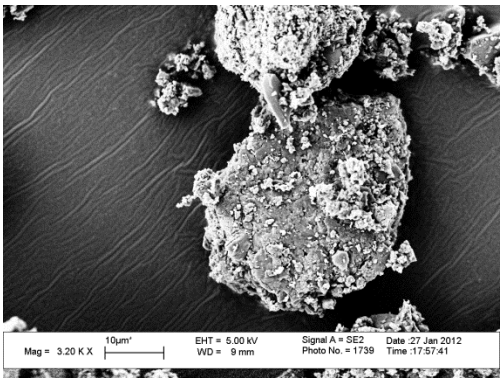

Texas Lignite (Pyrolysis Conditions: 5 bar, 1000 ^{o}C)

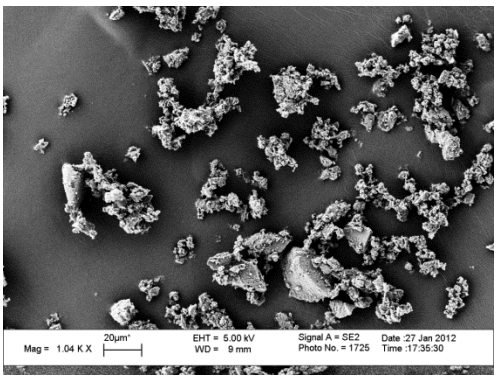

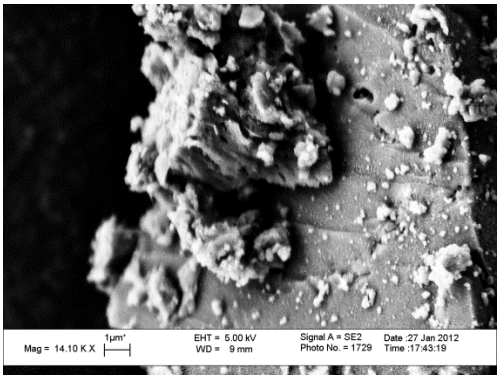

Char Surface Area Measurements

Briefly, chars have surface area that can be up to two orders of magnitude higher (more than a factor of 100) as compared to the starting biomass material. The effect of pressure results in a slight reduction in the char BET surface area. In our earlier studies on another project, we have seen pine char surface area increase by an order of magnitude. The basic question needs to be answered is whether this increased char surface area results in a proportional increase in the char gasification activity.

The numbers in the below table were all obtained using N_2 physisorption, at liquid nitrogen temperature. There are only a few inferences in the literature about other biomass species that support these observations. The question, whether we should be concerned about the pore diffusion effects as chars become more porous, would be of interest in char gasification step. We wanted to determine pore size distribution for the chars. It was not possible to get that information for pores smaller than 1.5 nm using N_2 physisorption. Literature suggested the difficulty in measuring pore size distribution for nano-size pores at liquid nitrogen temperatures (kinetics of nitrogen diffusion in nano-pores is very slow). Instead CO_2 adsorption at 0 ^{o}C has been suggested for carbonaceous materials. Therefore we attempted to use this method for surface area determination. The results are summarized in the below table.

BET Surface Area of Switchgrass Chars generated at various conditions

(reference: switchgrass starting material BET area 0.8 m^2/gm)

	600 ^{o}C	**800 ^{o}C**	**1000 ^{o}C**
1 bar	1.8 m^2/gm	2.9 m^2/gm	75 m^2/gm
5 bars	3.0 m^2/gm	187 m^2/gm	321 m^2/gm

10 bars	3.3 m^2/gm	175 m^2/gm	278 m^2/gm
15 bars	5.2 m^2/gm	108 m^2/gm	198 m^2/gm

Surface area of switchgrass chars measured by CO_2 adsorption

(reference: switchgrass starting material BET area 0.8 m^2/gm)

	Surface area (m^2g^{-1})
Char SWG_1000C_5bar	235
Char SWG_800C_5bar	283
Char SWG_600C_5bar	274
Char SWG_1000C_10bar	299
Char SWG_800C_10bar	246

Pore Volumes of Switchgrass Chars generated at various conditions

	600 ^oC	**800 ^oC**	**1000 ^oC**
1 bar	0.0048 cm^3/gm	0.0085 cm^3/gm	0.0584 cm^3/gm
5 bars	0.0071 cm^3/gm	0.1145 cm^3/gm	0.2039 cm^3/gm
10 bars	0.0123 cm^3/gm	0.1084 cm^3/gm	0.2003 cm^3/gm
15 bars	0.0146 cm^3/gm	0.0711 cm^3/gm	0.1339 cm^3/gm

BET Surface Area of Texas Lignite Chars generated at various conditions

(reference: Texas Lignite starting material BET area m^2/gm)

	600 ^oC	**800 ^oC**	**1000 ^oC**
5 bars	84 m^2/gm	99 m^2/gm	25 m^2/gm
10 bars	73 m^2/gm	94 m^2/gm	207 m^2/gm
15 bars	5 m^2/gm	156 m^2/gm	178 m^2/gm

Pore Volumes of Texas Lignite Chars generated at various conditions

	600 ^{o}C	800 ^{o}C	1000 ^{o}C
5 bars	0.087 cm^3/gm	0.0912 cm^3/gm	0.0426 cm^3/gm
10 bars	0.0735 cm^3/gm	0.0718 cm^3/gm	0.1555 cm^3/gm
15 bars	0.0270 cm^3/gm	0.1115 cm^3/gm	0.1361 cm^3/gm

The morphological changes in biomass char are caused to a great extent by the melting and swelling of the pyrolyzing biomass, as well as by the escape of volatiles. These are much less dramatic in Texas Lignite chars.

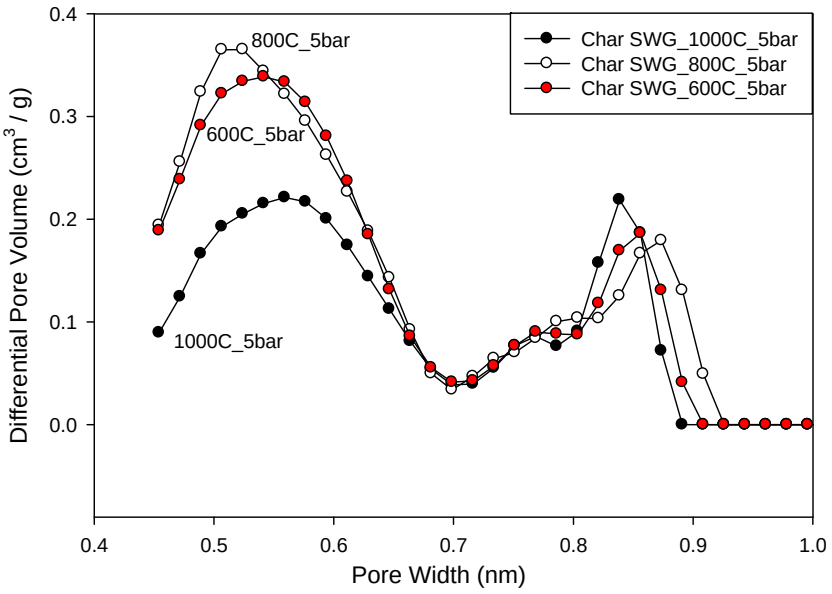

Figure 10. Pore-size distribution for switchgrass chars obtained from CO_2 adsorption at 0 ^{o}C. The chars were obtained at 5 bar pyrolysis at different temperatures.

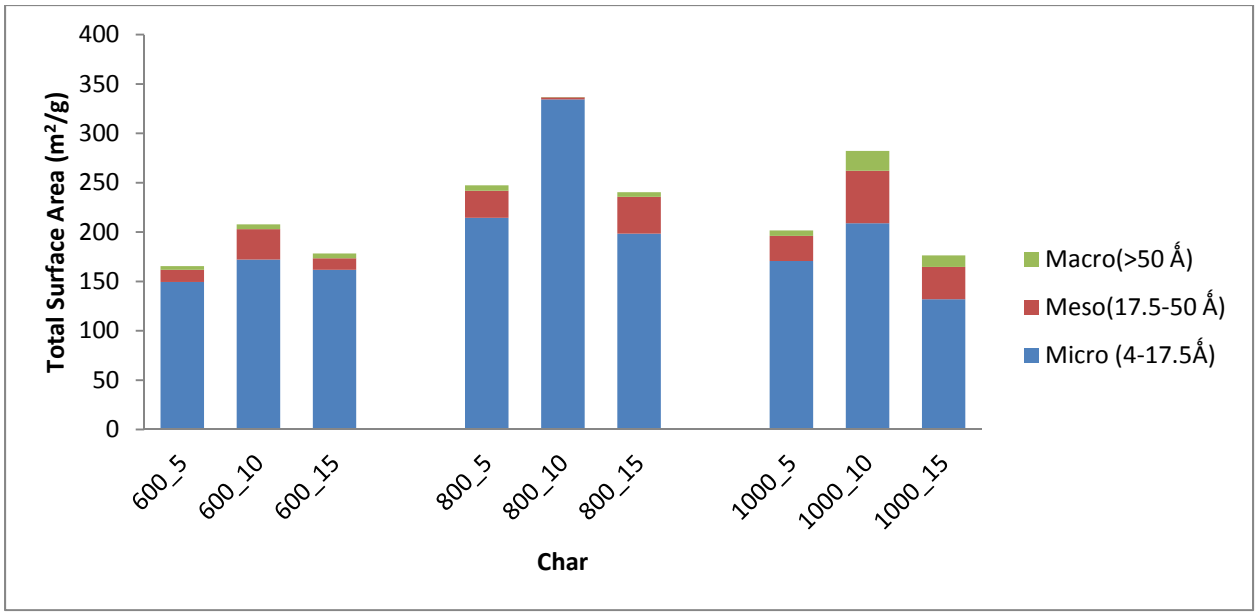

Figure 11. Total surface area of switchgrass chars generated at different pressures and temperatures.

Above figure 11 shows the total surface area of various switchgrass chars as well as the distribution of total area into micro-pores, meso pores, and macro-pores. Micro-pore contribution is calculated using DFT model, while BJH is used for both meso and macro pores. Total surface area is calculated using DFT. Regardless of the pyrolysis conditions, micro-pores are the dominant region where gasification occurs. Thus one should be mindful of the diffusion effects during gasification. Below figure 12 shows the micro-pore size distribution for one of the SG chars obtained from DFT model using the CO_2 adsorption data. Micropores below 1 nm are dominant in the chars formed during the SG pyrolysis.

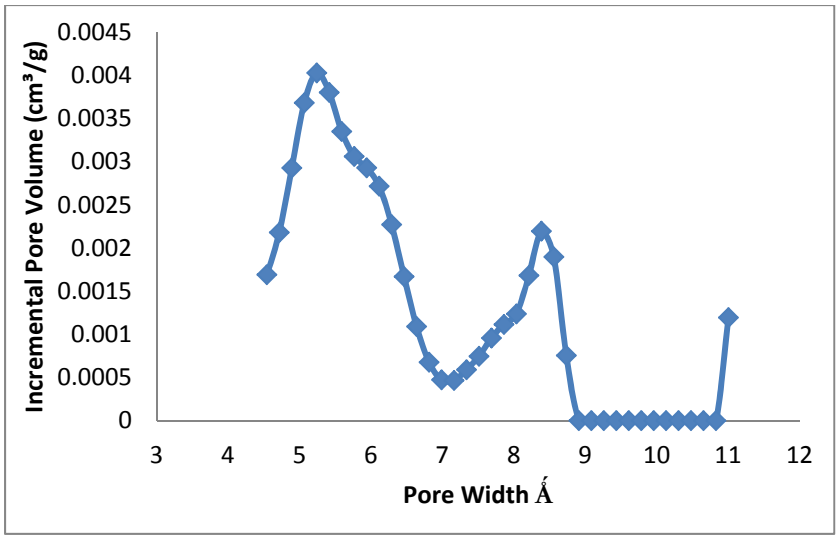

Figure 12. Micro-pores size distribution in a switchgrass char generated at high pressure and temperature in an entrained flow reactor

Below figures 13 and 14 show the H/C ratios for SG chars generated at different pyrolysis conditions.

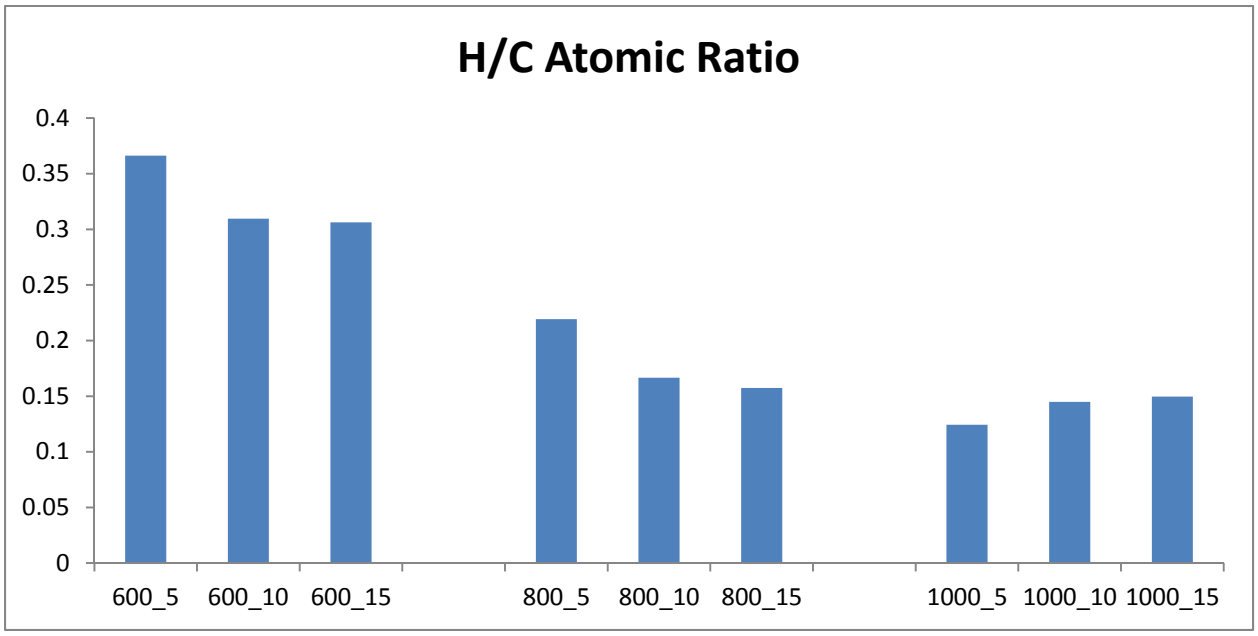

Figure 13. H/C atomic ratios for SG chars generated at different pyrolysis conditions

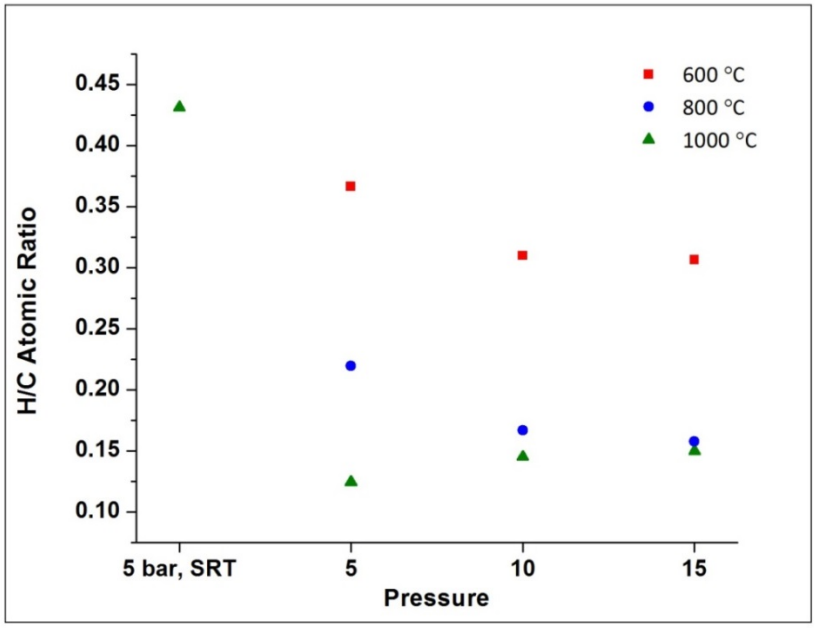

Figure 14. H/C atomic ratios for SG chars generated at different pyrolysis conditions

As seen in the above two figures, the effect of temperature is far more dramatic on the H/C ratio; pressure does not seem to have much of an effect on this ratio. The data shown in the above figure represent chars generated by pyrolyzing switchgrass for 28 sec at different pressures and temperatures. The exception is single point on the extreme left in the plot of the above figure- this green triangle represents the 1000 ^{o}C pyrolysis carried out for short residence time (4 sec). The H/C ratio for this char is 0.43, much higher than the range of 0.12-0.14 observed for other 1000 ^{o}C chars. This has important implication for the higher gasification reactivity of short time chars, as we will observe in the next section on graphitic chars.

C, H, N, O Analysis of Switchgrass Chars

Nine (9) different switchgrass chars were generated at three different pressures and three temperatures. The char samples were analyzed for C, H, N, and O. The results are shown below:

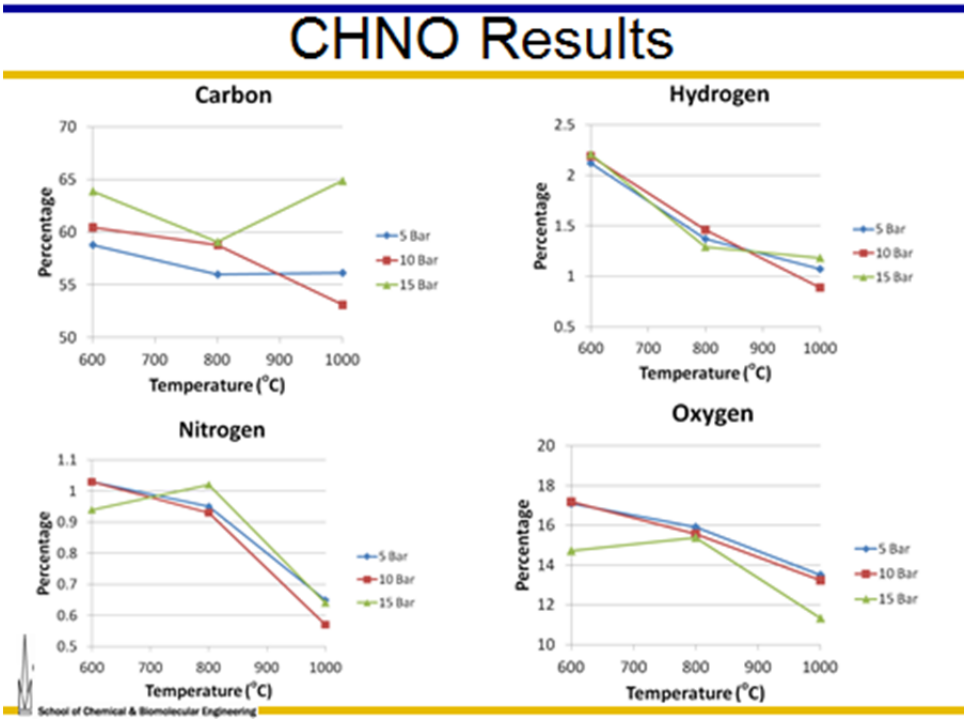

The effect of temperature appears to be more significant on H, N, and O content of the char, than the effect of pressure. As temperature is increased, all three decrease.

Formation of Graphitic Chars during pyrolysis

Our results on char gasification reactivity show the presence of heterogeneity in char gasification reactivity. It has been well established, at least qualitatively, that amorphous or active carbon can transform itself to graphitic form of carbon which has much lower reactivity towards gasification, oxidation etc. A char sample was held at 800 ^{o}C for 10 min before starting gasification at 800 ^{o}C in 100% CO_2. The reactivity profile is shown in the below figure. This char was active till nearly 30% conversion, before losing its gasification activity. The same char, in another experiment, was held at 1200 ^{o}C for 10 min. It lost most of its gasification reactivity during this 10 min holding period at 1200 ^{o}C. These transformations to graphitic chars are irreversible, and efforts must therefore be made to understand the role of process variables in such transformations. Our data indicate that pyrolysis pressure, temperature, and holding period are the key variables, and are in general agreement with the published literature.

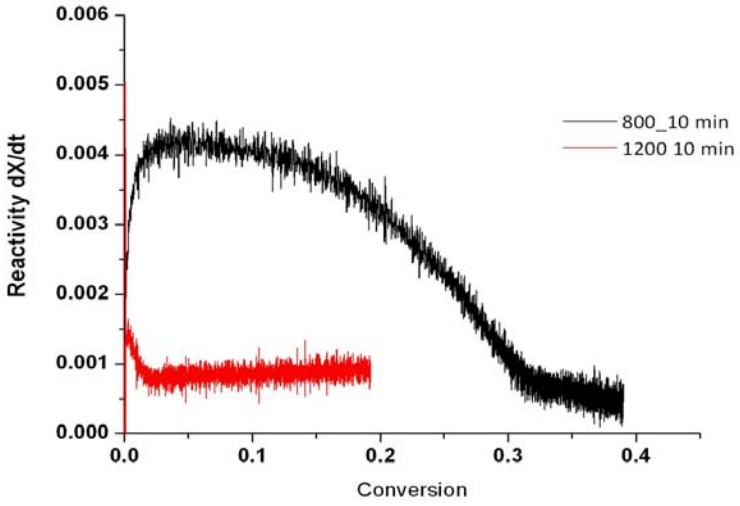

Figure 15. Effect of holding temperature on char gasification reactivity at 800 ^{o}C in 100% CO_2. The char sample was held isothermally at 800 ^{o}C, or 1200 ^{o}C for 10 min before starting the gasification.

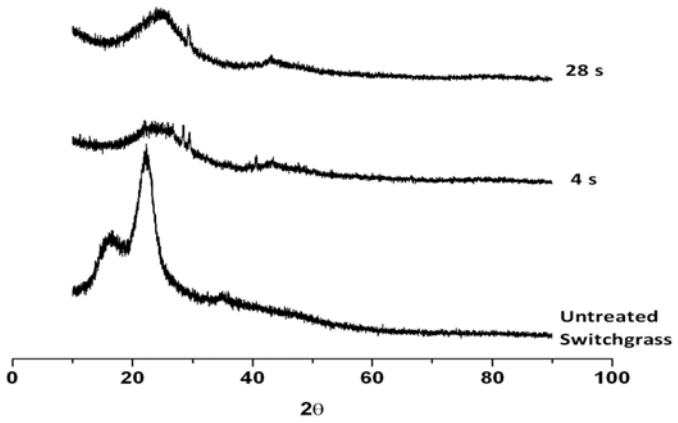

Figure 16. Effect of residence time during switchgrass pyrolysis on the formation of graphitic char in an entrained flow reactor (1000 ^{o}C, 5 bars).

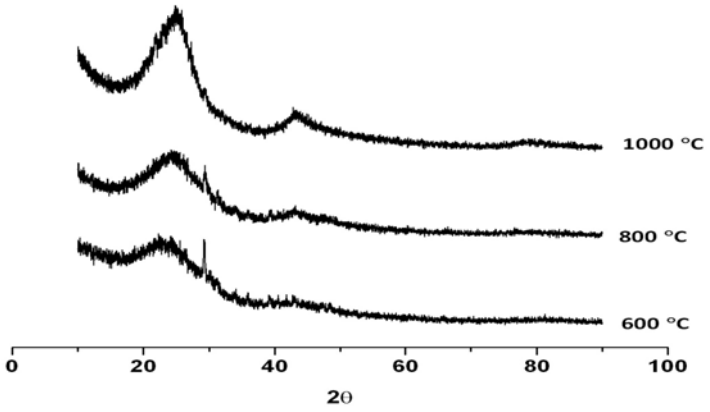

Figure 17. Effect of switchgrass pyrolysis temperature on the formation of graphitic char in an entrained flow reactor (P 15 bars, residence time 28 sec).

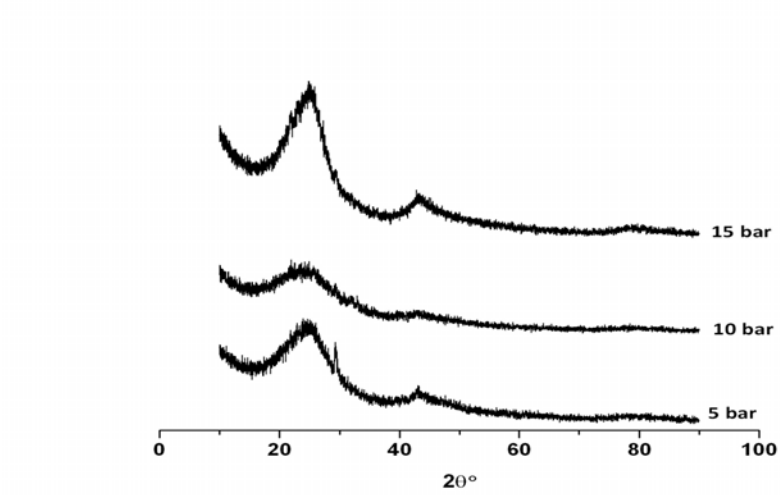

Figure 18. Effect of switchgrass pyrolysis pressure on the formation of graphitic char in an entrained flow reactor (1000 ^{o}C, residence time 28 sec).

The above three figures show the XRD results for switchgrass chars generated at different temperatures, pressures, and residence time. First figure shows the XRD of swicthgrass feedstock, and a sharp peak at ~ 24^o is characteristic of cellulose (the only crystalline material in the biomass). After pyrolysis at 1000 ^oC and 5 bars for 4 sec, the cellulose peak disappears, but instead a small broad peak at ~ 24^o attributed to graphitic carbon is quite visible. Pyrolysis for 28 sec results in a sharper peak at 24^o, and a small peak at 44^o also appears. Both these peaks correspond to different facets of graphitic carbon.

Figure 17 above shows the effect of temperature on the XRD chars generated at 5 bars and a residence time of 28 sec. The severity of graphitic carbon increases with increasing temperature. The third and final figure shows the effect of pressure on graphitic carbon structure formation. The behavior is a bit more complex here. As pressure is increased from 5 bars to 10 bars, less graphitic char is seen. When the pressure is increased to 15 bars, the trend reverses to the expected behavior. This observation, first thought to be an anomaly, has been verified multiple times and appears consistent with the char reactivity data as well as certain other metrics (H/C and O/C ratios in the char). Our results lead us to believe that there are two primary sources of graphitic char: (i) lignin, and (ii) oligomerization reactions occurring within the biomass particle where pyrolysis gaseous products such as ethylene and propylene are trapped due to higher pressure and undergo secondary reactions. Kinetic effects can be primarily due to the temperature and residence time, but the effect of pressure is more directly related to this trapping. Similar behavior is observed for other biomass species (i.e., pine and sugarcane bagasse).

A more quantitative approach to understanding the various grapheme-like structures is Raman spectroscopy. The technique is well established and has been documented in the literature for transformation of amorphous carbon structures to grapheme-like structures. Attempts are made to fit the observed spectra with 3-, 5-, 7-, and 10-peak model (1-4). The real utility of Raman spectroscopy is not to fit the data in a quantitative sense, but to use one of these several models for comparison purposes. We have used the 5-peak model to understand the effect of pyrolysis variables on the formation of these structures. The table below offers an interpretation of the various bands observed. The relative intensity values can be used to decipher the transformations and relate these to other parameters.

In summary, the highest temperature and intermediate pressure char possess the characteristics least suited for gasification. As we shall show in the next sections, the variations in the above properties have a significant impact on the reactivity of chars during gasification.

Table. Raman spectroscopy on chars – peak assignments for a 5 peak model

Band Name	Shape	Location*	Description	Other Comments
D_4	Lorentzian	1150-1200 cm^{-1}	Very poorly ordered materials [3] (sp^2 and sp^3 hybridized carbon bonds, C–C and C=C stretching vibrations of polyenes, etc.)	
D_1	Lorentzian	1350 cm^{-1}	Defect band in graphite, C-C between aromatic rings and aromatics with ≥ 6 rings [4]	
D_3	Gaussian	1500-1530 cm^{-1}	Small aromatic systems (3-5 rings) and amorphous carbon [3]	
G	Lorentzian	1580 cm^{-1}	Graphite E^2_{2g} stretching, aromatic ring quadrant breathing	
D_2	Lorentzian	1620 cm^{-1}	Lattice vibration involving graphene layers [3]	

*For a laser excitation wavelength of 488-514 nm

[1] Sadezky et al., (2005). *Carbon*, *43*(8), 1731-1742.
[2] Sheng, C. (2007). *Fuel*, *86*(15), 2316-2324.
[3] Wang et al., (2012). *Energy & Fuels*, *26*(3), 1565-1574.
[4] Li et al., (2006). *Fuel*, *85*(12), 1700-1707.

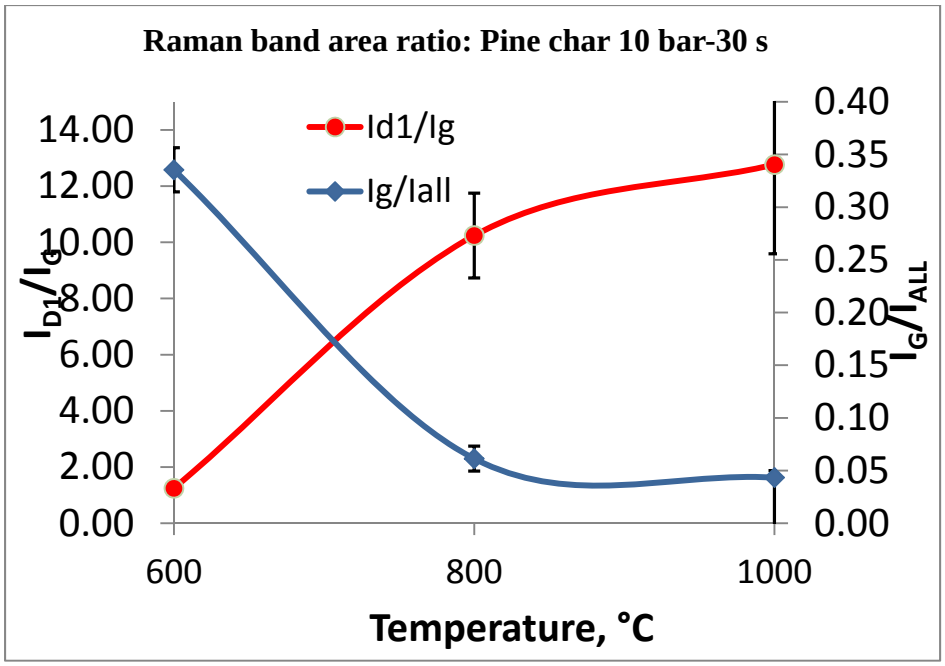

Figure 19. Effect of pyrolysis temperature on the evolution of Raman bands

D_3 = 3-5 Aromatic ring, amorphous carbon
D_1 = Medium rings (≥6)
G = Graphitic (large # rings)

With increase in temperature, Id1/Ig increases, which means, more medium sized aromatic rings are formed. The below figure shows that as this ratio increases, the char reactivity decreases.

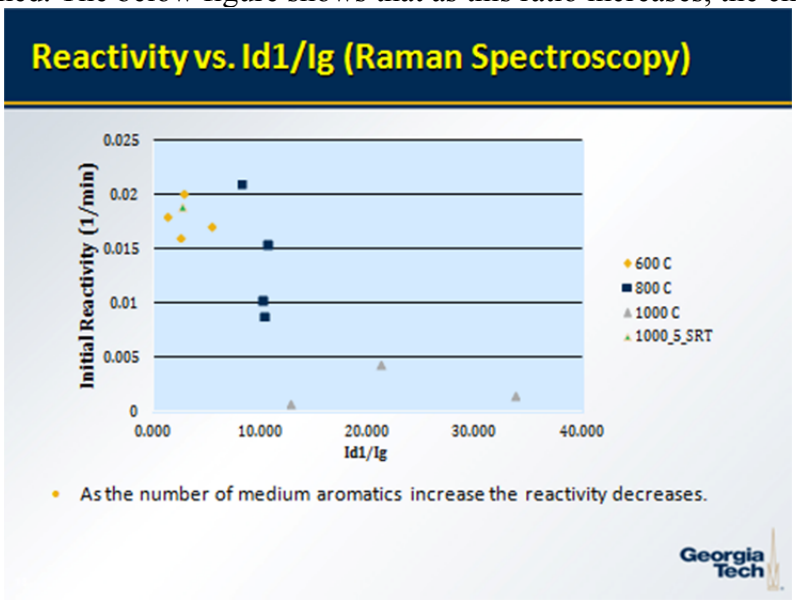

Figure 20. Initial gasification reactivity vs Raman Band ratio Id1/Ig

Task 7.0 Kinetic Models of Coal/Biomass Blends Pyrolysis

This task was included in the original plans of the proposal. However, no synergy was observed during the PTGA pyrolysis runs blends of switchgrass and T. lignite coal. Moreover, the limiting factor appeared to be the gasification step. Thus no efforts were undertaken to develop a kinetic models for pyrolysis. Such efforts have been useful in describing low temperature pyrolysis where the goal is to produce bio-oils. One likes to develop kinetic models to show the impact of operating parameters on the formation of certain bio-oil species. However, that approach would appear to be a waste of time. The most important take-away from our pyrolysis work is that although a fast step, pyrolysis conditions dictate the reactivity of the chars generated during pyrolysis.

Task 8.0 TGA / PTGA Gasification of Chars using CO_2

Figure 21 shows the results obtained using nine different chars, obtained by PEFR pyrolysis at three different temperatures and three different pyrolysis pressures (5, 10, and 15 bars). All

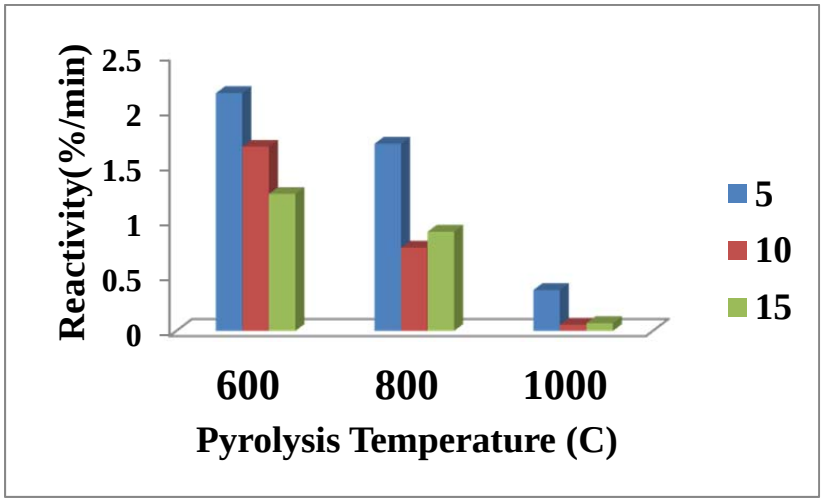

Figure 21. TGA results for initial char gasification activity in pure CO_2 at 800 ^oC and 1 atm. The chars were generated via pyrolysis in PEFR at three different pressures: 5 bars, 10 bars, and 15 bars and three different temperatures.

gasification runs were carried out at 800 ^oC and 100% CO_2. Initial char reactivity (5-10% conversion) decreases with increasing pyrolysis temperatures. In addition, the char gasification activity decreases with increasing pyrolysis pressure. We are focusing on the initial rate because this char is already well characterized. After a fraction of the char has been gasified, its porosity,

surface area, active site density are likely to be different than the starting char. As the below figure shows transient activity profile, it is clear that the chars generated at highest temperature (1000 ^{o}C) have the lowest gasification activity, whereas the chars generated at the lowest temperature (600 C) have the highest activity. The only exception is the dark blue line which shows the char produced at short residence time (4 sec) at 1000 ^{o}C and 5 bars. All other chars were produced at a residence time of 30 sec. The char gasification reactivity can be affected by several parameters: (i) char surface area, (ii) char active site density or catalytic content (e.g., inorganics), (iii) intrinsic char reactivity. This last point corresponds to the difference between and active char (amorphous char) and inactive char (graphitic char).

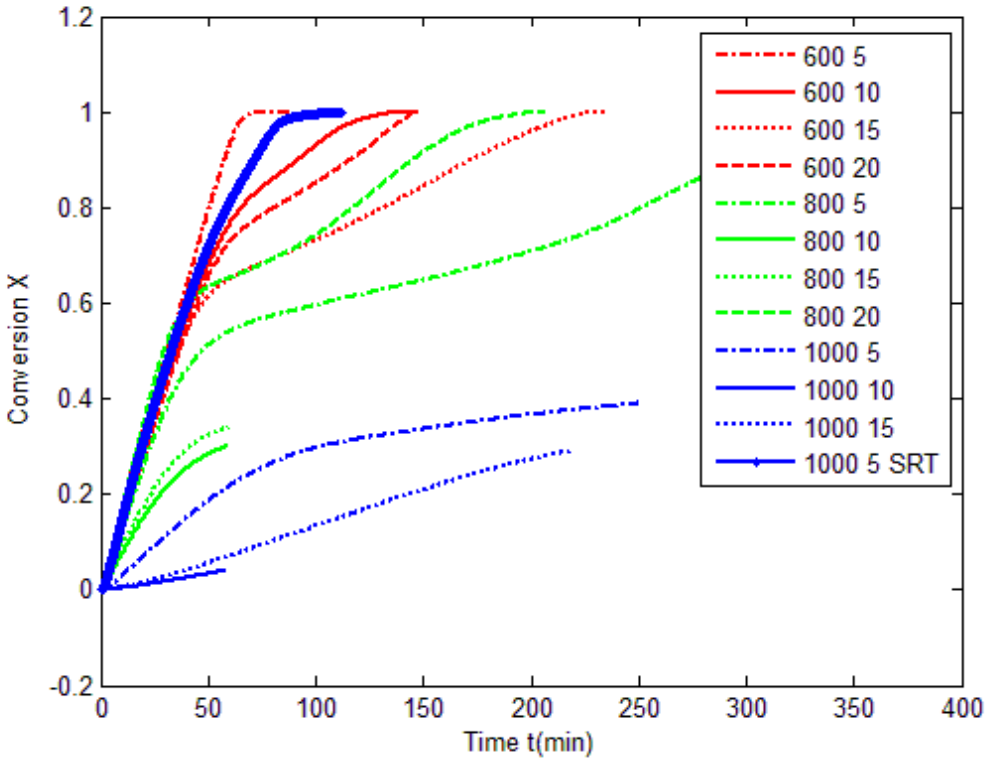

Figure 22. Effect of char pyrolysis pressure, temperature, and pyrolysis residence time on gasification activity in 100% CO_2 at 800 ^{o}C.

The below figure shows the switchgrass char reactivity profile over the entire conversion range. There are two main observations from: (i) chars generated at lower temperatures (e.g., 600 ^{o}C) are more reactive than the chars generated at higher temperatures, and (ii) chars generated at 600 ^{o}C retain their higher activity over the entire range of conversion, whereas the chars generated at 800 ^{o}C lose most of their reactivity at conversions between 60-80% (depending on pyrolysis

pressure). The chars generated at 1000 ^{o}C lose most of their reactivity between 30-50% conversion.

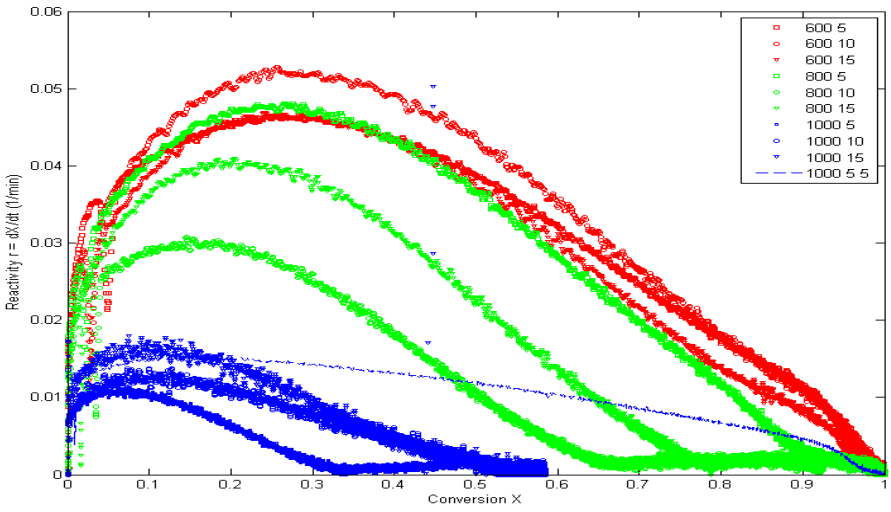

Figure 23. Gasification reactivity of switchgrass chars at 800 ^{o}C in 100% CO_2. The chars were generated via pyrolysis at 600 ^{o}C, 800 ^{o}C, or 1000 ^{o}C (at different pressures).

These results suggest that the char generated during pyrolysis has varying levels of reactivity depending on the pyrolysis temperature and pressure. In general higher temperatures and higher pressures lead to less reactive chars. It is fair to conclude that the transformation of chars from more reactive to less reactive state is a time-dependent process. The plausible variables for the formation of these less reactive chars include pressure, temperature, and residence times.

Texas Lignite char vs Switchgrass Char Gasification

Figures 24 and 25 below compare the intrinsic activity of lignite and switchgrass chars, generated through pyrolysis in an entrained flow reactor. In both cases, the gasification activity of Texas lignite char is higher than that for corresponding switchgrass char.

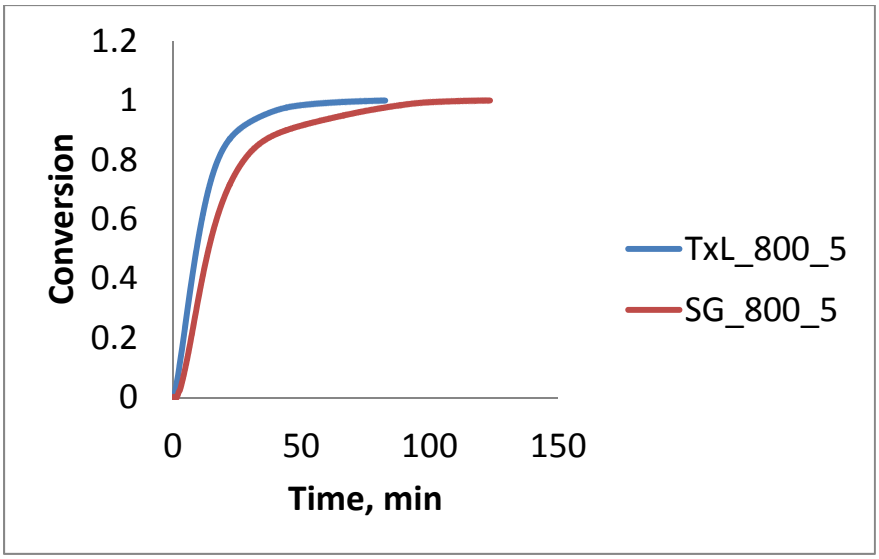

Figure 24. Char gasification profile in 100% CO_2 at 800 ^oC and 1 atm for switchgrass char and Texas lignite char. Both chars were generated through pyrolysis in an entrained flow reactor at 800 ^oC and 5 bars.

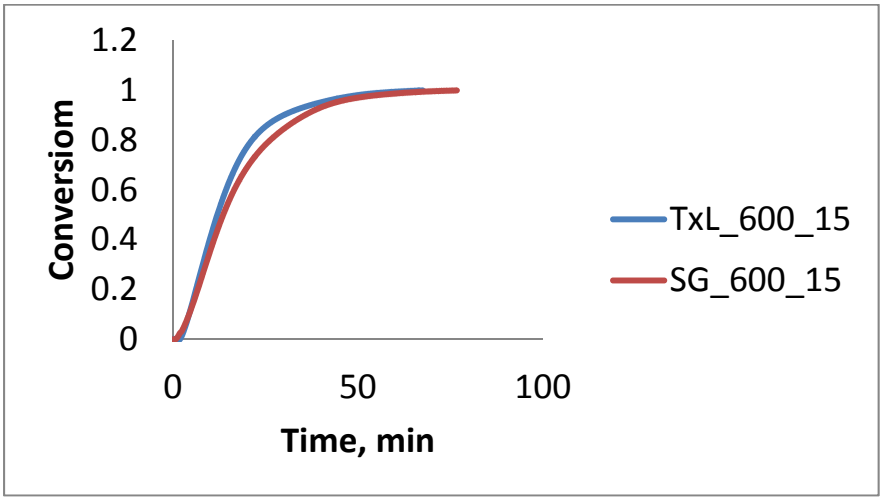

Figure 25. Char gasification profile in 100% CO_2 at 800 ^oC and 1 atm for switchgrass char and Texas lignite char. Both chars were generated through pyrolysis in an entrained flow reactor at 600 ^oC and 15 bars.

The results shown in above figures were obtained in order to establish a baseline behavior of individual components and were not quite what we had anticipated. We had expected the Texas lignite char to be far less active than the switchgrass char. In an effort to understand the reasons for this unusual activity behavior, we considered the compositions of the Texas lignite and the switchgrass, inorganic content and composition, and nature of carbon in the char (amorphous vs graphitic).

Table. Elemental composition of Texas lignite and switchgrass

sample	C	H	N	O by diff.	S	Ash
	wt%	wt%	wt%	wt%	wt%	wt%
Texas Lignite	61.99	4.44	1.17	**18.85**	0.69	**12.86**
Switchgrass	47.59	5.83	0.56	**42.20**	0.08	**3.74**

Table. Inorganic species present in Texas lignite and switchgrass feeds and chars

	Al	**Ca**	**Fe**	**K**	**Mg**	**Si**
TXL feed	10.7	28.2	4.7	**0.4**	5.9	**50.0**
SG Feed	0.1	10.0	0.3	**32.7**	6.8	**50.1**
TxL 800_5	12.7	**20.7**	4.0	**0.0**	5.3	**57.2**
SG 800_5	0.7	**9.8**	0.2	**40.9**	6.0	**42.4**

As seen in the above tables, the ash content of Texas lignite is nearly three times the value for switchgrass. More importantly, the oxygen content of switchgrass is typical of most biomass species and is much higher than that for Texas lignite. This is not surprising since biomass contains sugar polymers in the form of hemi-cellulose and cellulose and aromatic rings (lignin) with many oxygen-containing functional groups. Second table above shows the ICP analysis results. Texas lignite has three major components that are known to catalyze char gasification: Ca, Mg, Fe. Although Si is the major inorganic species, it likely does not play a direct role in char gasification. It is quite likely that it is present in some aluminosilicate compound form. Switchgrass, on the other hand, has three main catalytic species: Ca, K, and Mg. Our previous work has shown potassium to be a very good catalyst for char gasification. Another aspect of K is that it readily spreads over the char surface at elevated temperatures, providing a more effective distribution. In contrast, Ca is known to sinter at elevated temperatures, causing to lose its activity slowly.

Table. Gasification rates for several biomass and coal species[1]

Species	Type	Gasification rate (g/cm^2-s)
Pine	woody biomass	0.0037
Switchgrass	Herbaceous biomass	0.0041
Beulah coal	lignite	0.0065
Lower Wilcox coal	lignite	0.0056
Smith Rowland coal	subbituminous	0.0065
Dietz coal	subbituminous	0.0061

[1]S.P. Huey, K.A. Davis, R.H. Hurt, M.J. Wornat, ACS Chicago meeting preprints (1995)

The results appear to be in agreement with the trends reported in the literature. Above table lists the gasification rates for switchgrass, pine, lignite, and subbituminous coal and the rates appear to fall within the same order of magnitude.

Task 9.0 PTGA Gasification of Chars using Steam

Similar to Task 8.0, this part was done using steam. Similar parameters were utilized. In the later experiments, the gas phase composition will include CO_2, steam, CO, and H_2. Attempts were made in a separate atmospheric pressure experiments (TGA) to examine the effect of CO and H_2 on the intrinsic gasification kinetics (free of mass transport limitations).

It is important to find the conditions at which gasification rates can be measured under transport-free conditions. Char particle size is used primarily to probe the internal mass transport effects at a given temperature, whereas the amount of char in the TGA was used to probe the role of external transport effects. This second variable is even more critical to keep an eye on since we are using 10-20% steam (balance N_2), unlike CO_2 gasification using pure CO_2. Even in pure CO_2, we had found the role of bed depth (char amount) to play a role. The preliminary results using steam pointed to the effect of varying char amount for steam gasification at 800 ^oC. We found that char can be gasified using 10% steam at 750 ^oC without any external transport effects. It should be recalled that a temperature of 800 ^oC was found to be adequate for CO_2 gasification, but pure CO_2 may have permitted us to use higher temperatures, while still avoiding external transport effects.

We, therefore, limited the amount of char to ~ 2 mg. In the results that follow, we will be comparing the char gasification reactivity in steam vs. CO_2 at two different conditions:

CO_2 Gasification: 100% CO_2, 800 ^oC

Steam Gasification: 10% steam, 750 ^oC

The figure 26 below shows the initial gasification reactivity data for steam vs. CO_2 , and a reasonably good correlation between the two activities is seen. It should be noted as well that the

chars generated at 600 °C are much more reactive than those generated at higher temperatures. Similar observation has been made previously for the CO_2 gasification activity. Based on the trend line shown in this figure, one might suggest that CO_2 gasification activity provides a good approximation for steam gasification activity. This implies that the same sites are active for both CO_2 and steam gasification. Thus one may not see much enhancement in gasification activity by having both CO_2 and steam. However, this comparison does not hold over the entire conversion range.

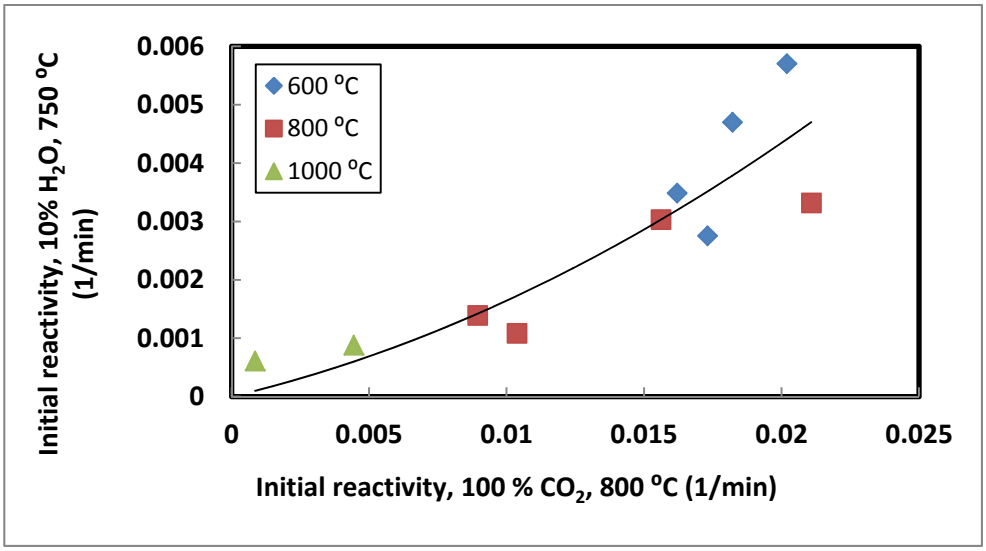

Figure 26. Char initial gasification reactivity in 10% steam at 750 °C vs. 100% CO_2 at 800 °C. All chars were generated in pressurized entrained flow reactor (PEFR) at different pressures (5-20 bars) and at different temperatures (600-800 °C).

Several variables were identified to which the char gasification reactivity (in CO_2) has been attributed: char surface area, char ash content, char quality (amorphous vs. graphitic), H/C and/or O/C ratio, and density of active sites. We do not yet have a measurement on the density of active sites, but we will look at the role of these other variables. Several figures below show that each of these parameters appear to play a role in char reactivity. Thus it is hard to rule out the role of any specific process variable. It is also not very feasible to separate these variables that might enable one to study the effect of one variable at a time.

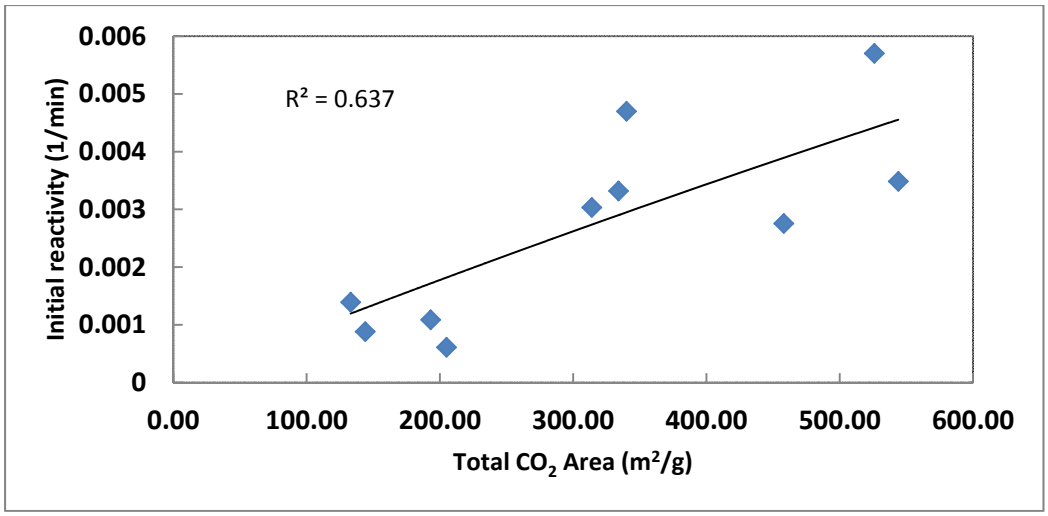

Figure 27. Char initial gasification reactivity in 10% steam at 750 ^{o}C vs. total surface area as measured by CO_2 adsorption . All chars were generated in pressurized entrained flow reactor (PEFR) at different pressures (5-20 bars) and at different temperatures (600-800 ^{o}C).

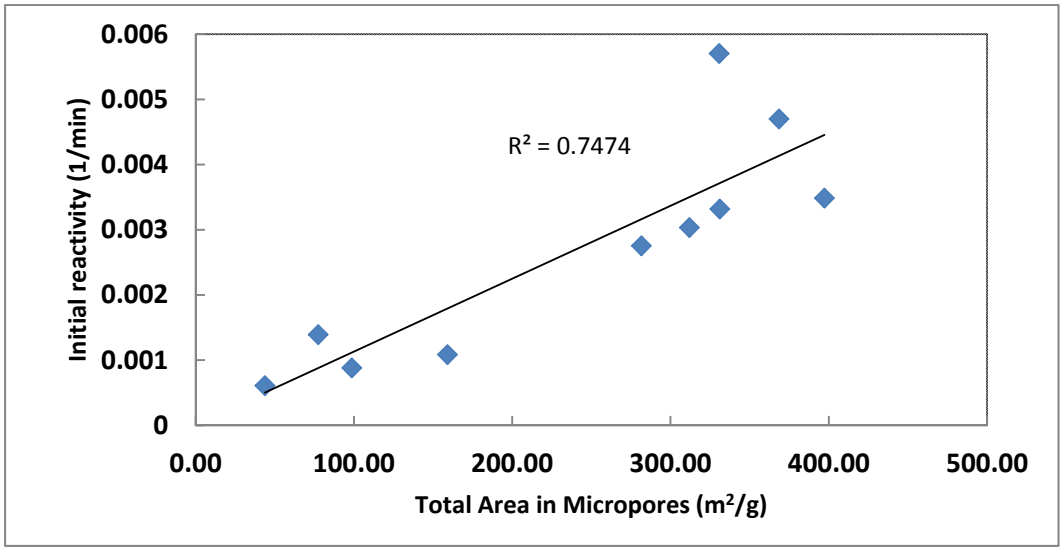

Figure 28. Char initial gasification reactivity in 10% steam at 750 ^{o}C vs. microporous area (excludes mesopores and macropores). All chars were generated in pressurized entrained flow reactor (PEFR) at different pressures (5-20 bars) and at different temperatures (600-800 ^{o}C).

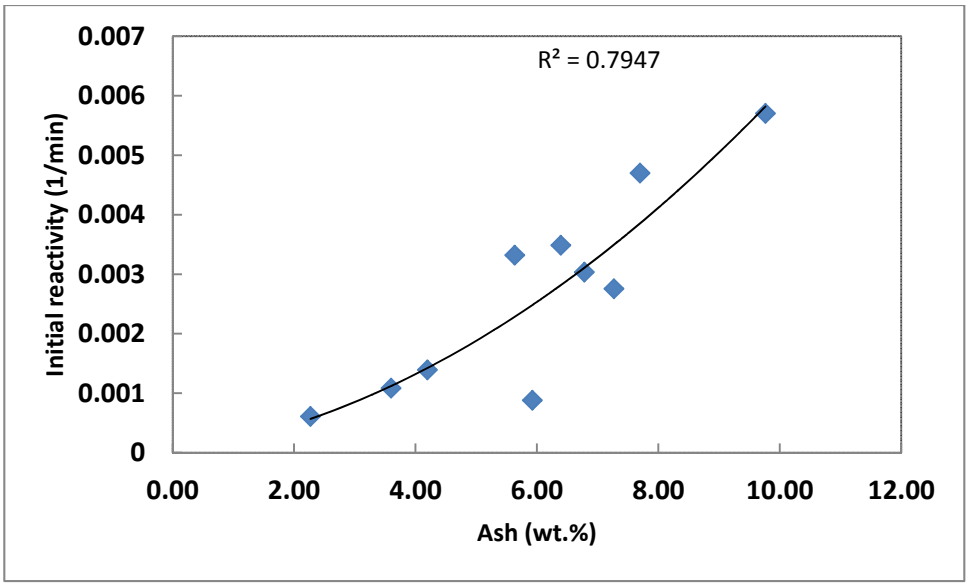

Figure 29. Char initial gasification reactivity in 10% steam at 750 °C vs. ash content. All chars were generated in pressurized entrained flow reactor (PEFR) at different pressures (5-20 bars) and at different temperatures (600-800 °C).

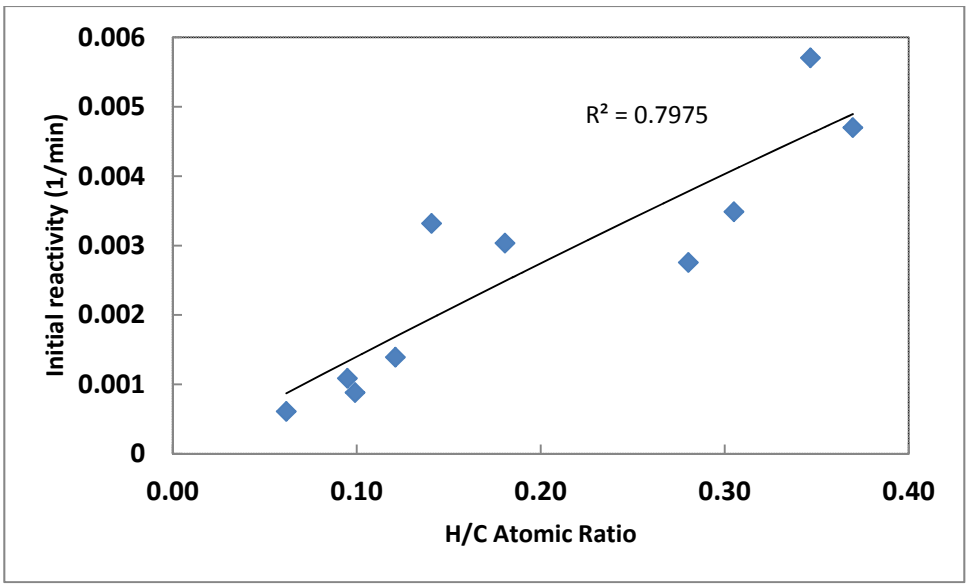

Figure 30. Char initial gasification reactivity in 10% steam at 750 °C vs. H/C atomic ratio. All chars were generated in pressurized entrained flow reactor (PEFR) at different pressures (5-20 bars) and at different temperatures (600-800 °C).

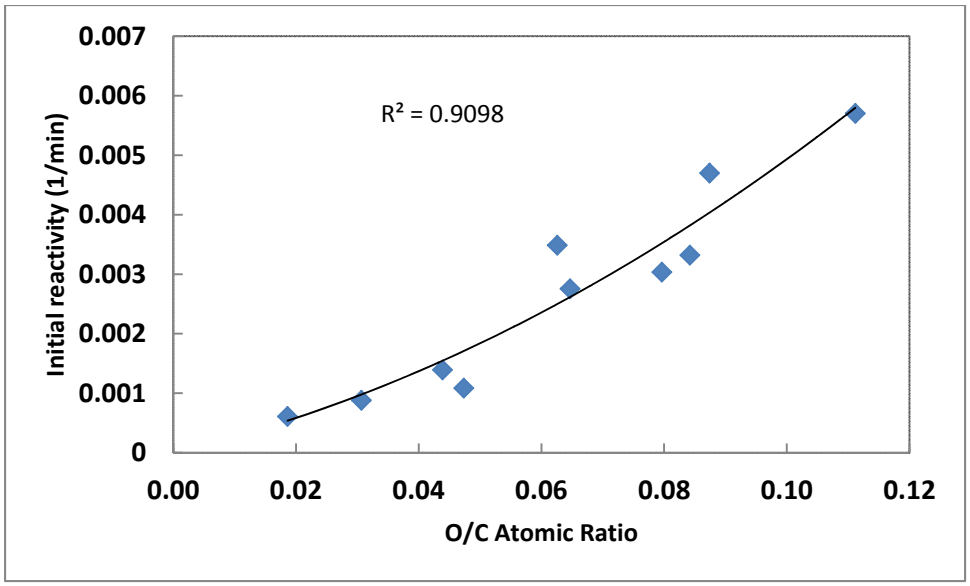

Figure 31. Char initial gasification reactivity in 10% steam at 750 ^{o}C vs. O/C atomic ratio. All chars were generated in pressurized entrained flow reactor (PEFR) at different pressures (5-20 bars) and at different temperatures (600-800 ^{o}C).

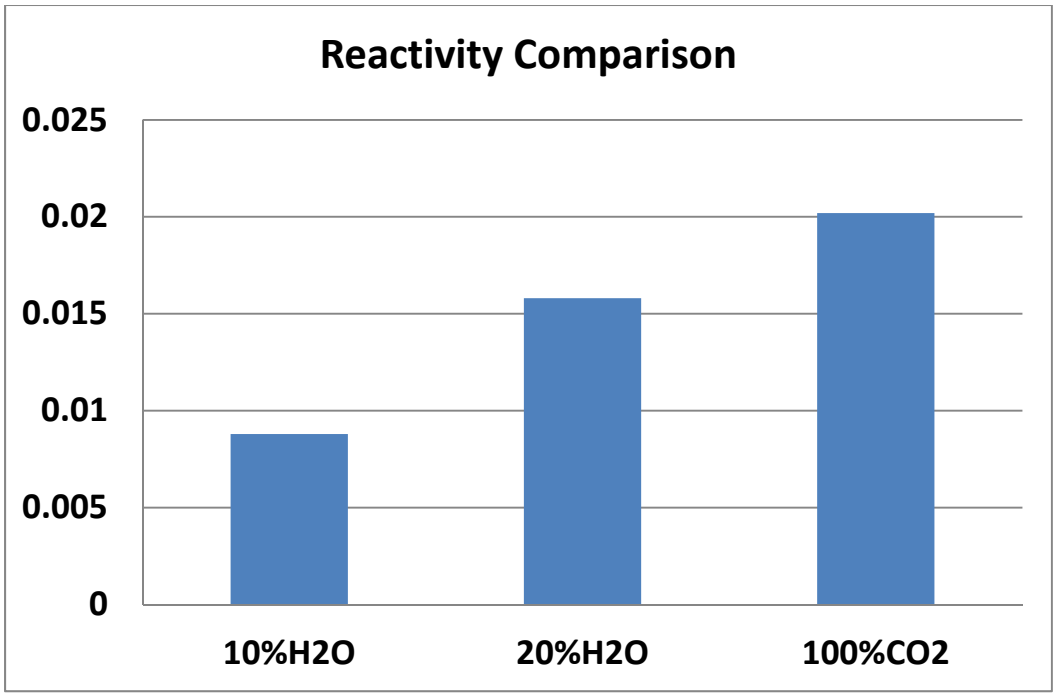

Figure 32. Char initial gasification reactivity in 10% steam at 750 ^{o}C, 20% steam at 750 ^{o}C, and in 100% CO_2 at 800 ^{o}C. The char used was generated in pressurized entrained flow reactor (PEFR) at 600 ^{o}C and 10 bars.

Task 10.0 Mathematical Models of Char Gasification Kinetic

Kinetic Study of Gasification of Switchgrass Char

Several sources for mass transfer limitations exist in TGAs: external mass transfer from the bulk gas into the sample, inter-particle mass transfer inside the sample bed, and intra-particle mass transfer. Prior gasification research conducted in the same PTGA has shown external mass transfer limitations to be negligible. We tested the rates for inter-particle mass transfer limitations by changing the sample mass and for intra-particle mass transfer limitations by changing the char particle size. For the particle size test, the original 125-180 μm particles were crushed and used as such. The results are summarized in 33. As can be seen, the gasification rates were identical regardless of the initial sample mass or particle size under the conditions tested. It was therefore deduced that mass transfer considerations could be ignored at 800°C for 50 mg samples if the rate was slower than tested here (50% conversion in about 20 minutes).

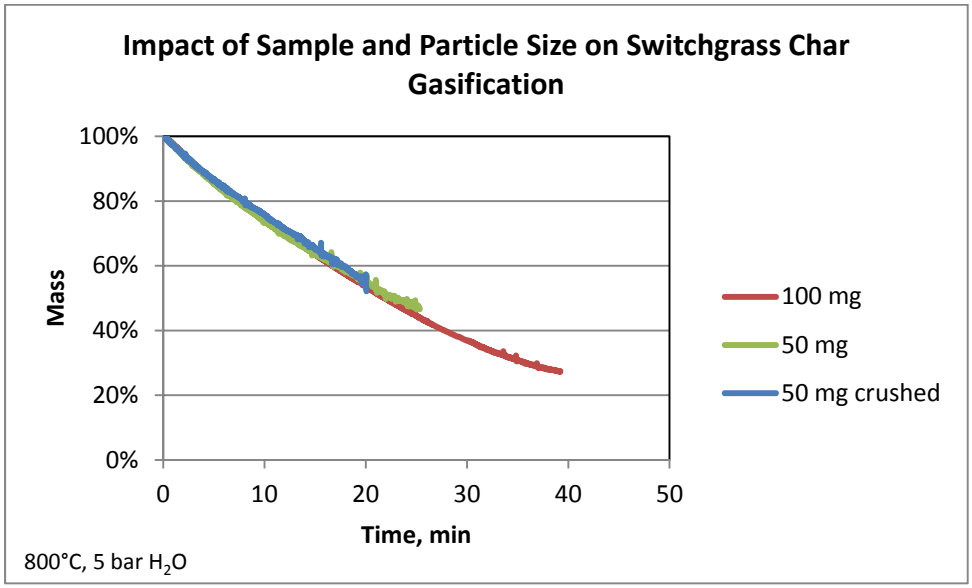

Figure 33. Impact of sample mass and particle size on gasification of switchgrass char in the PTGA. The char was prepared in the PEFR at 600°C and 15 bar, original particle size 125-180 um. Gasification conditions: 5 bar H_2O, 800°C.

The reaction rates were tested for the assumption of first order reaction with respect to char by testing the linearity of -ln(1-X) vs. time according to the integrated first order reaction rate equation.

$$-\ln(1-X) = kt \qquad (1)$$

Where k= reaction rate coefficient, min^{-1}

X = conversion

t = time, min

An example of the test for gasification of switchgrass char is shown in Figure 34. A good linearity was obtained, indicating that the gasification rate could be modeled as a first order reaction with respect to the char. For each experiment, the reaction rate coefficient k was obtained by a least square fit to the mass loss. The fit was not always as shown in the example, and in those cases the coefficient was determined for gasification at conversions between 10 and 35% in which range a linear relationship was typically obtained.

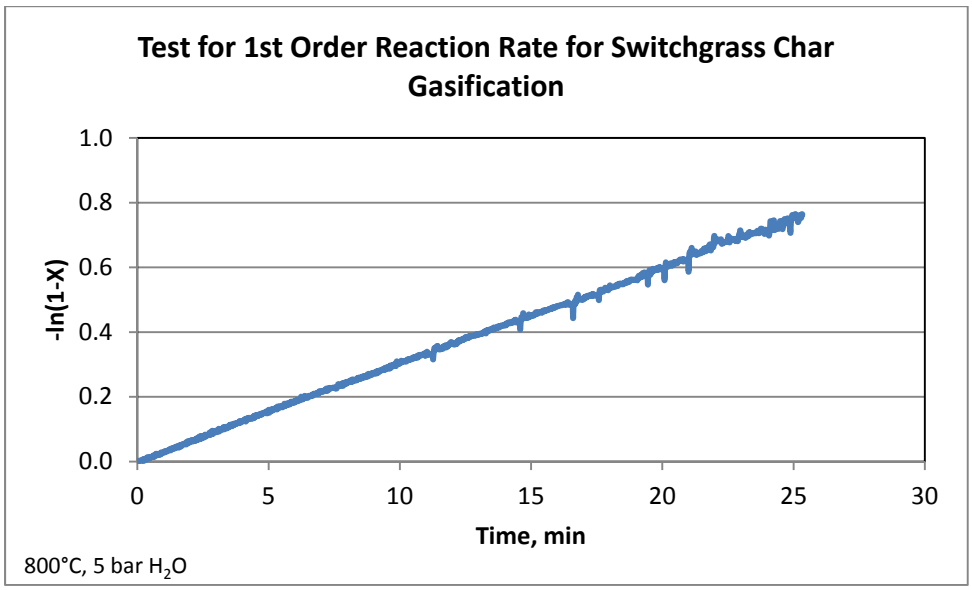

Figure 34. Test for 1st order reaction rate according to equation (1) for switchgrass char. Biomass: 50 mg of switchgrass char prepared in the PEFR at 600°C and 15 bar, particle size 125-180 um. Gasification conditions: 5 bar H_2O, 800°C.

The reaction rates obtained from the first order approximations to the rate data were tested for a general Langmuir-Hinshelwood type kinetics using the following overall kinetic expression.

$$k = \frac{k_{CO2}p_{CO2} + k_{H2O}p_{H2O}}{1 + K_{CO2}p_{CO2} + K_{H2O}p_{H2O} + K_{CO}p_{CO} + K_{H2}p_{H2}} \quad (2)$$

This general equation has been found to represent biomass gasification rate over a range of conditions.[i] Experiments were initially conducted in atmospheres containing either H_2O or CO_2 in the presence of the inhibiting gases (CO and H_2), and the validity of the model was tested under these conditions. Finally, experiments were conducted in the presence of all four gases, and the coefficients k_i and K_i were determined by a least squares fit to all of the experiments.

The switchgrass char used in these and all subsequent tests was prepared in the PEFR at 10 bar and 600°C. The impacts of CO_2, CO, and H_2 on the gasification rate in the absence of H_2O are depicted in Figure 15. As expected, increasing CO_2 partial pressure increased the gasification rate whereas increasing either CO or H_2 partial pressure inhibited the gasification rate.

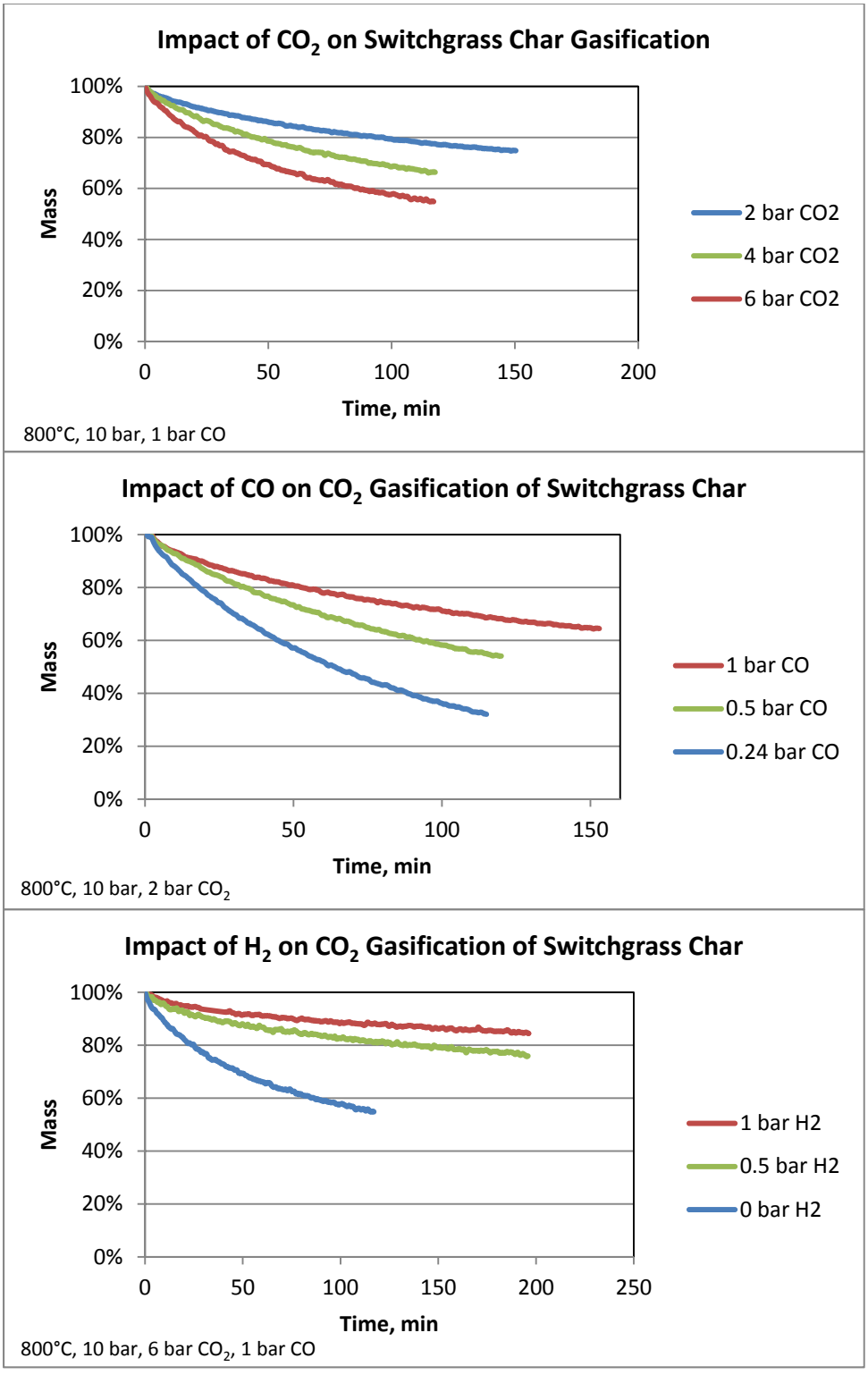

Figure 15. Impact of CO_2, CO, and H_2 on gasification of switchgrass char prepared in the PEFR at 600°C and 10 bar. Top: Impact of CO_2 at 800°C, 10 bar total pressure, 1 bar CO, 2-6 bar CO_2; Middle: Impact of H_2 at 800°C and 10 bar, 2 bar CO_2, 0.24-1.0 bar CO; Bottom: Impact of H_2 at 800°C, 10 bar total pressure, 2 bar CO_2, 1 bar CO, 0-1 bar H_2.

In the absence of H_2O, the general Langmuir-Hinshelwood equation reduces to the following form.

$$k = \frac{k_{CO2}p_{CO2}}{1 + K_{CO2}p_{CO2} + K_{CO}p_{CO} + K_{H2}p_{H2}} \tag{3}$$

Taking the inverse of this equation, we obtain:

$$\frac{1}{k} = \frac{1}{k_{CO2}p_{CO2}} + \frac{K_{CO2}}{k_{CO2}} + \frac{K_{CO}p_{CO}}{k_{CO2}p_{CO2}} + \frac{K_{H2}p_{H2}}{k_{CO2}p_{CO2}} \tag{4}$$

If only one of the partial pressures is varied at a time, this equation can be used to visually test how well the model fits the data. Thus for experiments varying CO_2 partial pressure, 1/k should be a linear function of $1/p_{CO2}$; for experiments varying CO partial pressure, 1/k should be a linear function of p_{CO}; and for experiments varying H_2 partial pressure, 1/k should be a linear function of p_{H2}. See equations below.

$$\frac{1}{k} = \left(\frac{1}{k_{CO2}} + \frac{K_{CO}p_{CO}}{k_{CO2}} + \frac{K_{H2}p_{H2}}{k_{CO2}}\right)\frac{1}{p_{CO2}} + \frac{K_{CO2}}{k_{CO2}} \tag{5}$$

$$\frac{1}{k} = \left(\frac{K_{CO}}{k_{CO2}p_{CO2}}\right)p_{CO} + \frac{1}{k_{Co2}p_{CO2}} + \frac{K_{CO2}}{k_{CO2}} + \frac{K_{H2}p_{H2}}{k_{CO2}p_{CO2}} \tag{6}$$

$$\frac{1}{k} = \left(\frac{k_{H2}}{k_{CO2}p_{CO2}}\right)p_{H2} + \frac{1}{k_{CO2}p_{CO2}} + \frac{K_{CO2}}{k_{CO2}} + \frac{K_{CO}p_{CO}}{k_{CO2}p_{CO2}} \tag{7}$$

Rate constants obtained via first order approximations to the gasification rates in each experiment were tested according to equations 5 through 7 for linearity. The resulting graphs are depicted in Figure 36. Very good linearity was obtained for all of the graphs in the range studied. Hence it was concluded that the equation can be used to represent gasification of the switchgrass char in CO_2.

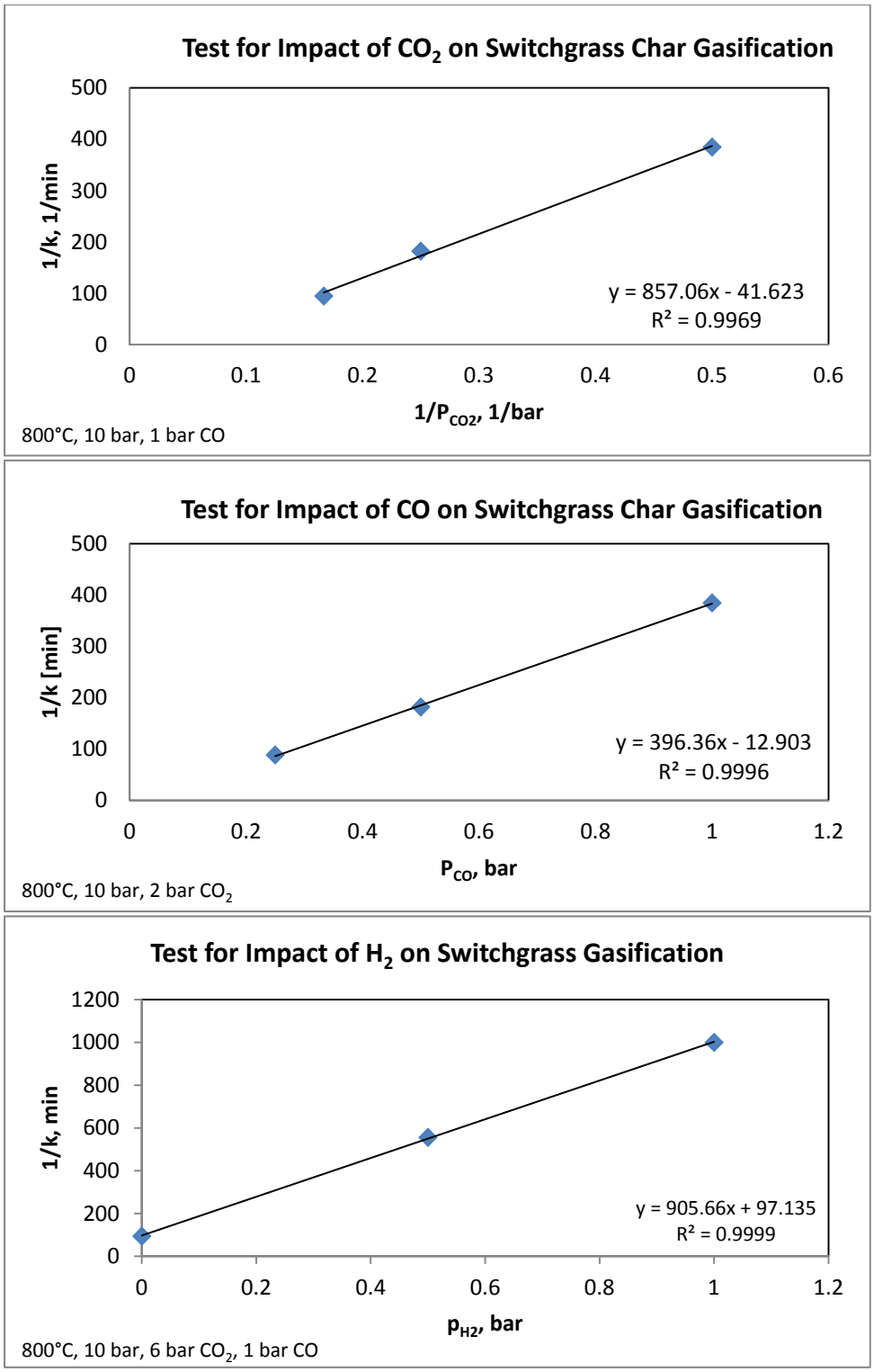

Figure 36. Tests for Langmuir Hinshelwood type kinetic rate expression according to equations 5-7 for gasification of switchgrass char in the absence of H_2O. Top: Impact of CO_2; middle: impact of CO; bottom: impact of H_2.

Next, the values for the coefficients k_{CO2}, K_{CO2}, K_{Co}, and K_{H2} were determined by minimizing the sum of the square of errors for all experiments performed in the absence of H_2O. A comparison of the predicted rates and the measured rates is shown in Figure 37 and the values for the coefficients in Table 1. A good correspondence was obtained, and the reaction rates could be modeled well with the chosen model. The graph includes additional points made at higher pressure. The reaction rate coefficients (Table 1) show that H_2 has a much higher inhibiting impact on the gasification rate than CO does. This has been found in other studies as well.[i]

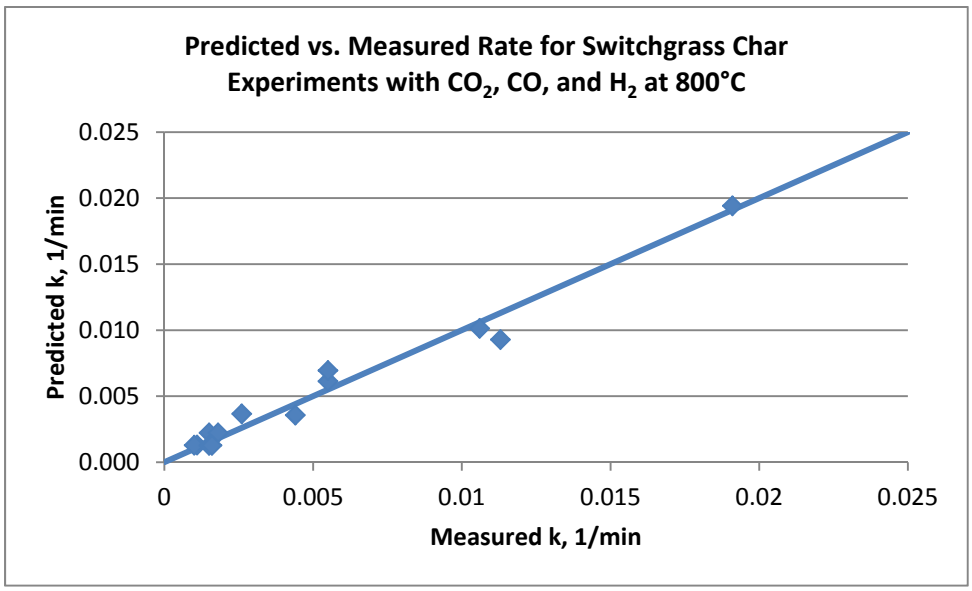

Figure 37. Experimental vs. predicted reaction rate constant for switchgrass char gasification at 800°C in the absence of H_2O according to Equation 3. The coefficients obtained are shown in Table 1.

Table 1. Reaction rate coefficients for gasification of switchgrass char at 800°C in the absence of H_2O according to equation 2.

Constant	Value
k_{CO2}	0.017 min^{-1}
K_{CO2}	0.15 bar^{-1}
K_{Co}	6.29 bar^{-1}
K_{H2}	60.5 bar^{-1}

To test for the impact of H_2O, experiments were performed while keeping the partial pressures of CO_2, CO, and H_2 constant. The increase in the gasification rate as the H_2O partial pressure was increased is seen in Figure . Increasing H_2O partial pressure increased the gasification rate) whereas increasing either CO or H_2 partial pressure decreased the rate (not shown).

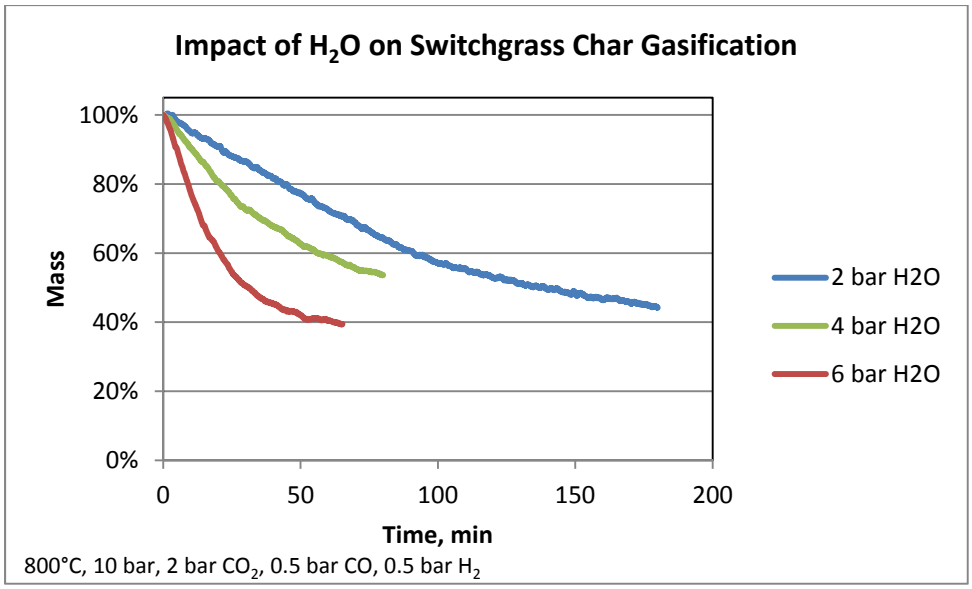

Figure 38. Impact of H_2O on gasification of switchgrass char. Switchgrass char prepared in the PEFR at 600°C and 10 bar. Gasification conditions: 800°C, 10 bar total pressure, 2 bar CO_2, 0.5 bar CO, 0.5 bar H_2, 2-6 bar H_2O.

Additional experiments with all four gases (CO_2, CO, H_2O, H_2) were conducted. The data from all experiments were used to obtain the coefficients for the Langmuir-Hinshelwood type kinetic expression shown in Equation 2. The comparison of the predicted and the measured rates is in Figure 39 and the coefficients are included Table 2. A good correspondence between the measured and predicted rates was obtained, and Equation 2 was deemed to represent the experimental data adequately. The coefficient k_{H2O} was almost an order of magnitude larger than k_{CO2}, indicating faster gasification by H_2O than by CO_2. K_{H2O} was found to be 0, indicating no inhibiting effect on the gasification rate by H_2O. H_2, CO, and CO_2 were all found to inhibit the reaction rate. The largest impact was by H_2, and its inhibiting impact was over an order of magnitude larger than that of CO; the inhibiting impact of CO_2 was minor compared to either CO or H_2. These observations are in accordance with literature results.[i] The high inhibiting impact of H_2 has been attributed to reverse oxygen exchange reaction ($C(O) + H_2 \rightarrow C + H_2O$) at high hydrogen coverages and conversions below 60%.[ii,iii]

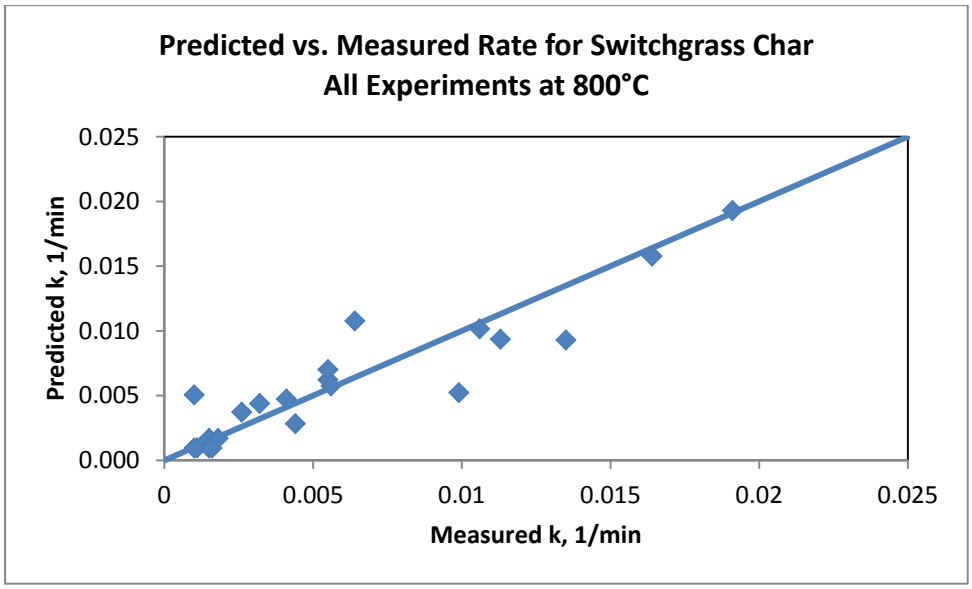

Figure 39. Measured vs. predicted reaction rate constant for switchgrass char gasification at 800°C according to equation 2. The coefficients obtained are shown in Table 2.

Table 2. Reaction rate coefficients for gasification of switchgrass char at 800°C.

Constant	Value
k_{CO2}	0.018 min^{-1}
k_{H2O}	0.12 min^{-1}
K_{CO2}	0.19 bar^{-1}
K_{H2O}	0
K_{CO}	6.39 bar^{-1}
K_{H2}	87.9 bar^{-1}

The experiments were not conducted at gas concentrations corresponding to the water gas shift equilibrium, and it possible that some water gas shift equilibrium reactions took place. To estimate for the impact of the water gas shift reaction, the water condensed after the reactor was compared to the water fed via the liquid pump. In most cases, there was a good agreement between the numbers with the water condensed somewhat lower than the water input (78-100%). No consistent, systematic relationship between the difference in the water condensed and water fed and the deviation from water gas shift equilibrium was observed. For the experiments at 800°C, the impact of water gas shift equilibrium was determined to not to be large, and no corrections to the gas concentrations were made based on the water gas shift reaction.

A limited number of experiments were performed at 850°C. The activation energy for the overall reaction rate coefficient in the presence of all four gases was calculated to be 237 kJ/mol, which is typical for gasification rates reported in the literature. This further suggests that there were no mass transfer limitations in the experiments.

Kinetic Study of Gasification of Bituminous Coal Char

The bituminous coal char gasified at a significantly lower rate than the switchgrass char, and hence the coal char gasification experiments were conducted at higher temperatures. Tests for determining mass transfer limitations were performed at 950°C (Figures 40-42). For CO_2 gasification at a high gasification rate (low concentration of the inhibiting gas CO) changing the coal mass from 50 mg to 25 mg increased the reaction rate but decreasing the coal mass further to 12.5 mg did not impact the rate. The gasification rate did not change either when using 25 mg of crushed coal particles, and it was concluded that there were no mass transfer limitations within the particles. Thus at these conditions, the rate was not limited by mass transfer at 25 mg or below. At a lower gasification rate (higher partial pressure of CO, Figure), no inter-particle mass transfer limitations were detected for 50 mg samples. Similar tests in atmospheres containing H_2O and H_2 showed no inter-particle mass transfer rates for 50 mg particles (Figure). For future experiments, 25 mg of coal char was utilized and the gasification rate was kept below the rates in the mass transfer limitation tests (2.5%/min).

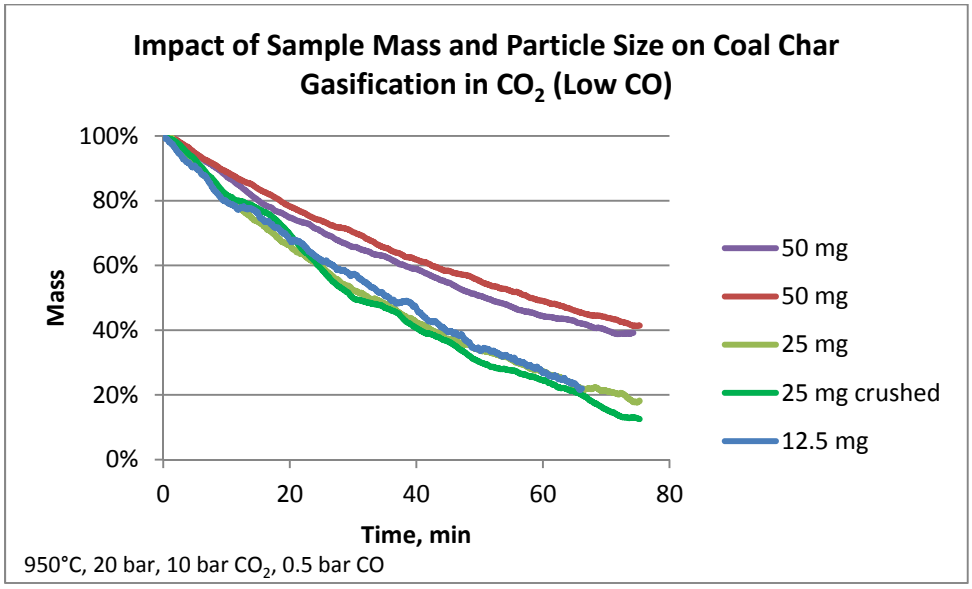

Figure 40. Tests for inter- and intra-particle mass transfer limitations at the conditions of high gasification rate (50% CO_2, 2.5% CO at 950°C and 20 bar).

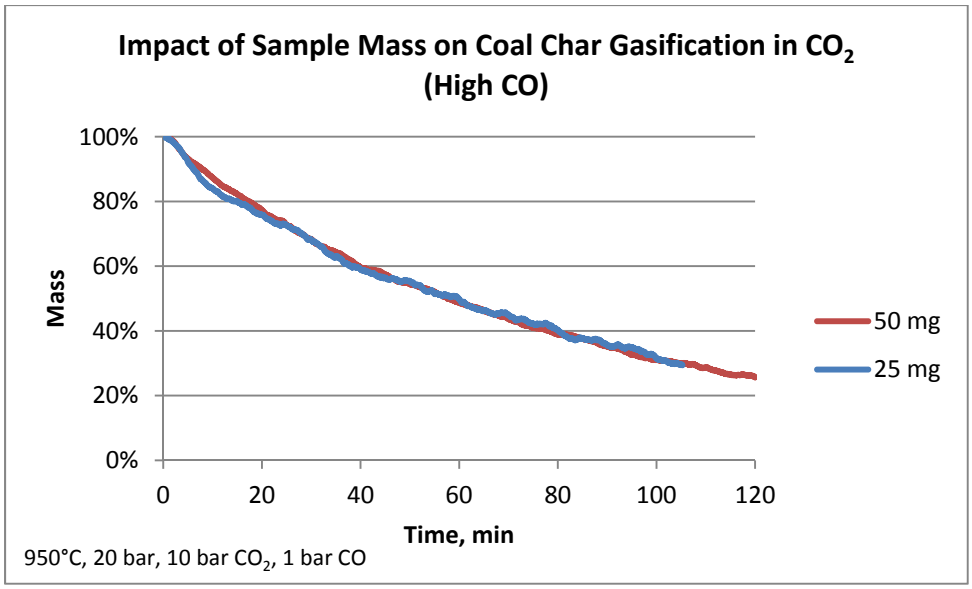

Figure 41. Tests for inter-particle mass transfer limitations for coal char at 950°C and 20 bar total pressure with 10 bar CO_2 and 1 bar CO.

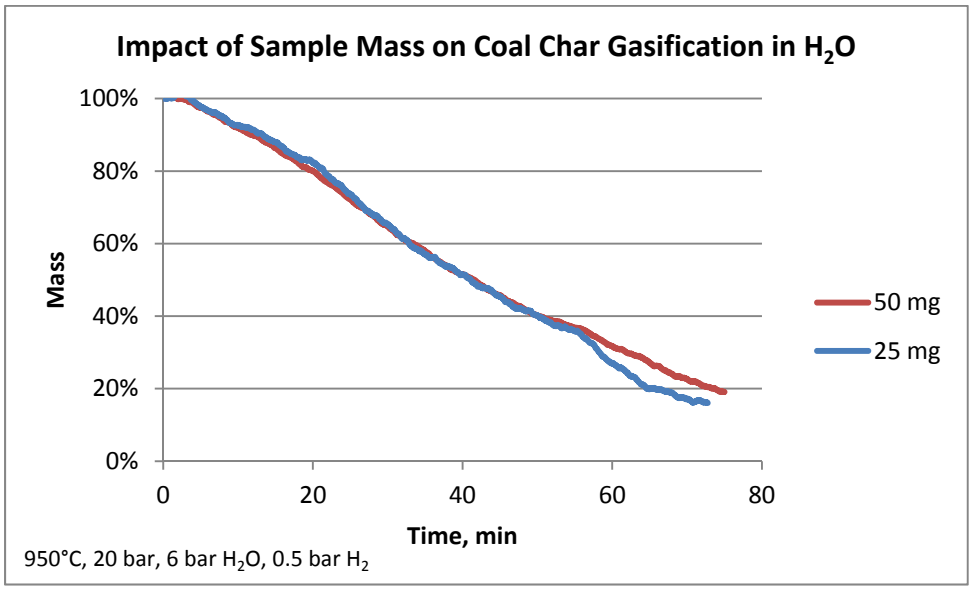

Figure 42. Tests for inter-particle mass transfer limitations for coal char at 950°C, total pressure 20 bar, 4 bar H_2O, 0.5 bar H_2

With the coal char, experiments were performed initially in atmospheres containing either CO_2 and CO or H_2O and H_2. The impact of CO_2 partial pressure on the gasification rate is depicted in Figure 43 and the impact of CO partial pressure in Figure 44. As expected, the gasification rate increased as CO_2 partial pressure increased or CO partial pressure decreased.

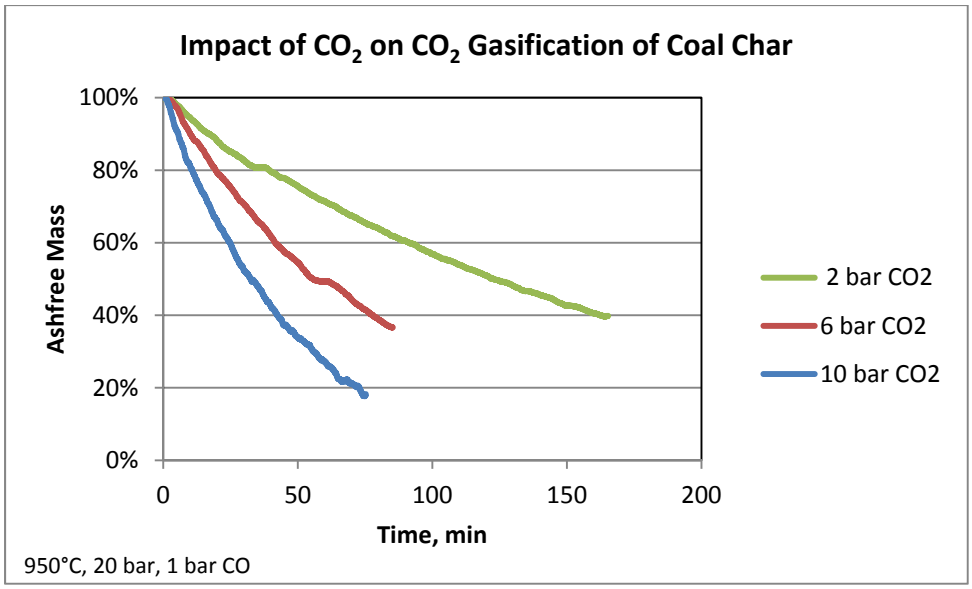

Figure 43. Impact of CO_2 partial pressure on CO_2 gasification rate of bituminous coal char. 950°C, 20 bar total pressure, 0.5 bar CO.

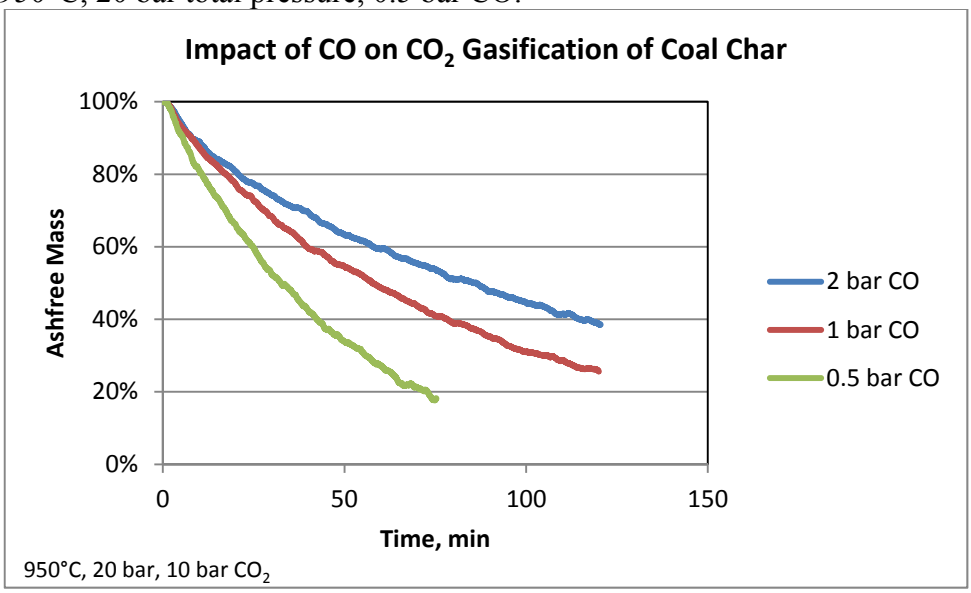

Figure 44. Impact of CO partial pressure on CO_2 gasification rate for bituminous coal char. 950°C, 20 bar total pressure, 10 bar CO_2

The reaction rates were tested for the assumption of first order reaction with respect to char by testing the linearity of -ln(1-X) vs. time according to the integrated first order reaction rate equation. An example of the test is shown in Figure 45. A good linearity was obtained over the entire reaction rate region. The first order assumption was applied to the data and an overall reaction rate coefficient k was calculated for each experiment.

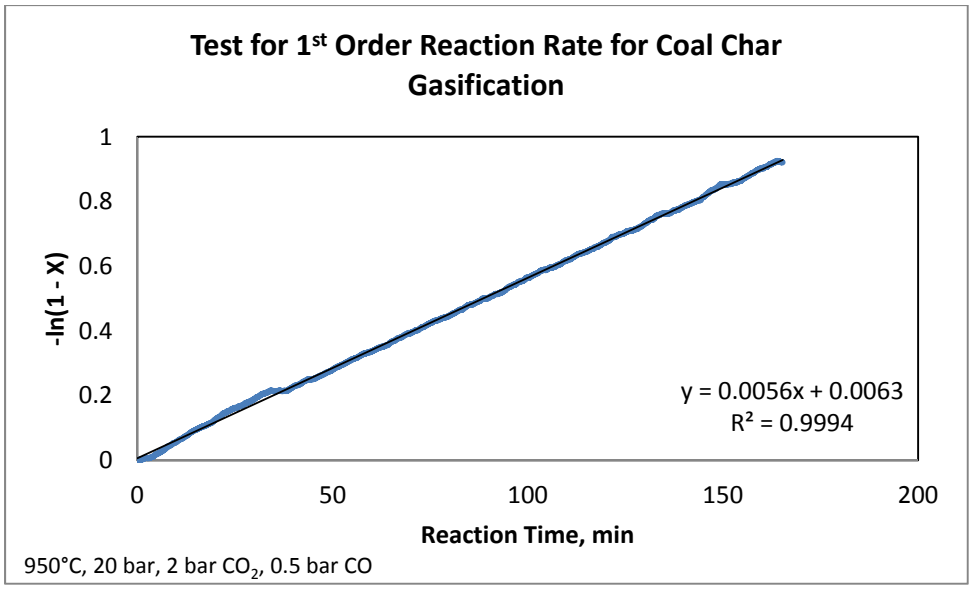

Figure 45. Test for first order reaction with respect to coal char. 950°C, 20 bar total pressure, 2 bar CO_2, 0.5 bar CO

The reaction rate coefficients were tested for the same kinetic expression as those for switchgrass (equation 2). For experiments at constant p_{CO}, 1/k was plotted vs. $1/p_{CO2}$ and tested for linearity. For experiments at constant p_{CO2}, 1/k was plotted vs. p_{CO}. The results for the tests are shown in Figure 46 and Figure 47. The rates could be adequately described by the chosen kinetic expression.

$$k = \frac{k_{CO2}p_{CO2} + k_{H2O}p_{H2O}}{1 + K_{CO2}p_{CO2} + K_{H2O}p_{H2O} + K_{CO}p_{CO} + K_{H2}p_{H2}} \quad (2)$$

$$\frac{1}{k} = \left(\frac{1}{k_{CO2}} + \frac{K_{CO}p_{CO}}{k_{CO2}}\right)\frac{1}{p_{CO2}} + \frac{K_{CO2}}{k_{CO2}}$$

$$\frac{1}{k} = \frac{1}{k_{CO2}p_{CO2}} + \frac{K_{CO2}}{k_{CO2}} + \left(\frac{K_{CO}}{k_{CO2}p_{CO2}}\right)p_{CO}$$

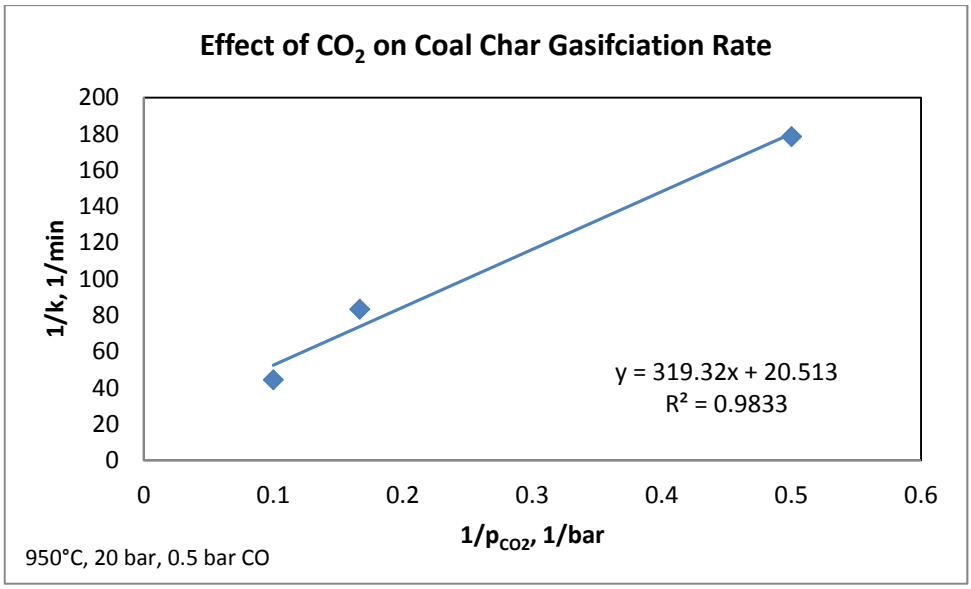

Figure 46. Test for impact of CO_2 partial pressure on gasification kinetics according to Langmuir-Hinshelwood kinetics.

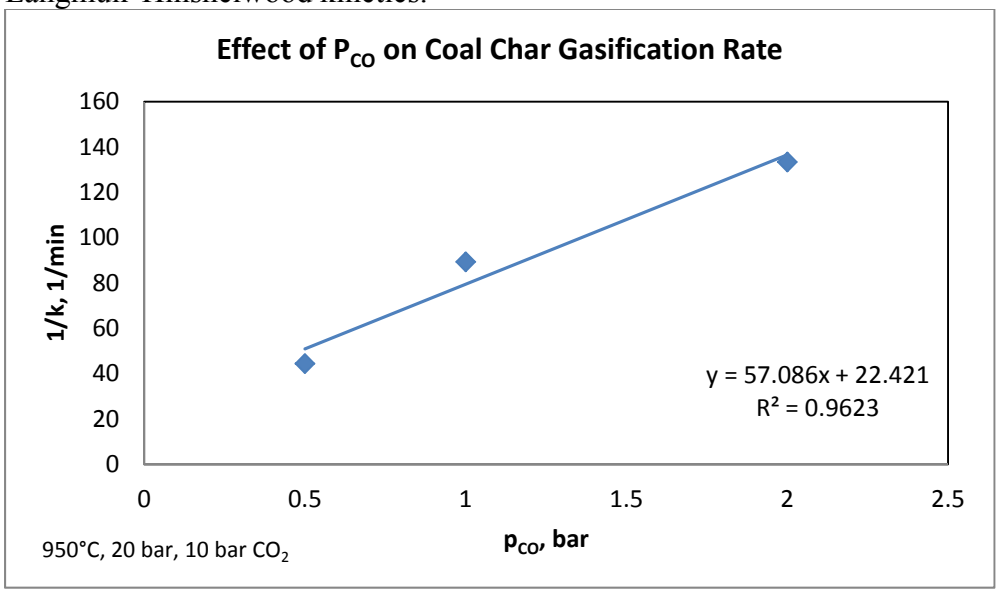

Figure 47. Test for impact of CO partial pressure on gasification kinetics according to Langmuir-Hinshelwood kinetics

All the data taken in the presence of CO and CO_2 were fitted to the reaction rate expression to obtain the rate coefficients. A comparison of the predicted vs. measured overall rate coefficients (k) is given in Figure 48. A good fit was obtained. The rate coefficients (Table 3) suggest that the rate was not inhibited by CO_2.

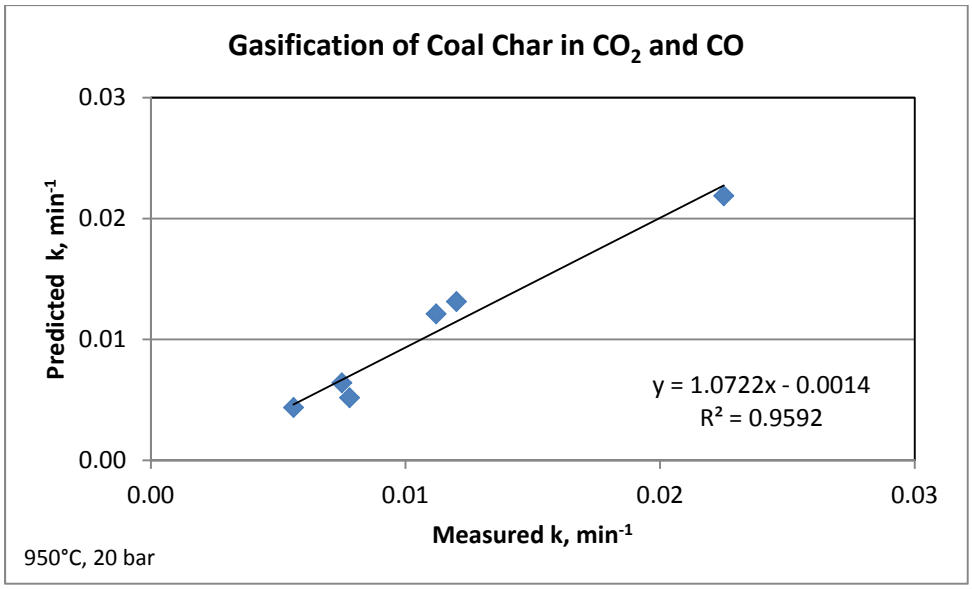

Figure 48. Measured vs. predicted reaction rate coefficients for coal char gasification in CO_2 and CO. Coefficients are in Table 3

Table 3. Reaction rate coefficients for gasification of bituminous coal char in the presence of CO_2 and CO.

Coefficient	Value
k_{CO2}	0.0113 min^{-1}
K_{CO2}	0
K_{CO}	8.29 bar^{-1}

The impacts of H_2O partial pressure and H_2 partial pressures on the gasification rate are shown in Figure 49 and Figure 50. The rate increased as H_2O partial pressure increased and H_2 partial pressure decreased.

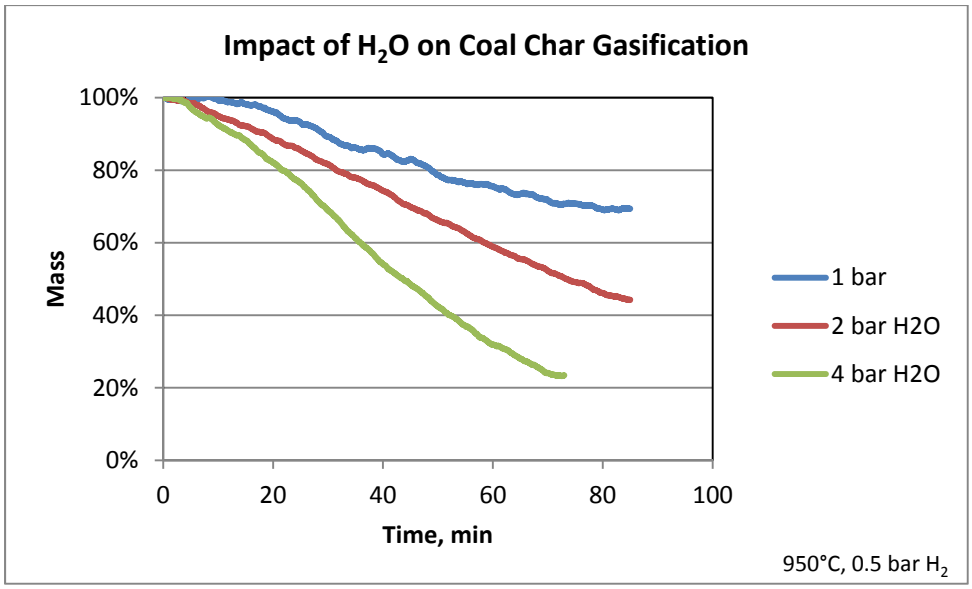

Figure 49. Impact of H_2O partial pressure on gasification of coal char. Temperature 950°C, 20 bar total pressure, 0.5 bar H_2.

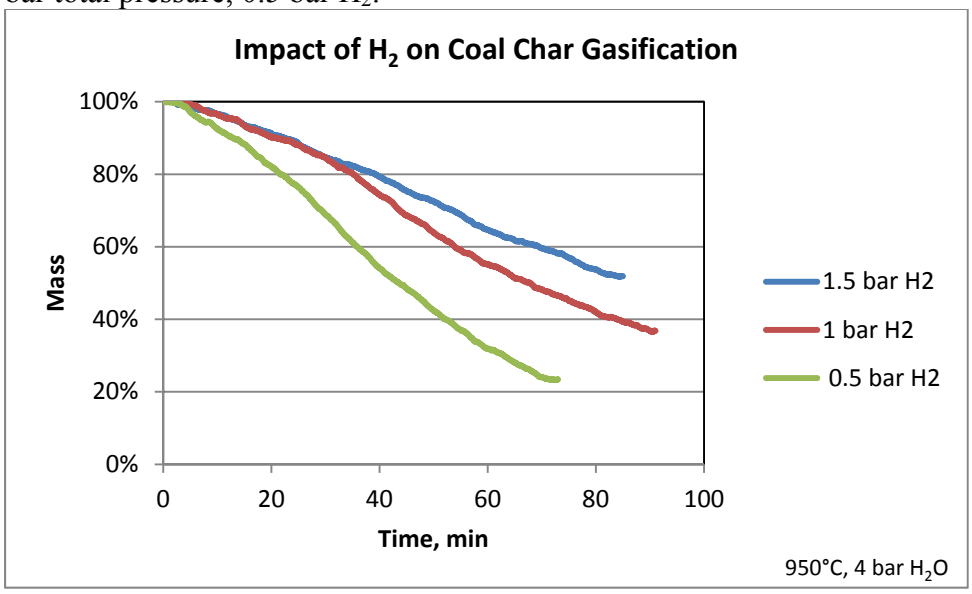

Figure 50. Impact of H_2 partial pressure on gasification of bituminous coal char. Temperature 950°C, 20 bar total pressure, 4 bar H_2O.

The reaction rate coefficients extracted from the data via the first order assumption were tested for Langmuir-Hinshelwood type kinetics according to the reduced form.

$$k = \frac{k_{H2O} p_{H2O}}{1 + K_{H2O} p_{H2O} + K_{H2} p_{H2}} \qquad (6)$$

To test whether the gasification rate could be presented by that rate expression, for experiments at constant hydrogen partial pressure, 1/k was plotted vs. $1/p_{H2O}$ and tested for linearity. At constant steam partial pressure, 1/k was plotted vs. p_{H2}. Excellent linearities were obtained (see Figure 51 and Figure 52), and the rates can thus be well described by the chosen kinetic expression.

$$\frac{1}{k} = \left(\frac{1}{k_{H2O}} + \frac{K_{H2}p_{H2}}{k_{H2O}}\right)\frac{1}{p_{H2O}} + \frac{K_{H2O}}{k_{H2O}}$$

$$\frac{1}{k} = \frac{1}{k_{H2O}p_{H2O}} + \frac{K_{H2O}}{k_{H2O}} + \left(\frac{K_{H2}}{k_{H2O}p_{H2O}}\right)p_{H2}$$

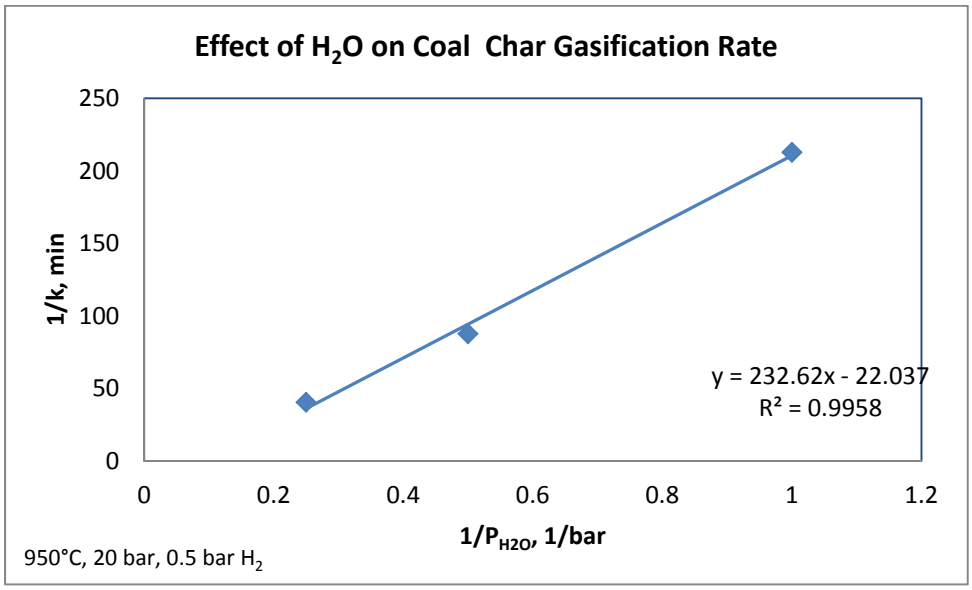

Figure 51. Test for impact of H_2O partial pressure on coal char gasification rate according to Langmuir-Hinshelwood kinetics.

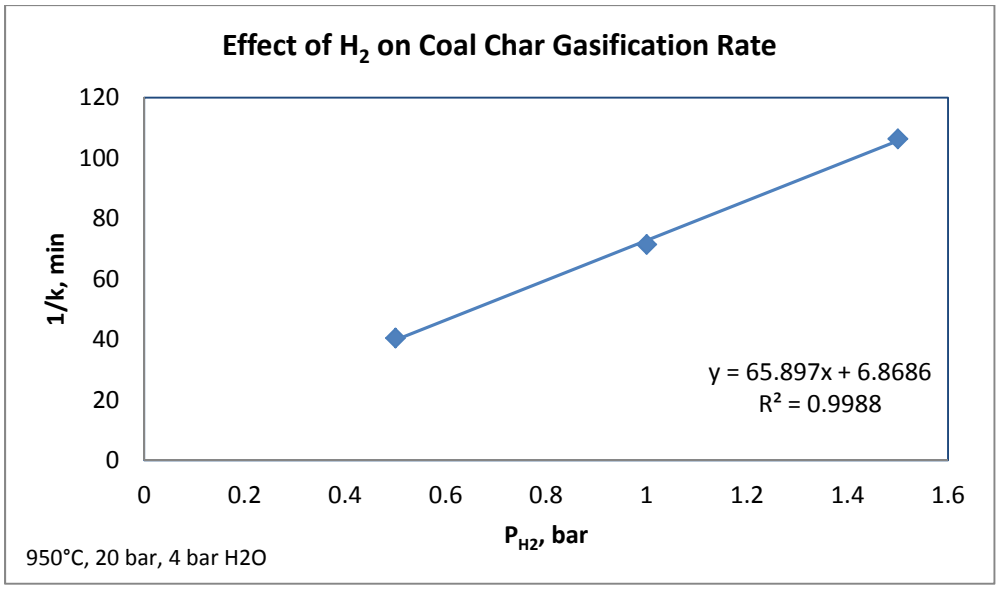

Figure 52. Test for impact of H_2 partial pressure on coal char gasification rate according to Langmuir-Hinshelwood kinetics.

A parity plot of the measured and predicted reaction rate coefficients is given in Figure 53. The optimized coefficients show no inhibiting impact by H_2O for the gasification rate in H_2O and H_2 mixtures.

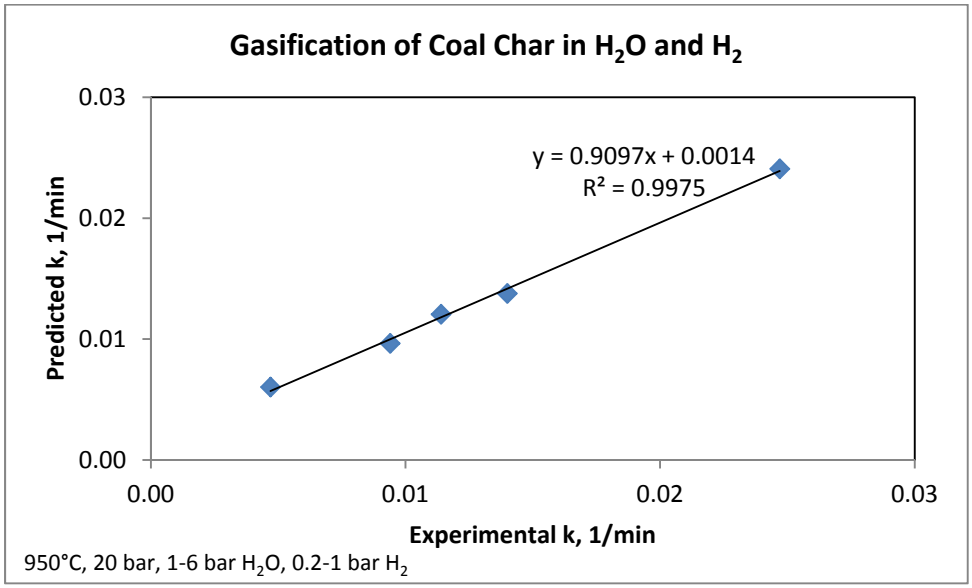

Figure 53. Measured vs. predicted reaction rate for coal char gasification in H_2O and H_2 according to equation 6. Coefficients in Table 4.

Table 4. Rate coefficients for gasification of bituminous coal char at 950°C in H_2O and H_2.

Constant	Value
K_{H2O}	0.0240 min^{-1}
K_{H2O}	0
K_{H2}	5.98 bar^{-1}

Experiments were further conducted in mixtures containing all four gases (H_2O, H_2, CO_2, and H_2). The gas conditions were chosen to correspond to the water gas shift equilibrium. All the data was fitted to the complete rate expression, and the measured vs. predicted rates are presented in Figure 54. No terms for inhibition by H_2O or CO_2 are shown. The gasification rate kinetic constant was higher for H_2O than for CO_2 and the inhibiting impact of H_2 is higher than that for CO.

$$k = \frac{k_1 p_{CO2} + k'_1 p_{H2O}}{1 + K_2 p_{CO2} + K p_{H2O} + K_4 p_{CO} + K_5 p_{H2}}$$

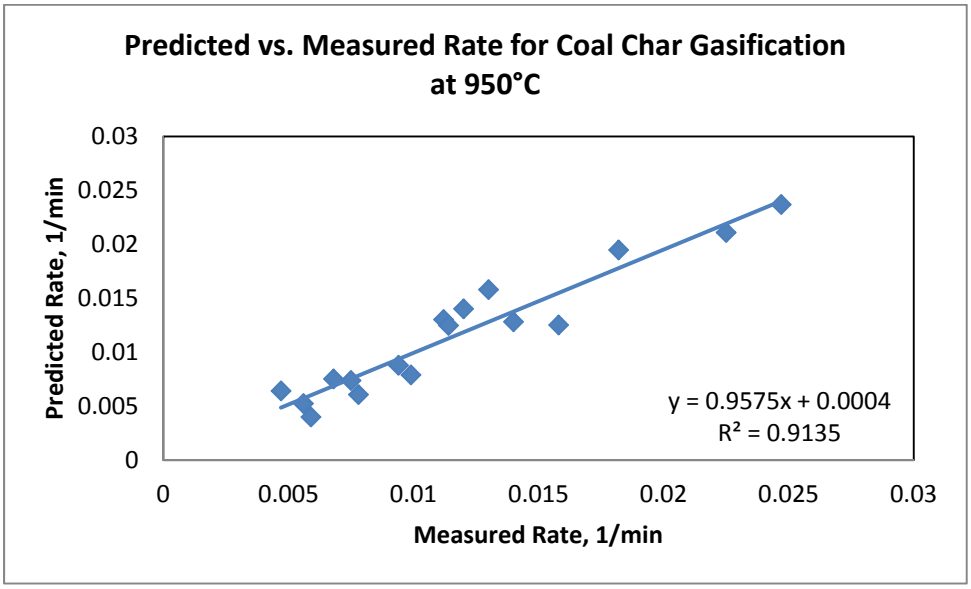

Figure 54. Experimental vs. calculated rates for coal char gasification in H_2O, H_2, CO_2, and CO. Temperature 950°C, total pressure 20 bar, 0-10 bar CO_2, 0-4 bar H_2O, 0-2.5 bar CO, 0-1.5 bar H_2. The values for the coefficients are in Table 5.

Table 5. Coefficients for gasification of bituminous coal char at 950°C according to equation 2.

Constant	Value
K_{CO2}	0.0154 min^{-1}
K_{H2O}	0.116 min^{-1}
K_{CO2}	0.177 bar^{-1}
K_{H2O}	0.498 bar^{-1}
K_{CO}	9.03 bar^{-1}
K_{H2}	33.2 bar^{-1}

The Arrhenius plot for the gasification rate is shown in Figure 55. The activation energy was 238 kJ/mol, which is in accordance with typical literature values. The high activation energy also confirms the absence of mass transfer limitations.

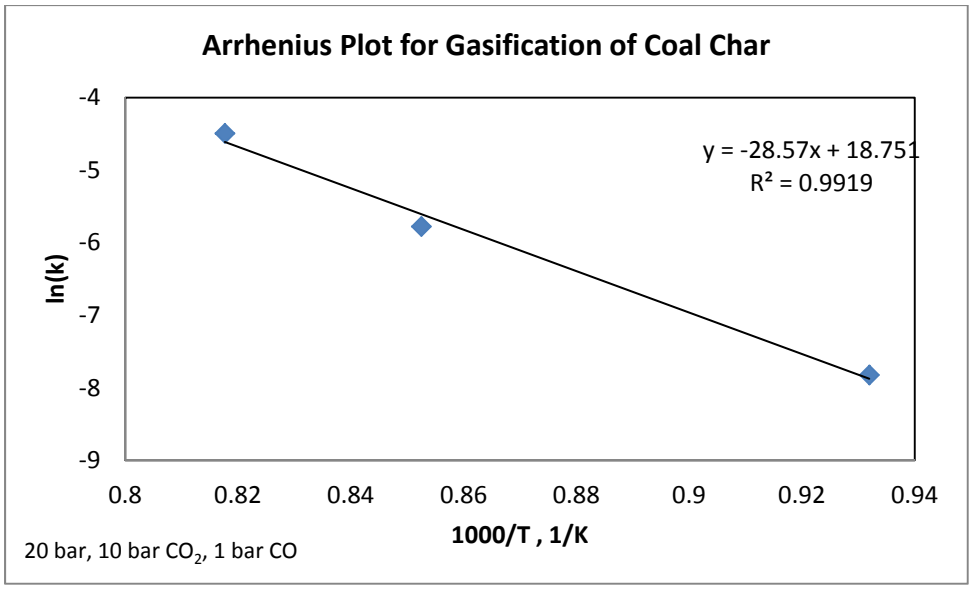

Figure 55. Arrhenius plot for coal char gasification at 20 bar total pressure, 10 bar CO_2, 1 bar CO, 800-950°C.

Gasification of Coal and Switchgrass Char Mixtures

Experiments were performed with mixtures of coal char and switchgrass char under various conditions. Figure 56 depicts the gasification of coal char, switchgrass char, and a 50%-50% blend of the two at 950°C in 10 bar CO_2 and 2 bar CO. The gasification of switchgrass char is very fast and complete in less than 10 min whereas only about 60% of the coal char becomes gasified in 120 minutes. In the gasification of the mixture of the two chars, initially one sees a rapid decrease in mass corresponding to the complete gasification of switchgrass char. After this initial mass loss, the gasification rate decreases. However, the gasification rate appears to be faster than the rate of coal char gasification only, and nearly complete gasification is achieved in 90 minutes.

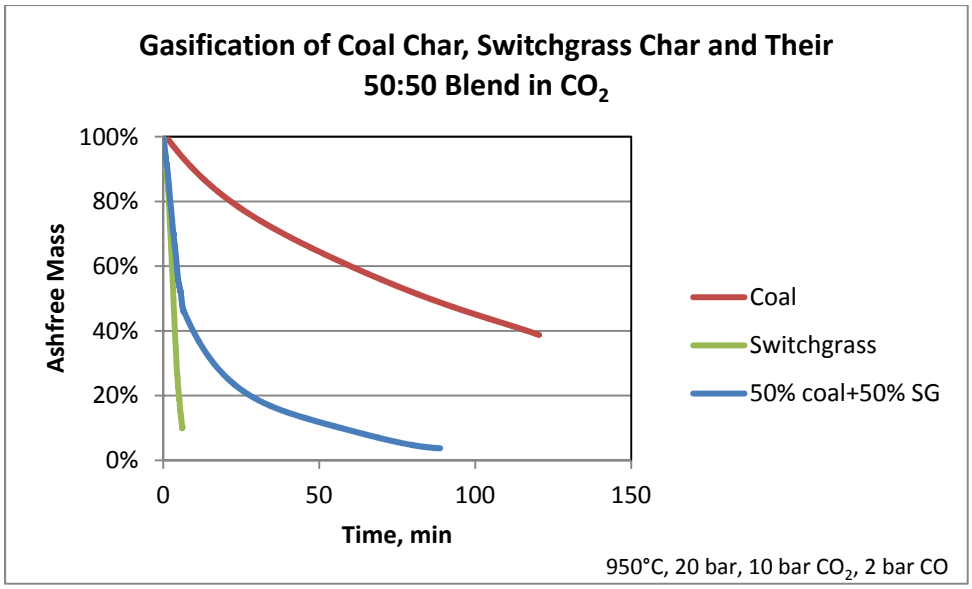

Figure 56. Gasification of coal char, switchgrass char, and a mixture of 50% coal and switchgrass char at 950°C in 10 bar CO_2 and 2 bar CO (total pressure 20 bar). Due to high noise, the signals have been smoothed by 6th order polynomial fits.

The reaction rate coefficients were determined by the first order tests (Figure 57). Two linear sections were obtained for the gasification of the char mixture, the first one corresponding to the initial period with rapid gasification of switchgrass char, and the second one to the gasification of coal char after complete gasification of switchgrass. The reaction rate coefficients were determined, and they are compared in Table 6. The initial rate is close to the weighted average of the reaction rates for coal and switchgrass chars. This suggest that the two chars gasified independently of each other in this region However, the gasification rate of coal char after the complete gasification of switchgrass is over three times higher than that for the coal char only. Thus the rate of coal char gasification was significantly increased after switchgrass was completely gasified. The result suggests that direct contact with switchgrass ash results in an enhancement of the coal char gasification rate.

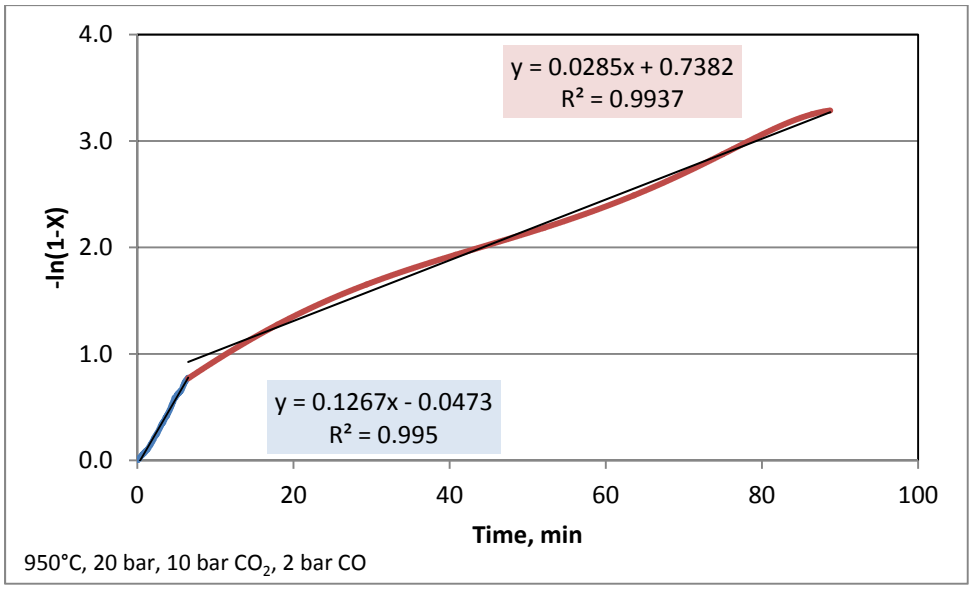

Figure 57. Gasification of a mixture of 50% bituminous coal char and 50% switchgrass char at 950°C with 10 bar CO_2, 2 bar CO (total pressure 20 bar).

Table 6. Reaction rate coefficients for bituminous coal and switchgrass char and their mixture at 950°C in 10 bar CO_2 and 2 bar CO.

Sample	k, 1/min
Coal char	0.0075
Switchgrass (SG) char	0.27
50% Coal + 50% SG, average	0.14
50% Coal + 50% SG, initially	0.13
50% Coal + 50% SG, after switchgrass char burn-off	0.029

Blends of switchgrass and coal chars were also gasified in atmospheres containing H_2O and H_2 (Figure 58). The result confirmed that the blends gasified at rates approximately equal to the weighted averages of the individual chars. These experiments were stopped at approximately the time when switchgrass char had become completely gasified. Hence it was not possible to ascertain if the coal char gasification rate became increased when only switchgrass ash remained.

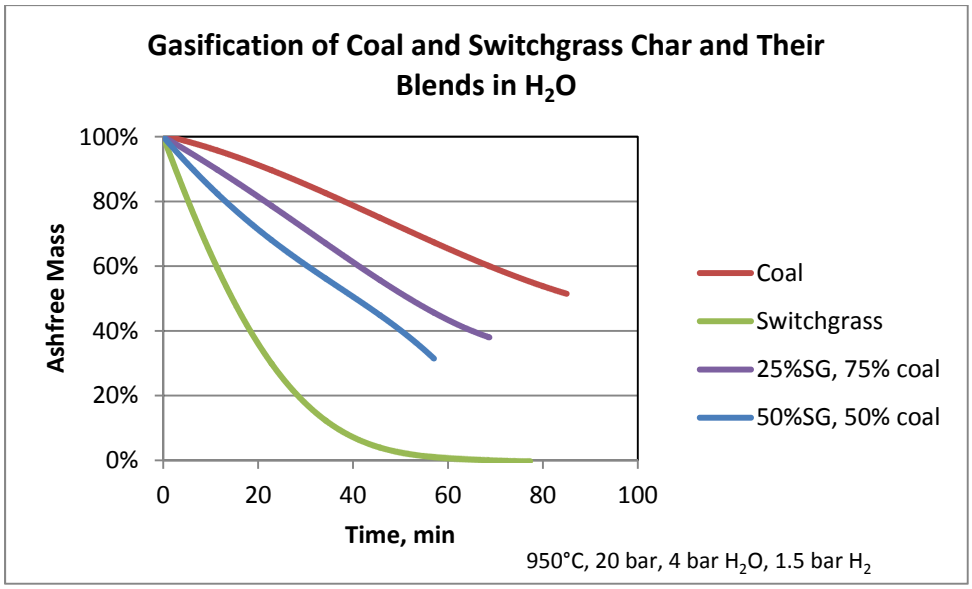

Figure 58. Gasification of switchgrass and coal char and their blends in atmospheres containing H_2O and H_2. Gasification conditions: 950°C, 20 bar, 10 bar H_2O, 1.5 bar H_2.

In the above experiment the rate of switchgrass char gasification was limited by mass transfer rates. Additional experiments were conducted under conditions in which both rates were kinetically controlled. Table 7 shows the reaction rates for experiments conducted at 800°C in 10 bar CO_2 and 1 bar CO (Figure 59). These conditions were chosen to obtain a measureable rate for both switchgrass and coal char. The rate coefficient obtained for the mixture of coal char and switchgrass was very close to the average rate coefficient of the two chars (0.061 vs. 0058 min^{-1}). This experiment confirmed that the mixtures gasified at rates similar to the weighted average rate of the two chars separately.

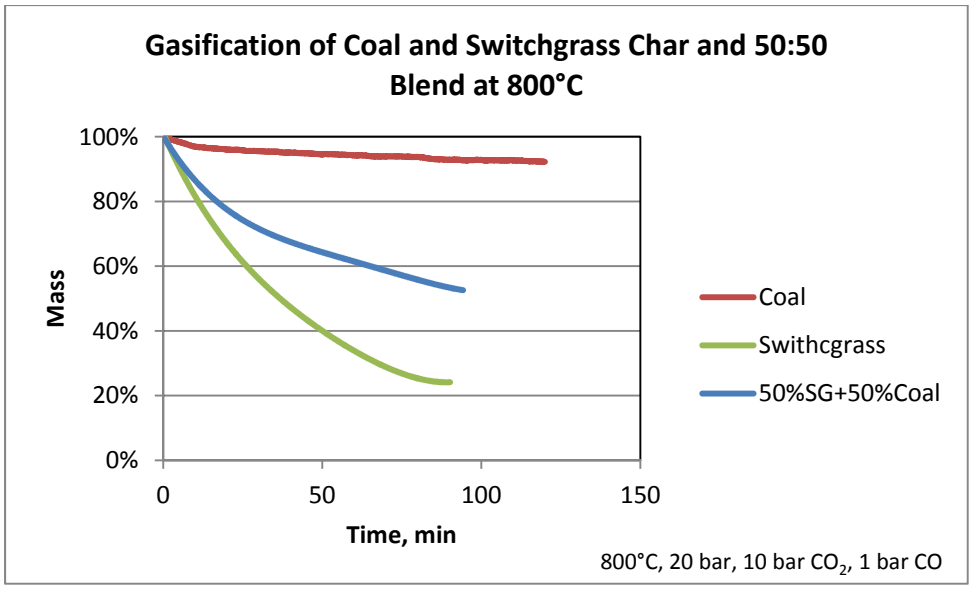

Figure 59. Gasification of switchgrass and coal char and a 50:50 blend at 800°C. 20 bar total pressure, 10 bar CO_2, 1 bar CO.

Table 7. Reaction rate coefficients for coal and switchgrass char and their mixture at 950°C in 10 bar CO_2 and 2 bar CO.

Material	Rate, 1/min
Coal	0.0004
SG	0.0166
50% coal + 50% SG	0.0061
Weighted average rate	0.0058

CONCLUSIONS

The experiments performed here in a pressurized thermogravimetric analyzer (PTGA) showed that switchgrass and coal devolatilized independently of each other. Switchgrass and coal char blends also gasified at rates equal to the weighted averages of the individual chars as long as the mixture contained gasifiable switchgrass char. Overall the results thus suggested no synergy during co-gasification of coal and switchgrass until switchgrass was completely reacted and had formed ash. However, in blends of switchgrass and coal char, the gasification rate of coal char increased after switchgrass had become completely gasified. The increased coal gasification rate was attributed to contact between the coal char and the switchgrass ash in these experiments. Thus the presence of biomass ash increases coal char gasification rates and thus provides synergy.

In an industrial gasifier processing coal and biomass, biomass will gasify faster than the coal and form ash. Hence there will be biomass ash present while coal char continues to react. If the biomass ash comes in close contact with coal char, it will increase the rate of coal char

gasification. It is expected that there has to be atomic level contact of the ash constituents with char. In the current experiments, a physical mixture of ash resulting from complete gasification of switchgrass char and coal char that was still undergoing gasification resulted in enhanced coal char gasification rates. Whether industrial gasifiers provide sufficient contact depends on many factors including the reactor type. At high gasification temperatures (>1000°C), there may also be significant devolatilization of the biomass ash constituents, in particular alkali metals that are known to be active for catalyzing gasification reactions. Whether vaporized alkali metals can interact with coal char and enhance the gasification rate, should be investigated further.

Task 11.0 Develop Char Porosity Models & Transport Effects into Kinetics

The chars collected from PEFR pyrolysis (Task 4.0) will be analyzed for porosity, pore size distribution (BET), and morphology (SEM) as described in Task 6.0. This information will be used to build quantitative models of the role of internal and external transport effects and how these would be influenced by the gasification conditions. The transport effects will be combined with the intrinsic kinetic models to provide an integrated model of the coal/biomass blend gasification process. No work was done on this task, as other leads appeared to be far more promising, and worth pursuing in greater detail.

Task 12.0 TGA/PTGA Gasification of Coal/Biomass Blends

Effect of Blending Texas Lignite with Switchgrass Biomass

The below figure shows the effect of blending Texas lignite with switchgrass biomass. Five different runs are reported here: (i) pure lignite, (ii) 90% lignite – 10% switchgrass, (iii) 50% lignite-50% SG, (iv) 10% lignite-90% SG, and (v) pure switchgrass.

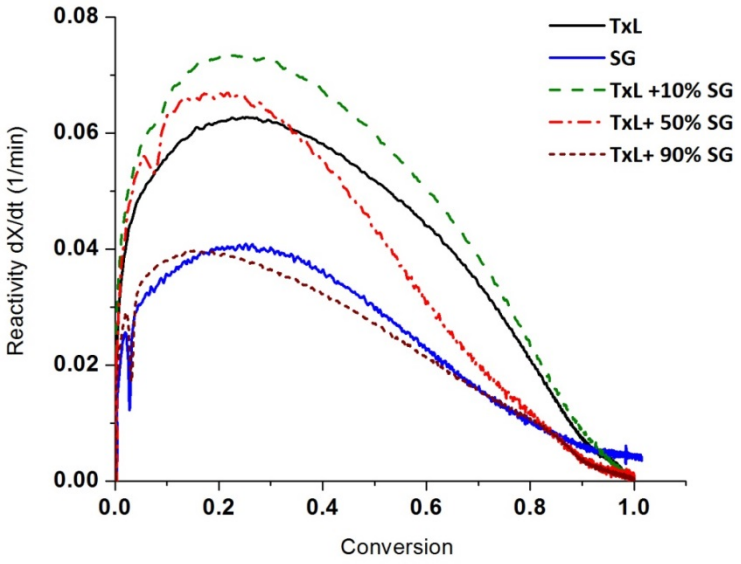

Figure 60. Gasification reactivity profiles in TGA using 100% CO_2 at 800 ^{o}C, 1 atm.

There is no strong evidence of a synergy between Texas lignite and switchgrass during the co-gasification process. In fact, as seen in the below figure, the profile seen for 50-50 blend can be thought of as a linear addition of the contributions coming from Texas lignite and switchgrass individual components. One should really be asking as to how would the inorganic species (particularly K) present in the biomass come in contact with the Texas lignite char. The only possibility would seem to be the spreading of potassium at elevated temperatures that has been reported.

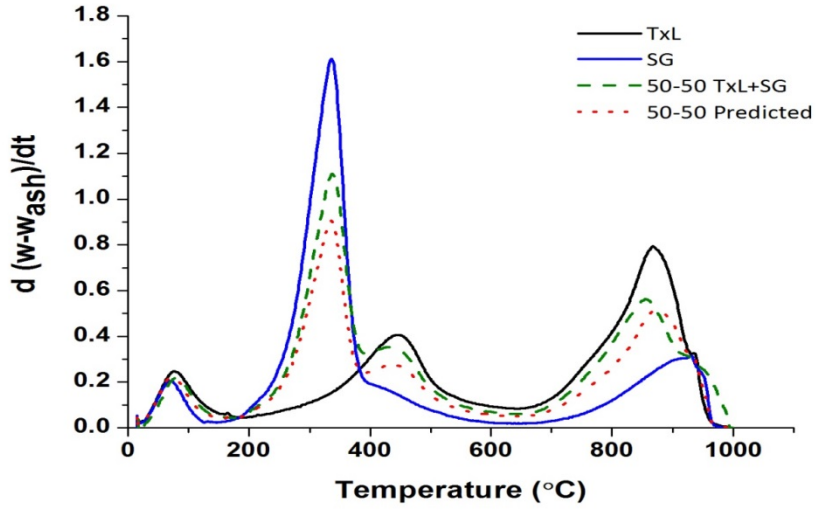

Figure 61. TGA reactivity profiles for Texas lignite, switchgrass, and 50-50 blend

Effect of Blending Texas Lignite with Inorganic Matter

We have attempted to blend Texas lignite char with various inorganic materials: switchgrass char, K_2CO_3, SiO_2 to see the impact on char gasification reactivity in CO_2. The below figure shows the activity profiles for Texas lignite char (generated in entrained flow reactor at 800 ^oC and 5 bars). Four different blends were made with switchgrass ash (5 wt%, 10 wt%, 20 wt%, and 40 wt%). As the SG ash content is increased, the gasification activity increases. This would appear to contradict the observations reported in the above two figures. It should be kept in mind that the blending is done with ash (not biomass), so the inorganic species are in direct contact with the Texas lignite char and can catalyze the gasification reaction.

The second figure below shows the summary of these results. The average reactivity was defined as that during the initial 10% conversion. A good linear increase in char reactivity is seen with increasing ash content. This is very encouraging result for it shows the feasibility of recycling ash by blending it with Texas lignite to achieve increased gasification reactivity.

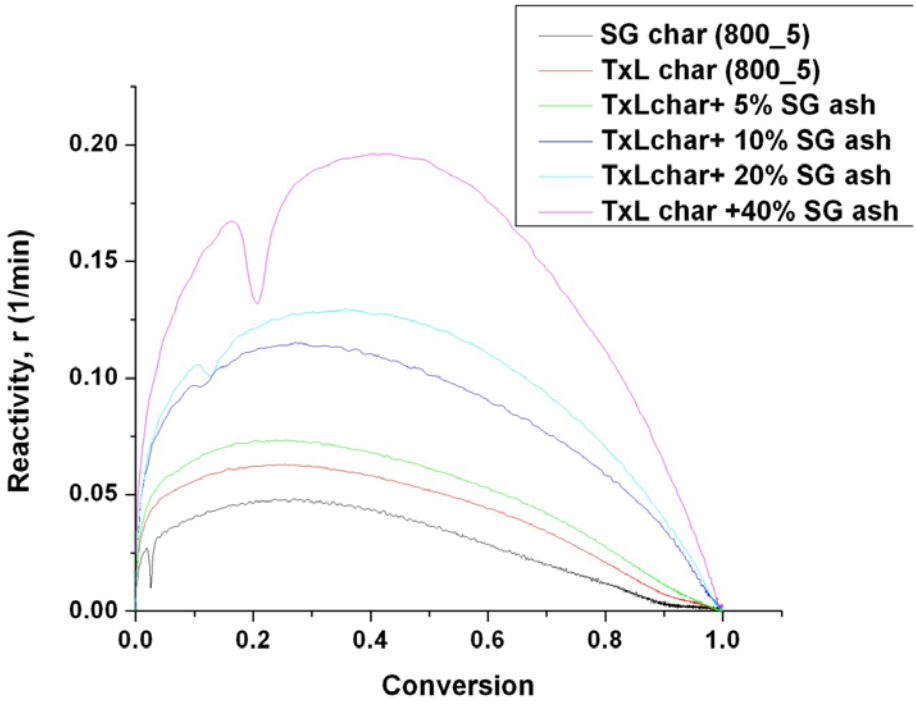

Figure 62. Char gasification reactivity profiles for the blends of Texas lignite and switchgrass ash. All runs were made at 800 ^oC, 100% CO_2 in TGA

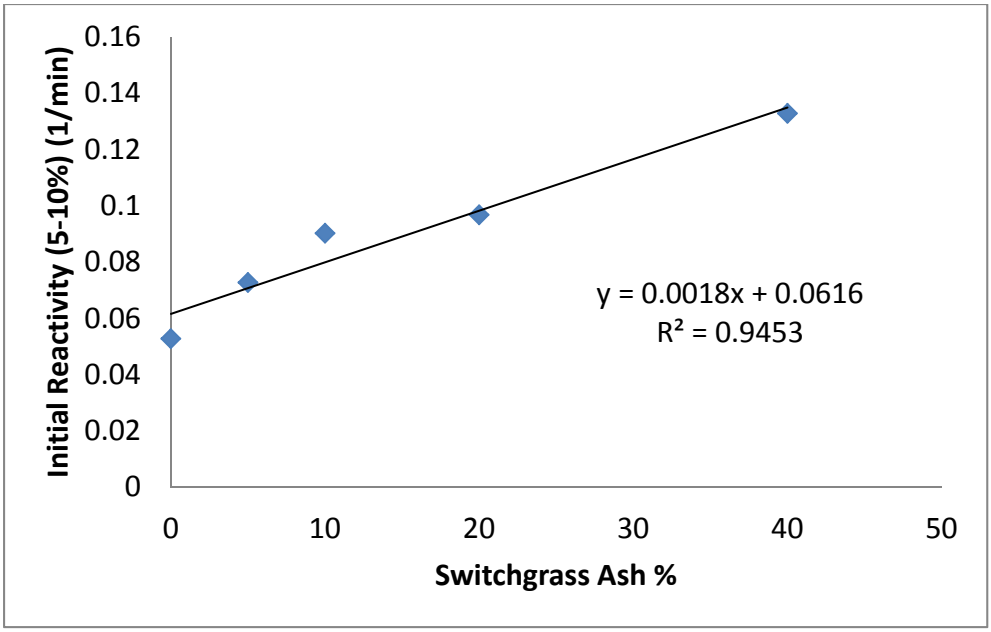

Figure 63. Initial gasification reactivity of Texas lignite blended with switchgrass ash. All runs were made at 800 ^{o}C, 100% CO_2 in TGA

The below figure shows the effect of blending Texas lignite char with different inorganic species: SG ash, CaO, and K_2CO_3. The effect of adding K_2CO_3 is most dramatic and is as expected. We also considered the role of SiO_2 since it is present in both SG ash and in Texas liognite char.

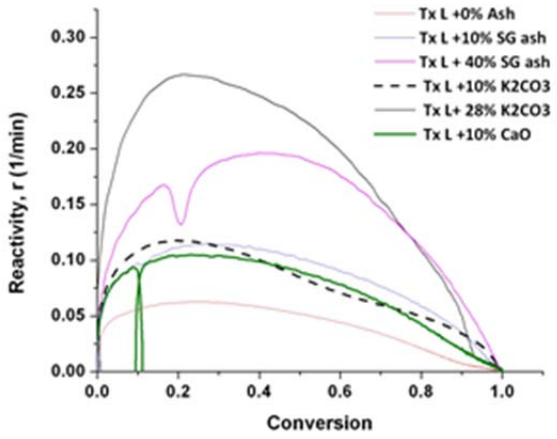

Figure 64. Effect of adding SG ash, K_2CO_3, and CaO on Texas lignite char gasification reactivity in 100% CO_2 at 800 ^oC.

The following figure shows the effect of adding varying amounts of silica on char gasification reactivity. The addition of just 2 wt% silica appears to decrease the reactivity of the char, but then increasing it to 20% does not appear to cause much more change in the decreased reactivity. We need to explore this observation in greater detail. It would seem intuitive that there are some transient effects associated with SiO_2 not being mobile. These effects are important to understand if we are to consider blending two feedstocks.

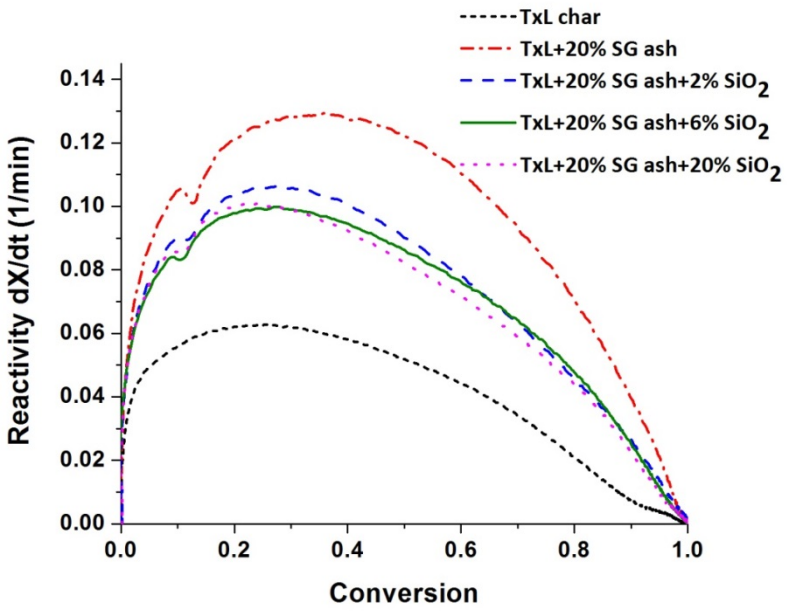

Figure 65. Effect of adding SG ash and SiO_2 on Texas lignite char gasification reactivity in 100% CO_2 at 800 ^oC.

Task 13.0 Char Gasification in PTGA - Catalytic Effect of Ash, Alkali, and Metals

As an extension of char gasification studies (Tasks 8.0 and 9.0), we studied the catalytic effect of various inorganic species typically present in coal and/or biomass. The effects of ash, alkali, and certain metals (e.g., Fe, Mg) will be examined under intrinsic kinetic conditions (no transport limitations) so that their true catalytic role can be identified.

Avicel char was generated in an entrained flow pyrolysis unit by pyrolyzing at 900 ^{o}C and 5 bars. Avicel is a form of pure cellulose and is not supposed to contain any inorganics. It is envisaged that the char generated from avicel can serve as a baseline char having zero or very little gasification activity. One can then add different inorganic species to examine the catalytic role these species play in char gasification. Figure below shows the effect of K_2CO_3 and CaO addition to avicel char on its gasification reactivity at 900 ^{o}C. A number of observations can be made from the results shown in the below figure. K_2CO_3 reduces to K_2O at ~ 900 ^{o}C which is then reduced to metallic K during gasification in the presence of carbon. Metallic potassium (K) migrates inside carbon matrix, enhancing its gasification activity. In contrast, Cao does not reduce to metallic Ca at the gasification temperature. In fact, CaO is known to undergo sintering at increasing conversion, which would cause it to lose its effectiveness as catalyst. It also points to the fact that as char is being gasified, its proportional ash content increases, resulting in increasing gasification activity. This will have implications for the next segment of results. However, at some stage, the system becomes starved of carbon and the rate will drop off.

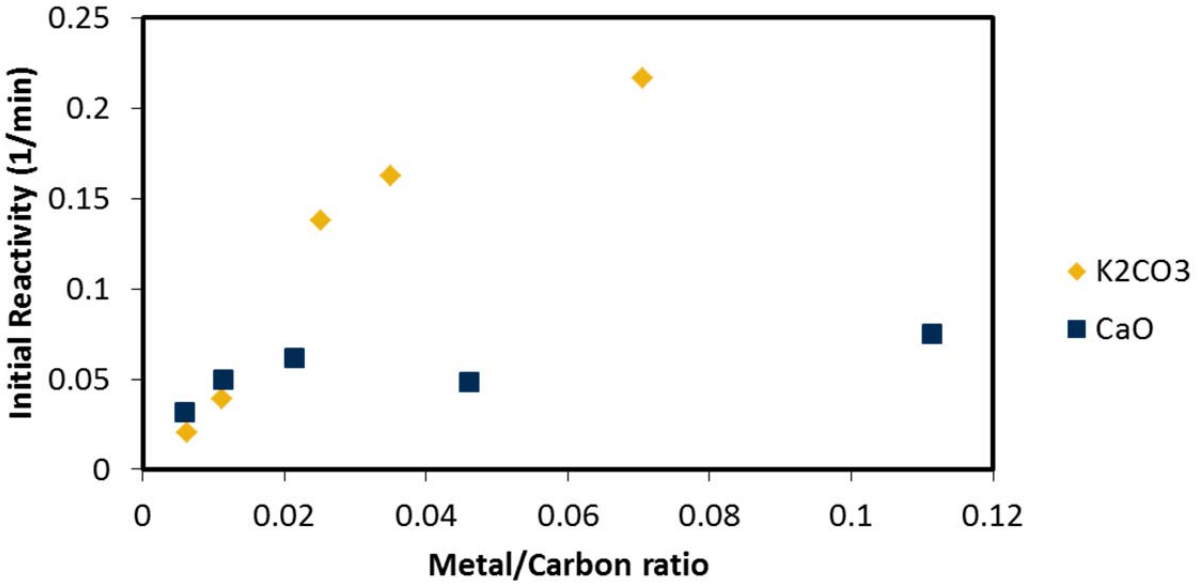

Figure 66. Catalytic effect of inorganic salts on avicel char gasification reactivity at 900 ^{o}C

Figure below shows the results obtained using different inorganics: MgO, CaO, Al_2O_3, and K_2CO_3. In all data shown below, the mixture contained 10 wt% inorganic – 90 wt% avicel char. Gasification runs were carried out at 900 ^oC in pure CO_2. The catalytic effect of inorganics decreases in the following order: K_2CO_3> CaO>MgO>Al_2O_3.

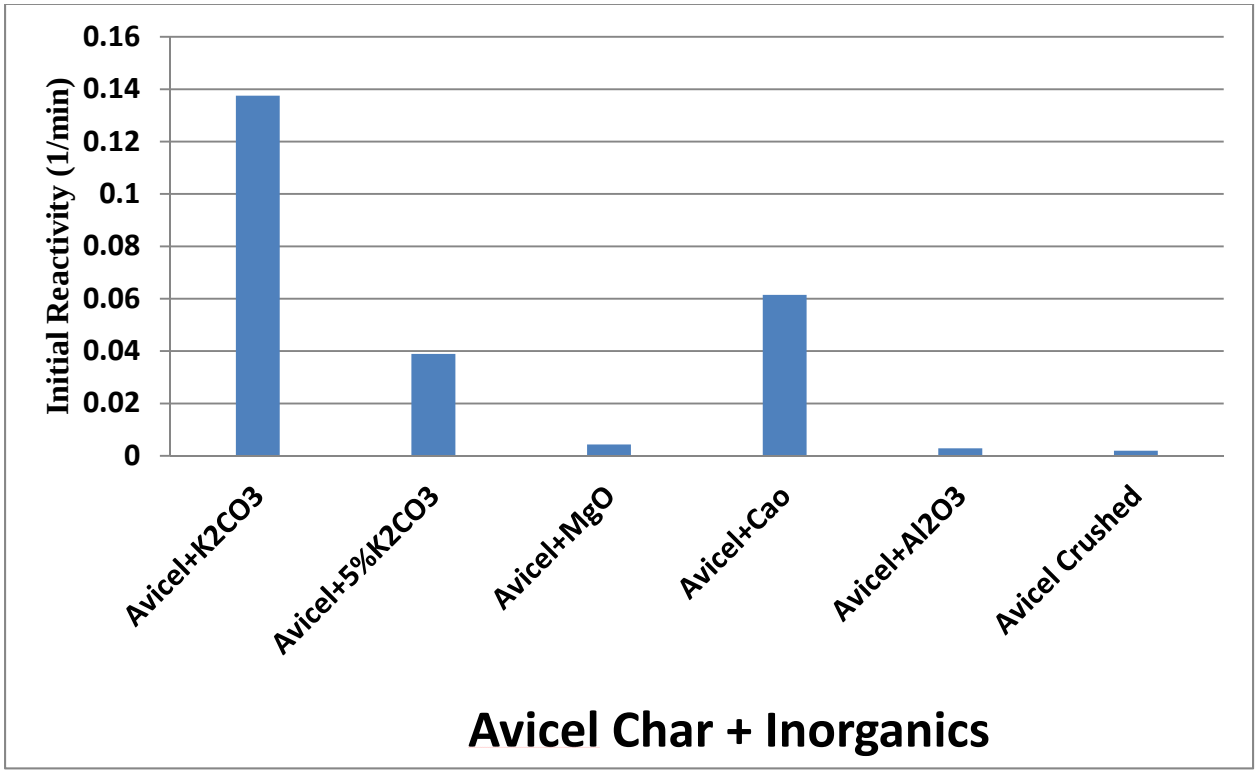

Figure 67. Reactivity of avicel char blended with 10 wt% inorganics (except where noted)

In the next set of experiments, we used a K/C atomic ratio of 0.045, and recorded the reactivity over the entire range of char conversion. Then we repeated the experiment with the same K/C ratio, but added certain amount of fumed silica (SiO_2). This was done to see if the presence of SiO_2 would cause an adverse effect on gasification reactivity. The results, shown in the below figure clearly point to the role of silica in reducing gasification reactivity.

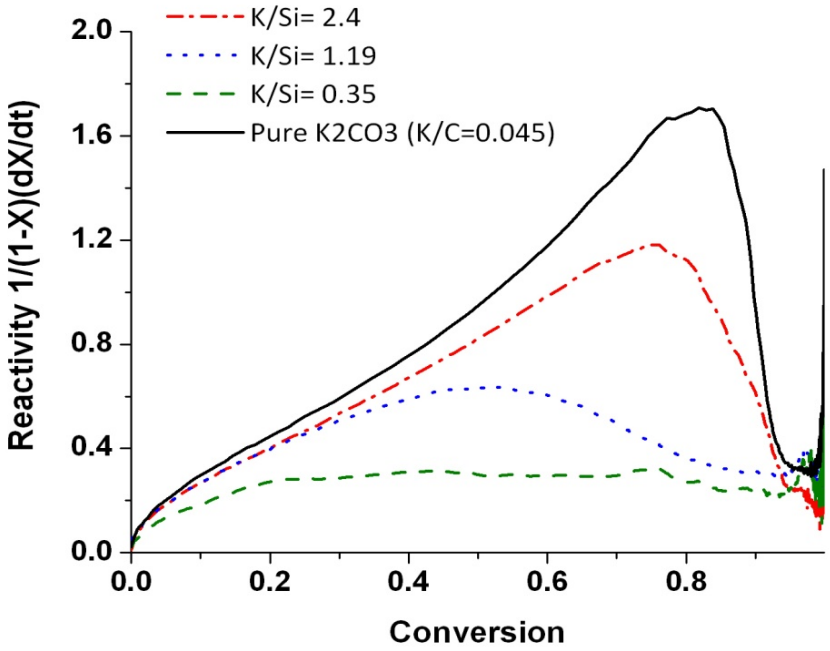

Figure 68. TGA gasification of avicel char at 900 C in 100% CO_2. Physical mixture of avicel char (800 C, 5 bar), fumed silica, and K_2CO_3 was used in the experiments. K/C ratio was kept constant at 0.045 in all four runs.

The below figure shows potassium deactivation by silica in avicel char. Increasing Si content in potassium activated avicel char does not afftect gasification reactivity until a threshold amount of Si is reached. This threshold value is K/Si ~ 1.3 and is similar for various K/C ratios. After this threshold, further increase in Si content lineraly decreases gasification reactivity.

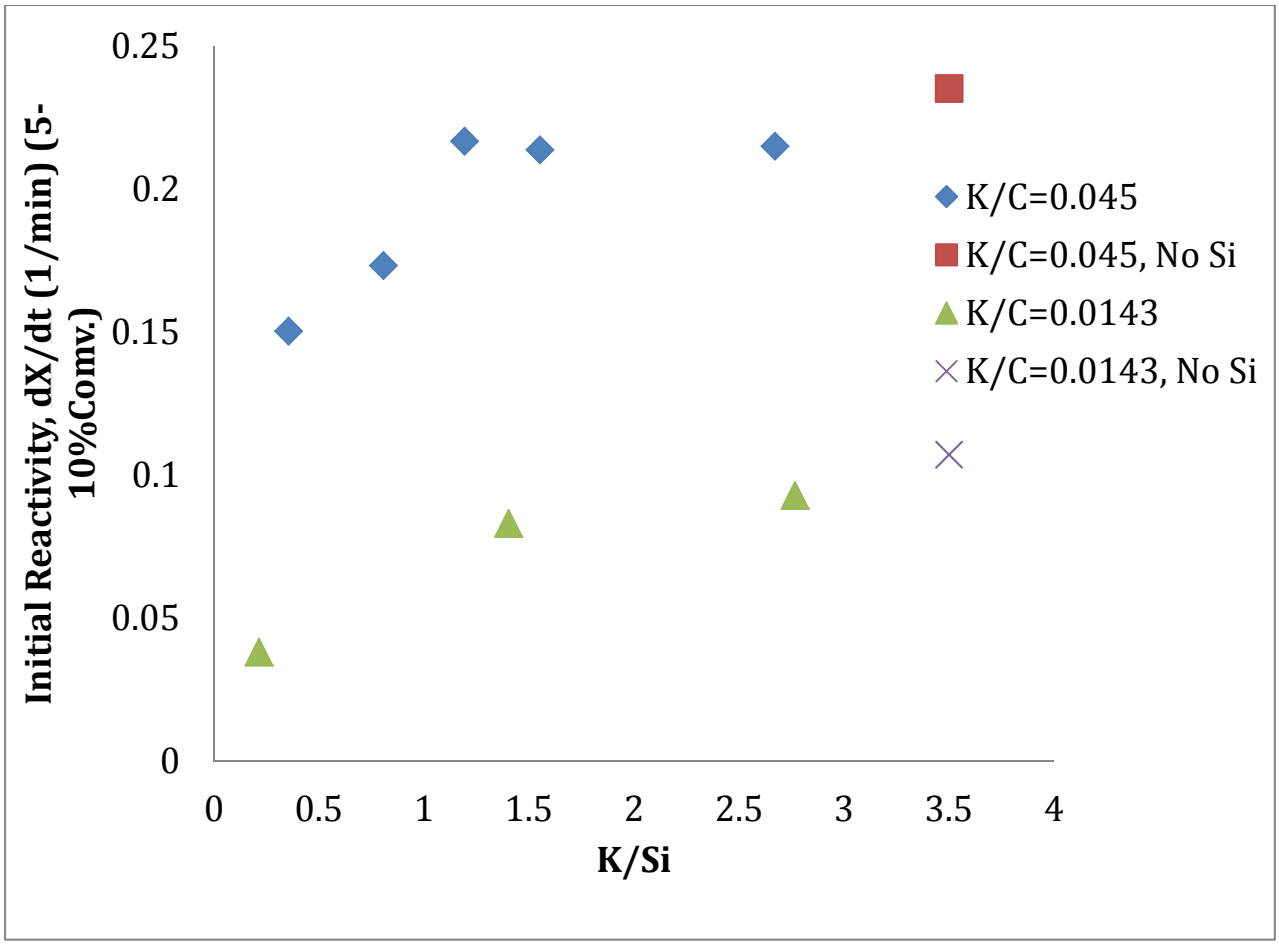

Figure 69. Potassium deactivation by silica in avicel char. The gasification reactivity was measured in TGA at 900 ^{o}C in 100% CO_2.

Task 14.0 Biomass Blends with Bituminous Coal Char

Bituminous Coal vs. Texas Lignite – Effect of Blends

As seen earlier, the gasification reactivity of switchgrass is lower than that for Texas lignite char. This is primarily due to the high Ca content of Texas lignite. Since bituminous coal is the primary feedstock for coal gasification, we thought it would be interesting to examine its gasification reactivity vs the gasification reactivity of Texas lignite char.

Table below summarizes the proximate and ultimate analyses of the two different coal species. The major difference appears to be in the moisture content, sulfur, and oxygen. A sample of Illinois No. 6 bituminous coal was pyrolyzed in a quartz tube reactor at 800 ^{o}C and 1 atm. The char thus generated was used for gasification studies. The below figures summarize the results from char gasification at 800 ^{o}C in 100% CO_2.

Table 1. Texas Lignite vs. Illinois # 6 Bituminous Coal

Rank	Lignite	Bituminous-Illinois #6 (Herrin)
Location	Texas	Franklin Co., IL
	Proximate Analysis (wt.% dry basis)	
Moisture	4.2	11.12
Ash	12.86	10.91
Volatile Matter	NA	39.37
Fixed Carbon	NA	49.72
	Ultimate Analysis (wt.% dry basis)	
C	**61.99**	**71.72**
H	4.44	5.06
N	1.17	1.41

O (by diff)	18.85	7.75
S	**0.69**	**2.82**
Ash	**12.86**	**10.91**

As the below figure shows, the char reactivity for Texas lignite is the highest over the entire conversion range. The reactivity of switchgrass char is nearly half of that for Texas lignite char, whereas the gasification reactivity of Illinois No. 6 coal char is at least an order of magnitude smaller than that for Texas lignite char or switchgrass char. These results suggest that bituminous coal would be a better co-gasification candidate than Texas lignite.

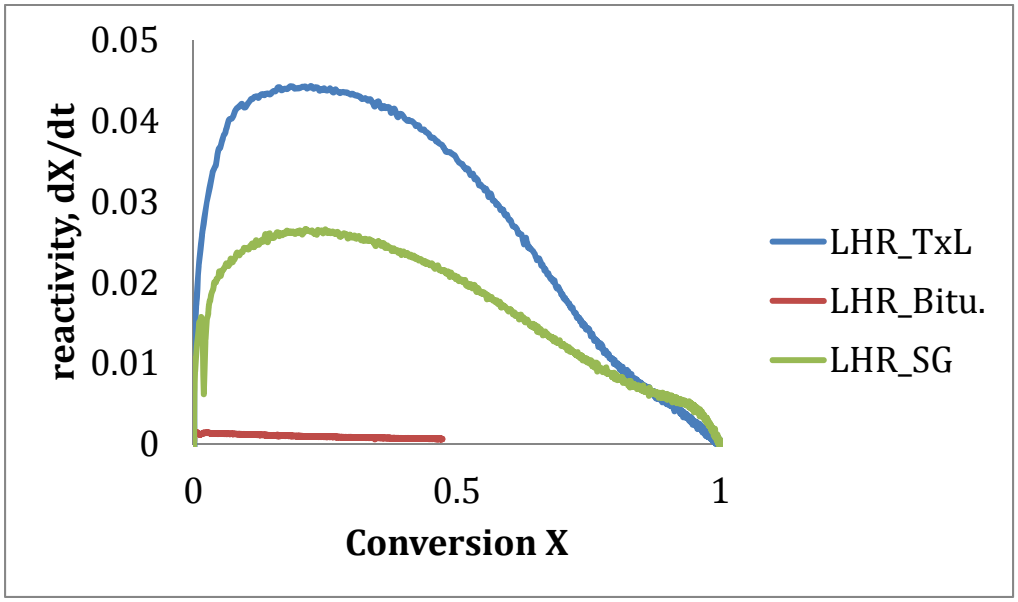

Figure 70. Char gasification reactivity of switchgrass, Texas lignite, and switchgrass chars. All chars were generated in quartz tube reactor at low heating rate (LHR, 15 ^{o}C/min) and held at 800 ^{o}C for 1 hr. Chars were then gasified in TGA at 800 ^{o}C in 100% CO_2.

The below figure shows the results using bituminous coal char. It takes ~ 450 min to achieve 40% conversion of bituminous char at 800 ^{o}C in 100% CO_2. Addition of 20 wt% pine ash, reduces time for 40% conversion to 70 min; SG ash addition reduces the time to ~ 40 min. Catalytic effect or synergy is obvious from the data shown in this below figure.

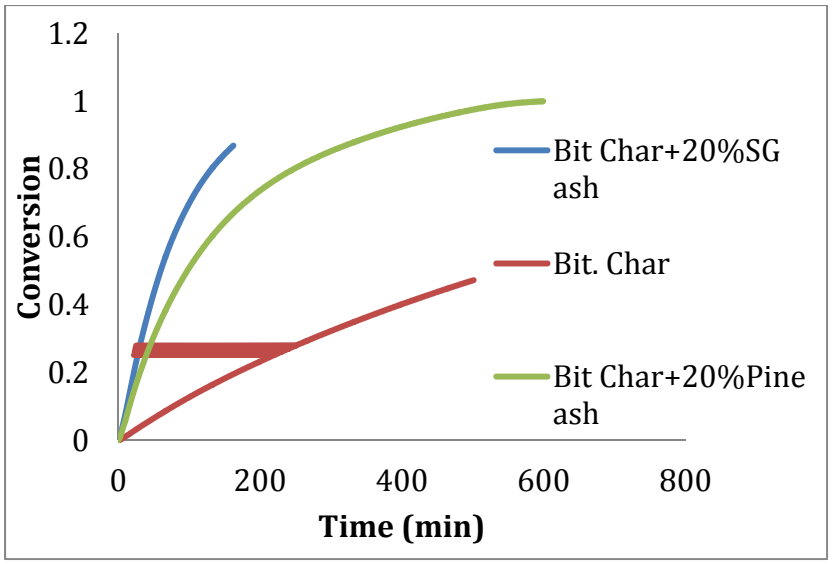

Figure 71. Catalytic effect of pine ash and SG ash on gasification reactivity of bituminous char. Bituminous char was generated in quartz tube reactor at low heating rate (LHR, 15 ^{o}C/min) and held at 800 ^{o}C for 1 hr. It was mixed with pine or SG ash and was gasified in TGA at 800 ^{o}C in 100% CO_2.

The below figure shows the same data (as the above figure) over the entire conversion range. We see a nearly a five–fold or larger increase in reactivity with the addition of the ash.

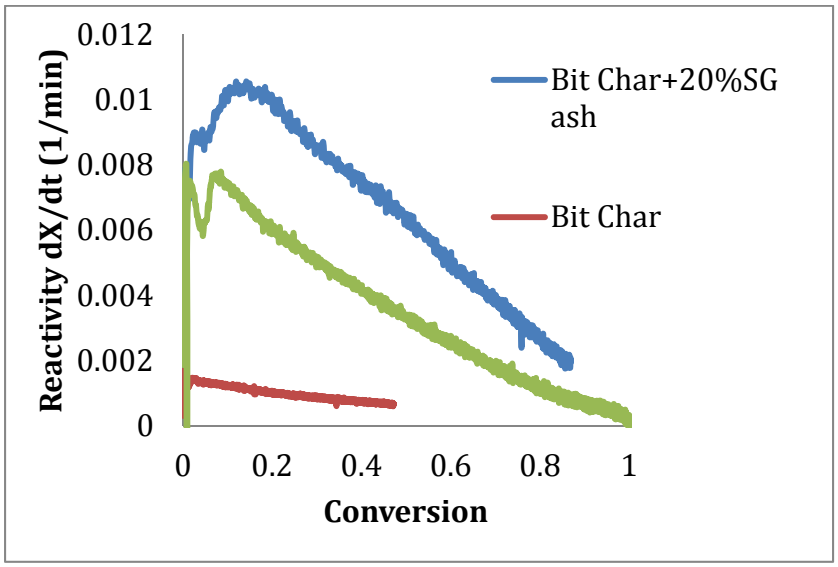

Figure 72. Catalytic effect of pine ash and SG ash on gasification reactivity of bituminous char.

Figure below shows the effect mixing SG char with bituminous coal char in various proportions for gasification at 800 ^{o}C in 100% CO_2. For reference purposes, the gasification reactivity curves of SG char, bituminous char amd Texas lignite char are also shown. The potential of using biomass with bituminous coal in enhancing the gasification reactivity is significant.

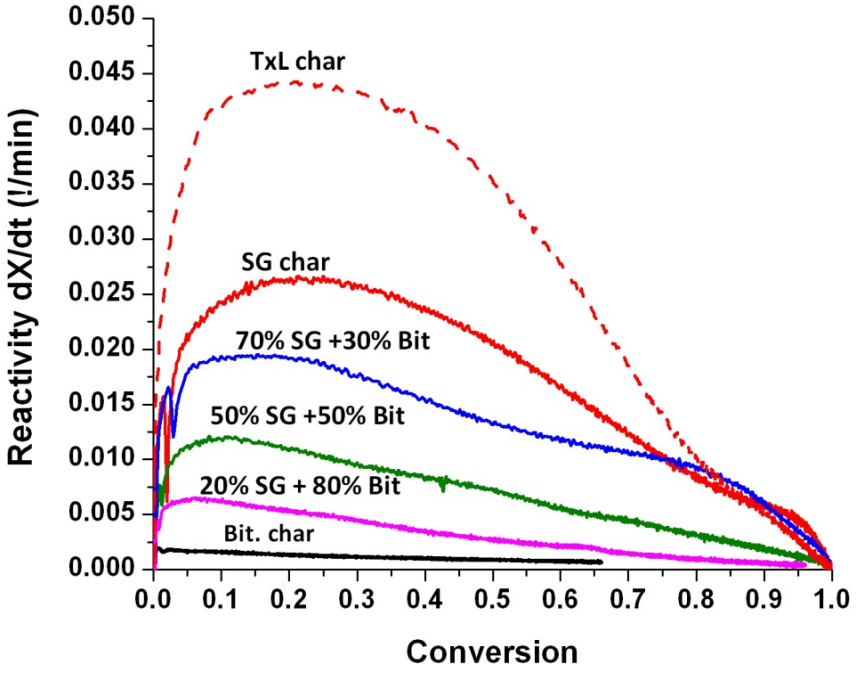

Figure 73. Catalytic effect of SG ash on gasification reactivity of bituminous char. Bituminous char was generated in quartz tube reactor at low heating rate (LHR, 15 ^{o}C/min) and held at 800 ^{o}C for 1 hr. It was mixed with SG ash in the varying proportions and was gasified in TGA at 800 ^{o}C in 100% CO_2.

Figure below shows that the catalytic effect or synergistic effects are not confined to just SG ash. Addition of SG char or pine ash have comparable effects on the gasification rates of bituminous coal.

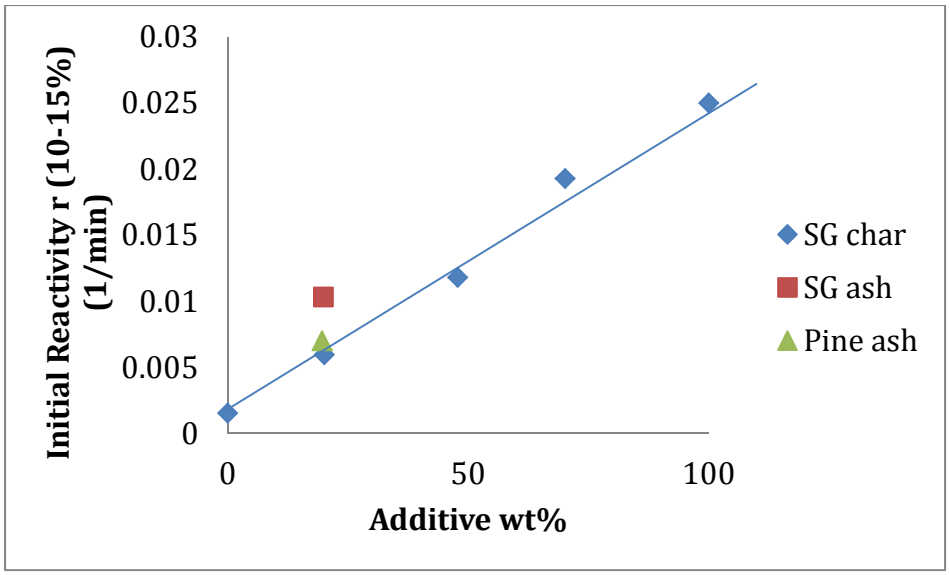

Figure 74. Catalytic effect of SG char, SG ash, or pine ash on initial reactivity of bituminous char at 800 ^{o}C in 100 CO_2.

Bibliography

1. Fermoso, J., Arias, B., Plaza, M.G., Pevida, C., Rubiera, F., Pis, J.J., Garcia-Pena, F., and Casero, P., "High pressure co-gasification of coal with biomass and petroleum coke", *Fuel Process. Technol*., **2009**, 90, 926-932.
2. Kumabe, K., Hanaoka, T., Fujimoto, S., Minova. T., and Sakanishi, K., "Co-gasification of woody biomass and coal with air and steam", *Fuel*, **2007**, 86, 684-689.
3. Kajitani, S., Zhang, Y., Umemoto, S., Ashizawa, M., and Hara, S., "Co-gasification reactivity of coal and woody biomass in high-temperature gasification", *Energy Fuels*, **2010**, 24, 145-151.
4. Larson, E., Fiorese, G., Liu, G., Williams, R.H., and Kreutz, T.G., "Co-production of decarbonized synfuels and electricity from coal + biomass with CO_2 capture and storage: an Illinois case study", *Energy Environ. Science*, **2010**, 3, 28-42.
5. Perlack, R.D., Wright, L.L., Turhollow, A.F., Graham, R.L., Stokes, B.J., and Erbach, D.C., "Biomass as Feedstock for a Bioenergy and Bioproducts Industry: The Technical Feasibility of a Billion-Ton Annual Supply". Report No. DOE/GO-102005-2135 and ORNL/TM-2005/66, Oak Ridge National Laboratory, April **2005**.
6. Gupta, R., "Advanced Coal Characterization: A Review", *Energy & Fuels*, **2007**, 21,451-460.Laurendeau, N.M., 1978. Heterogeneous kinetics of coal char gasification and combustion. *Progress in Energy and Combustion Science* **4**, 221–270.
7. Gøbel, B., Henriksen, U., Jensen, K.J., Qvale, B., Houbak, N., 2000. Dynamic modelling of char gasification in a fixed bed. In: Bridgewater, A.V. (Ed.), Proceedings of Progress in Thermochemical Biomass Conversion. Blackwell Science Ltd., Tyrol, Austria, pp. 92–108.
8. Gøbel, B., Henriksen, U., Jensen, T. K., Qvale, B., Houbak, N., The development of a computer model for a fixed bed gasifier and its use for optimization and control, *Bioresource Technology* **98** (2007) 2043–2052.

[i] B. Gøbel, U. Henriksen, T. K. Jensen, B. Qvale, N. Houbak, The development of a computer model for a fixed bed gasifier and its use for optimization and control, *Bioresource Technology* 98 (2007) 2043–2052.

[ii] M. G. Lussier, Z. Zhang, D. J. Miller, Characterizing rate inhibition in Steam/hydrogen gasification via analysis of adsorbed hydrogen, *Carbon* 36 (1998) 1361–1369.

[iii] C. Fushimi, T. Wada, A. Tsutsumi, Inhibition of steam gasification of biomass char by hydrogen and tar, *Biomass and Bioenergy*, 35 (2011) 179-185.